Stem cell mediated lung repair after influenza-induced injury: role of the Fgf10/Fgfr2b axis

Inaugural Dissertation
submitted to the
Faculty of Medicine
in partial fulfillment of the requirements
for the PhD-degree
in the Faculties of Veterinary Medicine and Medicine
of the Justus-Liebig University Giessen

by Jennifer Quantius
of Bonn, Germany

Giessen 2015

From the Department of Internal Medicine
Director/Chairman: Prof. Dr. Werner Seeger
Faculty of Medicine of the Justus-Liebig University Giessen

First Supervisor: Prof. Dr. Susanne Herold
Second Supervisor: Prof. Dr. Heinz-Jürgen Thiel
Committee Member (Chair):
Committee Member:
Date of Defense:

Table of contents

Figure legends

Abbreviations

3D	three dimensional
7-AAD	7-amino-actinomycin D
ACDU	Automated cell deposition unit
AEC	Alveolar epithelial cell
AEC I/II	Alveolar type I/II pneumocyte
ALI	Acute lung injury
APC	Allophycocyanin
APC-Cy7	Allophycocyanin-cyanin7
Aqp 5	Aquaporin 5
ARDS	Acute respiratory distress syndrome
AU	Arbitrary units
BADJ	Bronchoalveolar duct junction
BAL(F)	Bronchoalveolar lavage (fluid)
BASC	Bronchoalveolar stem cells
BSA	Bovine serum albumin
CC10	Club cell 10 kDa secretory protein
Ccnd1	Cyclin D1
CD	Cluster of differentiation
cDNA	Complementary deoxyribunucleic acid
c-kit	Mast/stem cell growth factor receptor kit
d	days
DASC	Distal airway stem cells
DMEM	Dulbecco's modified eagle medium
DMSO	Dimethyl sulfoxide
DNA	Deoxyribunuceic acid
DNase	Deoxyribunuclease
dNTP	Deoxyribonucleotide triphosphate
Dox	Doxycycline
DTT	Dithiothreitol
dsDNA	Double stranded DNA
EDTA	Ethylenediaminetetraacetic acid
EpCam	Epithelial cell adhesion molecule
EpiSPC	Epithelial stem/progenitor cells
FACS	Fluorescent activated cell sorting
FBS	Fetal bovine serum
Fgf (r)	Fibroblast growth factor (-receptor)
FiO_2	Fractional inspired oxygen
FITC	Fluoresceinisothiocyanat
FSC	Forward scatter
GF	Growth factors
GM-CSF	Granulocyte/macrophage colony-stimulating factor
h	hours
HA	Hemagglutinin
HBSS	Hanks balanced salt solution
hAEC	Human alveolar epithelial cell
HEPES	(4-(2-hydroxyethyl)-1-piperazineethanesulfonic acid
H&E	Hematoxylin Eosin
HGF	Hepatocyte growth factor

huEpiSPC	Human epthelial stem/progenitor cells
IFN	Interferon
IgG	Immunoglobuline
i.p.	intraperitoneal
IRF3	Interferone regulatory factor 3
i.v.	intravenous
kDa	kilodalton
kg	kilogramm
KGF	Keratinocyte growth factor
Klf4	Krueppel-like factor 4
Krt5	Keratin 5/ Cytokeratin 5
lgr6	Leucine-rich repeat containing G protein-coupled receptor
LNEP	Lineage-negative epithelial progenitors
M	mol
M1	Matrix protein 1
M2	Matrix protein 2
mAEC	Murine alveolar epithelial cells
MAVS	Mitochondrial associated antiviral signaling protein
MDCK	Madin darby canine kidney cells
MEM	Minimum essential medium
MFI	Median fluorescence intensity
mg	miligram
min	minute
ml	milliliter
mm	millimeter
mM	millimolar
MOI	Multiplicity of infection
mRNA	Messenger RNA
µg	mircogram
µl	microliter
µm	micrometer
NA	Neuraminidase
NANOG	Homeobox protein NANOG
NEB	Neuroendocrine bodies
NEP	Nuclear export protein
NFκB	Nuclear factor κ B
ng	nanogram
nm	nanometer
NP	Nucleoprotein
NS1	Non-structural protein 1
NS2	Non-structural protein 2
OAS	2`-5`- oligoadenylate synthetase
Oct3/4	Octamer binding transcription factor 3/4
p63	Tumor protein 63
PA	Polymerase acidic protein
PaO_2	Arterial oxygen partial pressure
PerCP Cy5.5	Peridinin-chlorophyll-protein cyanin-5.5
PB1	Polymerase basic protein 1
PB1-F2	Polymerase basic protein 1-F2

PBS	Phosphate buffered saline
PCR	Polymerase chain reaction
PDGF(R)	Platelet derived growth factor (-receptor)
PE	Phycoerythrin
PE-Cy7	Phycoerythrin-Cyanin 7
PFA	Paraformaldehyde
PFU	Plaque forming unit
pg	picogram
pH1N1	Pandemic H1N1
PKR	Protein kinase R
pmol	picomol
qRT-PCR	quantitative real time PCR
rFgf10	Recombinant Fgf10
rMC	Resident mesenchymal cells
RIG-1	Retinoic acid inducible gene-1
RNA	Ribonucleic acid
rpm	rounds per minute
RSP-18	Ribosomal protein subunit S-18
SAEC	Small airway epithelial cell
Sca-1	Stem cell antigen 1
sec	second
SMA	Smooth muscle actin
SMG	Submucosal gland
Sox2	Sex determining region Y-box2
SP-C	Surfactant protein C
SSC	side scatter
TPCK	L-(tosylamido-2-phenyl)ethylchloromethyl ketone
U	units
vClub cell	Variant club cell
vRNP	Viral ribonucleoproteins
w	week
Wnt7b	Wingless-type, mouse mammalian tumor virus integration site family, member 7B
w/o	without
WT	Wildtype
ZO-1	Zona occludens protein 1

1. Introduction

1.1 Influenza virus

1.1.1 Structure and replication cycle

Influenza A viruses are zoonotic pathogens which continuously circulate in several hosts including birds, pigs and humans (1). They belong to the family of *Orthomyxoviridae* and can be divided into influenza A, B and C viruses dependent on their viral antigens, whereby influenza A and B viruses are mostly relevant for humans (2-6). They are classified according to their hemagglutinin (HA) and neuraminidase (NA) properties. Currently, there are seventeen different HA and ten different NA protein subtypes known for influenza A viruses (1, 7). Their genome is composed of eight negative stranded RNA segments which encode eleven viral proteins (1): hemagglutinin (HA), neuraminidase (NA), matrix protein 1 (M1), matrix protein 2 (M2), non-structural protein 1 (NS1), non-structural protein 2 or nuclear export protein (NS2 or NEP), polymerase basic protein 1 (PB1), polymerase basic protein 2 (PB2), polymerase acidic protein (PA), nucleoprotein (NP) and polymerase basic protein 1-F2 (PB1-F2) (3). Influenza viruses are 80-120 nm in diameter and roughly spherical (3, 8). HA, NA and M2 are integrated in the viral envelope, (Figure 1) which consists of a lipid bilayer, originally derived from the host cell. HA is the most abundant protein in the envelope which makes up to 80% of the surface molecules. It is important for the entrance of the virus by binding to the host cell receptor (3). NA is the second most abundant protein on the virus surface, which is important for proper budding to release virions from the host cell (1, 3). M2 forms tetramers and acts as an ion channel which acidifies the viral core in endocytosed vesicles, enabling virus uncoating (1), whereas M1 is located underneath the viral envelope, holding the viral ribonucleoproteins (vRNP) together (3). The vRNPs are composed of negative, single-stranded RNAs bound to a trimeric RNA polymerase complex (PA, PB1, PB2) on the terminal side. The remaining sequence is wrapped around multiple NPs forming a rod-shaped structure (9).

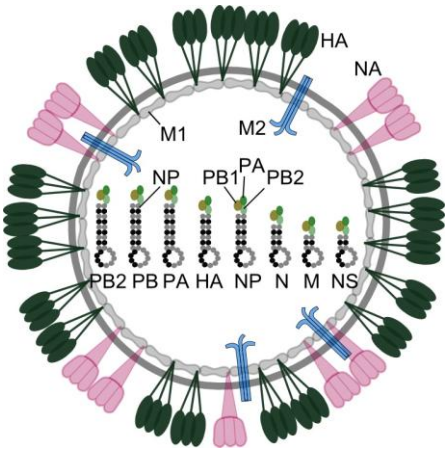

Figure 1: Schematic illustration of influenza A virus structure.
Influenza virus is composed of eight single-stranded RNA segments which encode 11 different proteins: hemagglutinin (HA), neuraminidase (NA), matrix protein 1 (M1), matrix protein 2 (M2), non-structural protein 1 (NS1), non-structural protein 2 or nuclear export protein (NS2 or NEP), polymerase basic protein 1 (PB1), polymerase basic protein 2 (PB2), polymerase acidic protein (PA), nucleoprotein (NP) and polymerase basic protein 1-F2 (PB1-F2).

The influenza virus life cycle can be divided into five main stages: 1) entry of the virus into the host cell, 2) vRNP transport into the host cell nucleus and 3) replication of viral genes, 4) export of vRNPs to the cytoplasm, 5) assembly of viral proteins and vRNPs at the host cell membrane and budding (3).

The initial step for virus propagation is the attachment to the host cell, via binding of HA to either α-2,6 or α-2,3 sialic acid (1). Human influenza virus strains primarily bind to α-2,6 sialic acid, in contrast to avian influenza viruses which mainly recognize α-2,3 linkages (3). In humans, the upper respiratory tract is primarily lined by α-2,6 sialic acid receptors, and α-2,3 sialic acid receptors are found in the lower, distal part (1).

The virus is internalized by endocytosis and decrease of pH in the endocytic vesicle causes the ion channel M2 to open leading to release of vRNP complexes into the cytoplasm followed by translocation to the nucleus (1). Therefore, the proteins of the vRNP complex have a nuclear localization signal (3) and bind to cellular nuclear import complexes (3, 9). The negative single-stranded RNA of influenza viruses is converted to positive RNA strands, which then serve as a template for further viral RNA production (3). The negative sense vRNPs are exported by the nuclear pores and viral proteins and vRNP complexes associate with the host cell membrane, where viral particles are formed using the host cell plasma membrane. The final step for virion release is the sialic acid cleavage by NA which releases the virion from the apical side of polarized host cells (3, 10).

During influenza virus evasion, three major antiviral pathways are activated by host cells to limit infection (11), whereas influenza virus manipulates and counteracts host innate immune responses in order to replicate efficiently (12). The innate immune response which is primarily triggered by viral RNA initiates Toll-like receptors, inflammasome and retinoic acid inducible gene-1 (RIG-1) (11, 13). Therefore, viral RNA is bound by RIG-1 and associates with mitochondrial associated antiviral signaling protein (MAVS) to induce NFκB (nuclear factor κ B) and interferon (IFN) production for viral clearance (11). Due to IFN production, the protein kinase R (PKR) is induced and usually gets activated by binding of dsRNA, which can initiate a general block of translation (14, 15). The viral NS1 protein is responsible for the inhibition of IFN production by limiting the activation of the transcription factor NFκB and dependent on the strain, also IRF3 (interferon regulatory factor 3) which is an interferon-inducible transcription factor (16, 17). Another cytoplasmatic antiviral protein which is activated by dsRNA binding is the 2`-5`- oligoadenylate synthetase (OAS), that initiates the activation of RNase and thereby the inhibition of virus replication. NS1 is able to interact with both proteins to block their antiviral properties (18).

1.1.2 Pathogenicity and epidemiology

Influenza virus infection of the human respiratory tract can result in respiratory disease and may lead to death. At times, it is the most common cause of respiratory tract infections (19, 20). After infection, the host cell protein biosynthesis is shut down to focus on the production of viral proteins (21). Influenza virus can adapt to the host with certain strategies and is able to evolve minor changes in their surface proteins and thereby evade immune recognition by host neutralizing antibodies, which is called antigenic drift and results in host susceptibility to infection (22). Another modification of influenza viruses or even generation of new strains can occur by antigenic shift, which requires infection of one host with two influenza virus strains followed by reassortment of gene segments between the two strains (1).

Influenza virus is usually airborne transmitted and causes a rapid onset of high fever, cough, headache, malaise and inflammation of the upper respiratory tract including trachea and upper respiratory tree, which persists for up to ten days.

Usually, people of all ages are affected, but severity is greatest in infants, aged persons and those with illness (19, 23). Interestingly, it has been demonstrated in an experimental approach that repair mechanisms after influenza infection are delayed in aged mice (24). In uncomplicated cases, influenza viruses only replicate in ciliated and non-ciliated cells of the nasal mucosa in the upper respiratory tract. Nevertheless, the virus can spread to the distal part of the lung, causing pneumonia with severe consequences. The cytolytic effect by the virus itself, or the indirect effects of host response causes damage of the alveolar epithelium, composed of type I and type II pneumocytes, leading to edema formation and severe respiratory dysfunction. Epidemics concerning all groups of ages occur each winter season, whereas worldwide pandemics appear irregularly (6). The most severe pandemic was the so-called spanish flu in 1918 which caused approximately 50 million deaths worldwide (2, 25).

1.2 Acute lung injury and acute respiratory distress syndrome

The most severe consequence which can result from influenza virus infection is the acute respiratory distress syndrome (ARDS) which was firstly described in 1967 (26, 27). Since a standard definition for acute lung injury (ALI) and ARDS was made in 1994, the mortality rate did not remarkably change and still accounts for 30-40% (28-30). However, in the last years, new definition criteria for ARDS were addressed (31, 32) and a new categorization has been applied subdividing ARDS into mild, moderate, or severe. This is based on the degree of hypoxemia levels, according to the ratio between arterial oxygen concentration and the fraction of inspired oxygen (PaO_2:FiO_2) (32-34). Other criteria include a rapid onset and bilateral infiltrates, usually diagnosed by chest x-ray, with the exclusion of left arterial hypertension (35, 36).

ARDS can have different causes. Some of the most common risk factors are pneumonia, sepsis, aspiration of gastric contents, inhalational injury and major trauma (36). The pathology can be divided into three main stages, which include the inflammatory, proliferative and fibrotic phase. The inflammatory phase is characterized by diffuse alveolar damage with disruption of the epithelial-endothelial barrier and edema formation (37). The proliferative phase is defined by further damage to the alveolar epithelium and capillary network, where type II

pneumocytes start to proliferate to restore barrier function, and the alveolar air space is filled with cell debris and erythrocytes and fibroblasts become more apparent (38). The fibrotic phase includes deposition of collagen, fibronectin and extracellular matrix components and is characterized by an imbalance of pro- and antifibrotic factors which may stimulate lung resident fibroblast, and aberrant repair (31, 39, 40).

The central role of ARDS treatment is protective ventilation, since mechanical ventilation can induce additional injury to the lung (41, 42). Severe life- threatening hypoxemia is treated by extracorporeal membrane oxygenation, if no other therapy is successful, to at least keep up oxygen levels and protect the lung (43, 44). Pharmacotherapeutic ARDS treatments include vasodilators, like nitric oxide which increases blood flow of ventilated alveoli, exogenous surfactant application, to decrease surface tension, or anti-coagulants to avoid thrombus formation to improve lung function (45, 46). Recent new therapies include mediators which promote cytoprotective or mitogenic effects, like KGF (keratinocyte growth factor) or GM-CSF (granulocyte/macrophage colony-stimulating factor) (47-49). Nowadays, also cell-based therapies with bone marrow derived mesenchymal stem cells are clinically tested. Nevertheless, new approaches for therapy of ARDS are required to decrease mortality rates and improve outcome (47, 50).

1.3 Structural and cellular compartments of the lung

The lung is a complex organ, which enables crucial oxygen supply and alterations in the lung structure may lead to impaired gas exchange (51). There is a clear hierarchy and branching morphometry in the lung (52). The human airway tree branches dichotomously about 23 times (51), which leads to about 480 million gas exchange units: the alveoli. This complex and delicate lung structure is supported by a fiber system which surrounds the entire conducting and alveolar structures (51). The upper, conducting airways are lined by bronchial epithelium (51). Ciliated cells remove potential harmful organisms or dust particles and filter the inhaled air by coordinated beating, whereas secretory cells, like goblet cells do not only keep the mucosa moist, but also bind particles and pathogens by their secreted mucus (53, 54). The bronchial epithelium contains club cells which produce surfactant (club cell 10 kDa secretory protein; CC10). They have multiple roles in lung

protection, for example by production of antimicrobial peptides or metabolism of toxic substances (54, 55). The alveolar compartment is lined by type I and type II pneumocytes. Type I pneumocytes are large squamous epithelial cells, which enable normal gas exchange (56). They are extraordinary thin (57) and share a basement membrane with the endothelial cells. The capillary is incorporated between the walls of two alveoli, allowing gas exchange on both sides of the septum (51). Type I pneumocytes cover 95% of alveoli, while they make up only 8% of total cells (57). The cuboidal type II cells are mainly located in the corner of the alveolus and express surfactant proteins (57) which mostly consist of lipids and line the inner alveolar surface. Surfactants are important for alveolar stability and surface tension and therefore regulate proper ventilation (58). Another function is their contribution to host defense by binding surface structures of various pathogens to promote their elimination by alveolar macrophages (58). Microenvironmental factors, necessary for epithelial cells are provided and regulated by lung resident mesenchymal cells. They are not only important for secondary septa formation during development, they also regulate elastin and collagen deposition (59-61).

1.4 Lung epithelial stem/progenitor cells

The lung is a very complex organ which contains more than 40 different cell types (51, 62). Therefore, different region-specific epithelial progenitor cells have been detected in tracheobronchial, as well as in distal alveolar tissue (63). Due to slow turnover of epithelial cells in the lung, the proliferative response of lung epithelial progenitor cells are preferentially studied in injury models (62, 64). These different injury models, involving proximal airway, broncho- and/ or alveolar injury suggest that the adult lung contains different epithelial progenitor cell niches, which are characterized by self-renewal potential, clonogenicity and multipotency, representing classical properties of stem/progenitor cells (62, 63, 65). In general, stem cells can either divide symmetrically or asymmetrically. Symmetric division leads to generation of identical daughter cells, in contrast to asymmetric division which leads to the generation of terminally differentiated cells in addition to new progenitors (65-68). Furthermore, the local microenvironment or “niche” which

includes for example extracellular matrix and a broad spectrum of autocrine and paracrine factors, plays a crucial role in the regulation of stem cells (66, 69).

1.4.1 Epithelial progenitor cells in rodents

In the adult lung, various stem/progenitor cells are responsible for homeostasis of cells, as well as for the repair of injured lung tissue (70). In the cartilage containing tracheobronchial region, basal cells, defined by various markers, like nerve growth factor receptor, Krt5/14 (Cytokeratin 5/14), p63 (tumor protein 63) and aquaporin 3 play an essential role during injury and can generate the major epithelial cell types found in the proximal airways, including basal cells, club cells, ciliated cells and goblet cells, which includes a Notch-mediated differentiation (71-76). Of note, cells located at the submucosal gland ducts (SMG), in between cartilage rings, are involved in repopulating processes of the SMG and its surface epithelium after injury. Therefore, the SMG is considered as a stem/progenitor cell niche (70, 77-79). In the trachea and bronchioles, CC10-expressing club cells can be found, which respond differently during injury or homeostasis (80). Moreover, the majority of club cells express the cytochrome P450 which plays an important role in detoxification processes (55, 81, 82). Application of naphthalene causes severe bronchiolar damage to the epithelial cells due to cytochrome P450-mediated conversion into a toxic intermediate (83, 84). A small naphthalene resistant club cell subpopulation (vClub cells) is located at the distal conducting airways (83) which lacks the cytochrome P450 and contributes to airway repopulating processes after injury. It has been demonstrated that club cells give rise to ciliated cells and self-renew. In injury models of severe alveolar damage, club cells can also repopulate type II pneumocytes, most probably after a bronchiolar epithelium transitional state (69, 85, 86).

A relatively undefined cell type is the neuroendocrine cell, located at airway branches or bronchoalveolar duct junctions (BADJ) and are usually clustered into neuroendocrine bodies (NEB). These cells are resistant to naphthalene injury and in close proximity to vClub cells, which suggests that the neuroendocrine body microenvironment habours a progenitor cell niche (87-89). Another cell population, located at the BADJ are the so-called bronchoalveolar stem cells (BASC), which were first described by Kim et al.. They express the type II pneumocyte marker

surfactant protein C (SP-C) and the club cell marker CC10. These cells are resistant to naphthalene treatment and increase in cell numbers after injury, which then return to baseline levels after restoration. Characterization of surface markers show a $CD45^{neg}CD31^{neg}Sca\text{-}1^{+}CD34^{+}$ signature. *In vitro* experiments revealed that these cells can give rise to alveolar type I and type II pneumocytes, as well as club cells, which suggests that BASC self-renew but also habour the potential for multilineage differentiation (90). Interestingly, bronchopulmonary dysplasia, induced by hyperoxia treatment of newborn mice does not increase BASC numbers compared to normoxia controls, suggesting that not all types of injury stimulate BASC proliferation. However, additional factors, like bone marrow derived mesenchymal stromal cells or conditioned medium of these cells, increase the BASC population in hyperoxia-treated newborn mice, suggesting a contribution of paracrine factors (91).

McQualter et al. defined a rare population with $EpCam^{high}\alpha6^{+}\beta4^{+}CD24^{low}$ signature. This multipotent epithelial stem/progenitor cell (EpiSPC) fraction gives rise to airway or alveolar epithelial lineages *in vitro* suggesting an organized stem cell hierarchy in the adult murine lung (92, 93). Additionally, undifferentiated lung stromal cells, in contrast to α-smooth muscle $actin^{+}$ ($\alpha\text{-}SMA^{+}$) myofibroblasts have a supportive influence on EpiSPC growth and upregulate genes which are associated with lung development, suggesting reactivation of developmental pathways during lung injury (94). Another progenitor cell type with the expression of integrin α6β4 was proposed by Chapman et al.. These cells clonally expand and proliferate *ex vivo*. This rare population possesses the ability to proliferate and form organoid structures after kidney capsule implantations (95).

Of note, it has been demonstrated that $p63^{+}Krt5^{+}$ expressing cells undergo rapid proliferation after influenza virus infection. These cells form clusters ("pods") which are found in interbronchial regions of damaged tissue (96). Lineage tracing studies of $p63^{+}$ cells after influenza virus infection or bleomycin treatment show that the majority of newly generated $p63^{+}$ cells derived from $CC10^{+}$ cells and not from pre-existing $p63^{+}$ basal cells located in the upper airways (97). These so-called distal airway stem cells (DASC) differentiate into alveolar and bronchiolar lung tissue, and selective depletion of these cells impairs the regenerative process *in vivo* (98). Another report describes migration and co-expression of $\alpha6\beta4^{+}$ cells in combination with Krt5, in influenza virus-challenged lung tissue and excludes the

contribution of basal cells for $Krt5^{+}p63^{+}$ pods. These lineage-negative epithelial progenitors (LNEP) are an important responder after severe lung injury. Interestingly, *ex vivo* culture of LNEP alone, or with various morphogenic factors does not stimulate Krt5 expression, in contrast to culture with bronchoalveolar lavage fluid (BALF) of influenza virus-infected mice which results in proliferation and Krt5 upregulation (99), suggesting that multiple factors induced in the stem cell niche contribute to their regenerative response. The distal lung is lined by two cell types, the squamous type I pneumocytes which enable gas exchange and the cuboidal surfactant protein-producing type II pneumocytes (100). Since a long time it has been suggested that type II pneumocytes act as progenitors for type I pneumocytes (101). A recent report demonstrates the self-renewal abilities of type II pneumocytes and differentiation into cells that express type I pneumocyte markers after bleomycin-induced injury (102), representing an important alveolar progenitor cell activated after mild injury.

Although the presence of different epithelial progenitor cell populations is well described, their lineage relation and particularly their defined roles in replenishing different epithelial components of the lung after injury is not well defined. In addition, the signals which stimulate them to drive coordinated repair processes without aberrant wound healing is still not well understood.

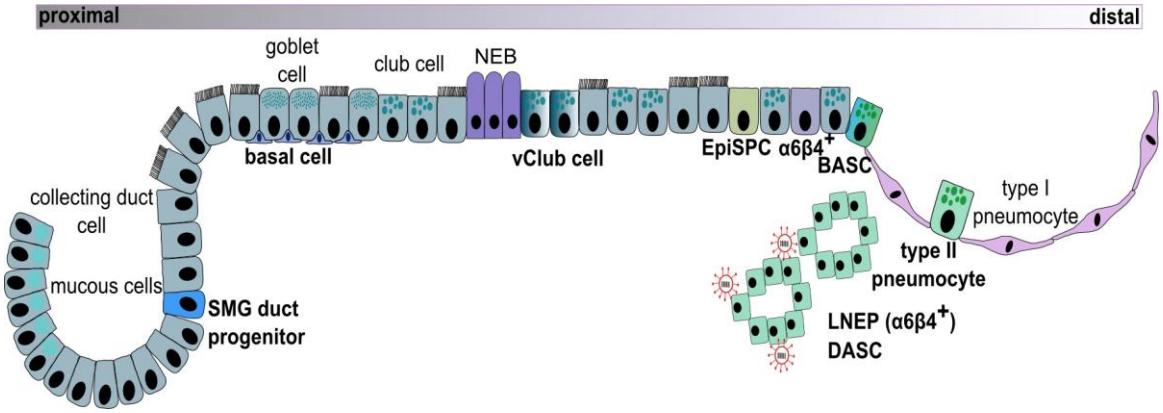

Figure 2: Schematic illustration of epithelial stem/progenitor cells in the murine lung.
Epithelial stem/progenitor cells of the adult murine lung are located at side-specific regions from the tracheobronchial until the distal alveolar tissue. They contribue to tissue repair processes after injury and are characterized by self-renewal, multipotency and clonogenicity; BASC, bronchoalveolar stem cell; DASC, distal airway stem cells; LNEP, lineage-negative epithelial progenitor; NEB, neuroendocrine bodies; SMG, submucosal gland; vClub cell; variant club cell.

1.4.2 Epithelial progenitor cells in the human lung

Although, the epithelial stem cell research in the adult murine model is well established, much less is known about epithelial progenitor cells in the adult human lung. In particular, the knowledge about defined markers to isolate a homogenous population is very limited (103). It has been described that different airway epithelial cells of the bronchial epithelium in the upper respiratory tract have the ability to form submucosal glands in xenograft models (104). In the tracheobronchial region, a side population of $CD45^{neg}$ cells is identified with clonogenic capacity. These cells express epithelial cell markers, like Krt5, E-cadherin, ZO-1 (zona occludens protein 1), p63 and are isolated according to their property to efflux hoechst stain (105). The hoechst stain is a vitality staining and primarily used to determine the DNA content for cell cycle studies, but it can be used to identify cells with stem or progenitor abilities (106). In the pseudostratified epithelium, $p63^{+}$ cells can be found, which are morphologically comparable to murine basal cells. These cells are able to either self-renew or differentiate into luminal or ciliated cells *in vitro* which is dependent on the Notch signaling pathway (72, 73). In the distal lung, it is demonstrated that type II pneumocytes form spheres in co-culture with a human lung fibroblast cell line (MRC-5), suggesting clonality and self-renewal properties of type II pneumocytes. Of note, culture of type II pneumocytes alone does not result in spheric outgrowth. Histological analysis revealed that most of the cells express the type II pneumocyte-specific membrane protein HTII-280 (102, 107). Another report describes the identification of multipotent human lung stem cells with the stem cell marker c-kit (mast/stem cell growth factor receptor kit). Cultured multicellular clones are negative for specialized cell types, like epithelial, smooth muscle, and endothelial cell markers but express NANOG (homeobox protein NANOG), Oct3/4 (octamer binding transcription factor 3/4), Sox2 (sex determining region Y-box2) and Klf4 (krueppel-like factor 4), and show mutipotency, clonogenicity and self-renewal capacity. Injection of these $c\text{-}kit^{+}$ cells into damaged mouse lung tissue result in the formation of bronchioles, alveoli and pulmonary vessels *in vivo* (65). Terminal bronchoalveolar tissue is generated by single cell injections of $E\text{-}cadherin^{+}/lgr6^{+}$ (leucine-rich repeat containing G protein-coupled receptor) human epithelial lung cells into kidney capsules (103). Of note, the $E\text{-}cadherin^{+}/lgr6^{+}$ cell population is a subpopulation of integrin $\alpha6^{+}$ cells, which show self-renewal and differentiation into

specialized epithelial cells, but not mesenchymal or endothelial differentiation (103).

1.5 Fibroblast growth factors and corresponding receptors

The first fibroblast growth factors (Fgf) were isolated from brain and pituitary gland. They were termed Fgfs due to their mitogenic activity on cultured fibroblasts (108-110). Today, the mammalian Fgf family comprises 22 members of structurally related polypeptides, which can be divided by their mode of action into endocrine, paracrine and intracrine members. The endocrine and paracrine Fgfs act via a cell surface tyrosine receptor, in contrast to the intracrine Fgfs which act intracellularly and independent of a receptor (111). The family of paracrine Fgfs is the largest family which comprises four subfamilies, including Fgf7 and Fgf10. Most of the paracrine Fgfs are secreted proteins and mediate biological responses by binding to cell surface tyrosine kinase receptor with heparin/heparan sulfate which acts as a cofactor and ensures stable interaction and signaling (111-113). The Fgf receptors are composed of an extracellular domain which is responsible for ligand binding, a transmembrane domain and an intracellular domain with the tyrosine kinase core as well as regulatory sequences (112). The extracellular ligand binding domain consists of immunoglobulin-like domains which can be alternatively spliced (112, 113). Four fibroblast growth factor receptor (Fgfr) genes have been identified, but due to splicing seven major forms exist with different ligand-binding specificities (1b, 1c, 2b, 2c, 3b, 3c, 4) (111, 112). The isoform b of the Fgfr is preferentially expressed by the epithelium, whereas the c isoform of the receptor is expressed mainly by mesenchymal cells (114, 115). Ligand binding induces functional dimerization, phosphorylation of tyrosine residues on the receptor, and activation of four major downstream signaling pathways RAS-RAF-MAPK, PI3K-AKT, STAT and PLCγ and may lead to migration, survival and proliferation (116).

1.6 Fibroblast growth factor 10 in the embryonic and adult lung

During lung organogenesis, Fgf10 is expressed in the distal mesenchyme where it activates the epithelial Fgfr2b to induce branching of the local epithelium whereat

Fgf10 dosage seems to be critical in the epithelial amplification process (117-119). The importance of Fgf10/Fgfr2b signaling during lung development is demonstrated in respective knockout animals which are not viable after birth. The absence of the receptor Fgfr2b or its ligand Fgf10 result in a wide range of phenotypic abnormalities in multi-organ development of all three germ layers including lung development failure, and the phenotype of Fgf10 knockouts correlates with Fgfr2b null mice (120-123). Fgf10 is structurally most related to Fgf7 (also known as keratinocyte growth factor; KGF) and both bind to the Fgfr isoform Fgfr2b which is present on epithelial components of various tissues including lung (123, 124). But in contrast to $Fgf10^{-/-}$ or $Fgfr2b^{-/-}$ animals, $Fgf7^{-/-}$ animals display not such remarkable abnormalities during lung development (120, 124-126). Of note, Fgf7 can only activate Fgfr2b, whereas Fgf10 is able to bind to Fgfr2b and Fgfr1b. However, Fgfr1b knockout animals do not show a lung-specific phenotype (112, 127), suggesting a minor importance of Fgfr1 in lung development or repair. Interestingly, Fgfr2b stimulation with different ligands results in different responses. Stimulation with Fgf7 results in rapid receptor degradation, whereat stimulation with Fgf10 results in prolonged signaling and receptor recycling (128).

During lung development, Fgf10 is secreted by mesenchymal progenitor cells, and acts on distal epithelial progenitor cells to keep them in a progenitor phenotype by preventing differentiation (129, 130). Furthermore, Fgf10 acts as chemoattractant for distal lung epithelial cells in a mesenchymal-free environment, promotes endodermal outgrowth and induces budding (131, 132). Inhibition with a dominant negative, soluble Fgfr2, which binds several ligands, including Fgf10, reveals a time-dependent Fgf requirement for lung formation, whereat postnatal suppression of Fgf signaling has no remarkable effect on late alveologenesis (133). However, in the adult lung it has been demonstrated that parabronchial smooth muscle cells get reactivated by epithelial Wnt7b (wingless-type, mouse mammary tumor virus (MMTV) integration site family, member 7B) signaling to express Fgf10 after epithelial injury caused by naphthalene. This paracrine Fgf10 signaling activates the remaining airway progenitor cell pool to proliferate and to promote restoration of the lung barrier. Interestingly, parabronchial smooth muscle precursors represent one of the pools for Fgf10 expression during development (129, 134). This demonstrates the ability to reactivate developmental pathways in the adult

lung after injury and to promote epithelial repair (134-136). In another lung injury model, induced by profibrotic bleomycin, Fgf10 overexpression in inducible transgenic animals attenuates the fibrotic phenotype, resulting in less collagen deposition, increased survival, and protection of epithelial cells (137). It also has been shown that overexpression of a soluble, dominant negative Fgfr2 expressed under the surfactant protein C (SP-C) promoter increases alveolar permeability, inflammatory cytokine expression and decreases surfactant protein expression. Additionally, adult mice fail to recover after hyperoxia treatment, when the dominant negative Fgfr2b is expressed (133, 138).

1.7 Aim of the thesis work

Influenza virus causes respiratory tract infections which may lead to acute lung injury or its severe form, the acute respiratory distress syndrome (ARDS). ARDS is characterized by epithelial cell apoptosis, disruption of the epithelial layer and edema formation which impairs gas exchange dramatically. The pathological consequences of influenza virus infection are well described, but regenerative pathways and host-pathogen interactions during these processes are poorly understood. Epithelial progenitor cells have been shown to proliferate after injury and contribute to repair processes to restore lung architecture and function.

The aim of this work was to investigate if repair processes after influenza virus infection are dependent on a distinct pool of distal epithelial progenitor cells, and thereby evaluating the role of contributing regenerative signaling pathways. Furthermore, the interaction between virus and host cell-mediated regenerative pathways is elucidated to finally find new therapeutic approaches to foster repair processes after influenza virus infection. Therefore, evaluation of the proliferative potential and differentiation properties of distal epithelial progenitor cells in three-dimensional cultures, as well as in *in vivo* mouse models with wildtype, inducible genetically modified, or knockout animals were performed.

2. Materials & Methods

2.1 Cell culture media

Medium	Ingredients
Avicel overlay medium	2xMEM (Gibco), 0.1% $NaHCO_3$ (Sigma-Aldrich), 0.2% BSA (Sigma-Aldrich), 1.25% Avicel (FMC Biopolymers), 1x penicillin/streptomycin (Sigma-Aldrich), 1 µg/ml trypsin TPCK (Worthington).
Basal medium 2	Basal Medium (Promocell), 0.02 ml/ml FBS (Promocell), recombinant human insulin [1 ng/ml] (Promocell), recombinant human basic FGF [5 µg/ml] (Promocell), 1x penicillin/streptomycin (Sigma-Aldrich).
DMEM/HEPES	DMEM (Gibco), 25 mM HEPES (Biochrom).
EpiSPC basic medium	MEM-alpha (Gibco), 10% FBS (Gibco), 1x insulin/ transferrin/ selenium (Gibco), 1x penicillin/streptomycin (Sigma-Aldrich), 0.0002% heparin (Stemcell Technologies), 2 mM L-glutamine (PAA).
EpiSPC expansion medium (murine and human)	EpiSPC basic medium, 50 ng/ml recombinant human Fgf10 (R&D Systems), 30 ng/ml recombinant murine or human HGF (R&D Systems). After influenza virus infection 1 µg/ml trypsin TPCK (Worthington) was added to the medium.
hAEC medium	F12 Nutrient Mixture (Ham) (Gibco), 10% FBS (Gibco), 1x penicillin/streptomycin (Sigma-Aldrich), 2.5 µg/ml amphotericin B (PAA).
Human co-culture medium	MEM-alpha (Gibco), 2% FBS (Gibco), 1x insulin/ transferrin/ selenium (Gibco), 1x penicillin/streptomycin (Sigma-Aldrich), 0.0002% heparin (Stemcell Technologies), 2 mM L-glutamine (PAA).

Medium	Ingredients
Infection medium	DMEM (Gibco), 1x penicillin/streptomycin (Sigma-Aldrich), L-glutamine (PAA), 0.2% BSA (Sigma-Aldrich), 1 µg/ml trypsin TPCK (Worthington).
Inoculation medium	$PBS^{Mg+/Ca+}$ (Gibco), 0.2% BSA (Sigma-Aldrich), 1x penicillin/streptomycin (Sigma-Aldrich).
mAEC medium	DMEM (Gibco), 25 mM HEPES (Biochrom), 10% FBS (Gibco), 1x penicillin/streptomycin (Sigma-Aldrich).
MDCK.2 medium	DMEM (Gibco), 10% FBS (Gibco), 1x penicillin/streptomycin (Sigma-Aldrich).

2.2 Buffers and solutions

Buffers /Solutions	Ingredients
FACS buffer	920 ml $PBS^{-/-}$ (Gibco), 74 ml 1% EDTA (Biochrom), 5 ml FBS (Gibco), 10 ml 9% Na-azide (Sigma-Aldrich), sterile filtered, pH= 7.4.
MACS buffer	920 ml $PBS^{-/-}$ (Gibco), 74 ml 1% EDTA (Biochrom), 5 ml FBS (Gibco), sterile filtered, pH=7.4.
PII-Solution	7.95 g/l NaCl (Carl Roth GmbH), 0.4 g/l KCl (Merck), 1.11 g/l glucose (Sigma-Aldrich), 0.46 g/l Na_2HPO_4 (Merck), 2.38 g/l HEPES (Sigma-Aldrich), 0.28 g/l $CaCl_2$ x $2H_2O$ [2mM] (Sigma-Aldrich), $MgSO_4$ x $7H_2O$ (Fluka) [1.3 mM] diluted in H_2O (B. Braun), pH= 7.2, sterile filtered.
Paraformaldehyde (PFA) 4%	4 g PFA (Sigma-Aldrich) in 100 ml $PBS^{-/-}$ (Gibco), pH= 7.4.
PBS/EDTA	2 mM EDTA (Biochrom) in $PBS^{-/-}$ (Gibco), sterile filtered.

2.3 Transgenic mouse strains

The following mice strains were used for experimentation.

Mouse strain	Features
C57BL/6N	Wildtype (WT)
Rosa26$^{rtTA/+}$;tet(O)sFgfr2b/+	Inducible overexpression of soluble, dominant negative Fgfr2b
Rosa26$^{rtTA/+}$;tet(O)Fgf10/+	Inducible Fgf10 overexpression
Fgf7$^{-/-}$	Fgf7 knockout

Generation of *Rosa26 rtTA* mice was achieved by crossing *CMV-Cre* mice with *rtTA^{flox}* mice (139, 140), which resulted in a ubiquitous expressed rtTA under the Rosa26 promoter. This constitutive *Rosa26$^{rtTA/+}$* strain was crossed with either *tet(O)sFgfr2b* (133, 141) or *tet(O)Fgf10* (134, 142) responder lines to allow expression of either soluble, dominant negative Fgfr2b or Fgf10 when doxycycline containing food (625 mg/kg, Harlan Teklad) was administered. *Rosa26$^{rtTA/+}$; tet(O)sFgfr2b/+* and *Rosa26$^{rtTA/+}$; tet(O)Fgf10* heterozygous mice were generated on a mixed background and genotyped as previously described (133, 140, 142, 143). *Fgf7* knockout animals were purchased from Jackson Laboratories (stock number 4161) on a mixed background and backcrossed for five generations into a C57BL/6N background. Animal experiments performed at the Justus-Liebig University were approved by regional authorities of the State of Hesse (Regierungspräsidium Giessen).

2.4 Influenza virus strains

The following virus strains were used for the experimental part:

Virus strain	Characteristics
A/Puerto Rico/8/34 (A/PR8)	H1N1 adapted to mice by passaging
A/X-31(H3N2) (x-31)	H3N2 in a A/PR8 backbone
A/Hamburg/04/09 (pH1N1)	H1N1 pandemic, human isolate

2.5 Human lung tissue

Human lung tissue was obtained from patients undergoing lobectomy for tumor removal after written consent in cooperation with the departments of Pathology and Surgery, Justus-Liebig-University, Giessen. Processing of human lung tissue was approved by the Ethics Committee of the University Giessen (Az. 10/06).

2.6 Preparation of virus stock

For the preparation of a virus stock, MDCK.2 cells (Madin darby canine kidney cells; ATCC number CRL-2936) were passaged. Therefore cells were washed twice with $PBS^{Mg+/Ca+}$ (Gibco) and trypsin EDTA (Biochrom) was added until the cells detached from the T75 culture flask (Greiner Bio-one), followed by addition of MDCK.2 medium and further incubation at 37°C, 5% CO_2. After 24h (confluency ~ 80%), cells were infected with a MOI (multiplicity of infection) of 0.01. Therefore, cells were washed twice with $PBS^{Mg+/Ca+}$ (Gibco) and 4 ml of inoculum were added to the cells, followed by incubation at room temperature for 1h. The inoculum was removed and infection medium was added to the cells, followed by additional incubation for 48h at 37°C, 5% CO_2. The infection medium was collected and centrifuged to remove cell debris (4,000 rpm, 15 min, 4°C). The supernatant was aliquoted and stored at -80°C until quantification of virus titers were performed.

$$\text{MOI calculation: } \frac{\text{Virus (plaque-forming units)}}{\text{Cell number}}$$

2.7 Quantification of virus concentration

To quantify virus concentration, a plaque assay was performed. MDCK.2 cells were passaged and seeded in 6-well plates (Greiner bio-one) one day prior infection. The cells were washed with $PBS^{Mg+/Ca+}$ (Gibco) and a dilution series of the virus stock or BALF was made and 1 ml of the inoculum was added to the MDCK.2 cells, followed by incubation at room temperature for 1h. 2 ml Avicel overlay medium were added to the cells, followed by incubation for 48h at 37°C, 5% CO_2. The Avicel overlay medium was removed, and cells were fixed with 1 ml 4% paraformaldehyde (PFA, Sigma-Aldrich) for 30 min at 4°C, followed by three times washing with $PBS^{Mg+/Ca+}$ (Gibco). After permeabilization with 1 ml of 0.3% Triton-X 100 (Roth) for 15 min at room temperature, 0.5 ml of the primary

antibody, detecting influenza A nucleoprotein (NP) 1:1000 (Meridian Life Science) in $PBS^{Mg+/Ca+}$ (Gibco), 0.1% Tween-80 (Sigma-Aldrich), 10% horse serum (PAA) was added and incubated for 1h at room temperature, followed by three times washing with $PBS^{Mg+/Ca+}$ (Gibco), 0.05% Tween-80 (Sigma-Aldrich). After addition of 0.5 ml of the secondary antibody (goat α-mouse horseradish peroxidase, Santa Cruz) in a 1:2000 dilution (diluent: $PBS^{Mg+/Ca+}$ (Gibco) in 0.1% Tween-80 (Sigma-Aldrich), 10% horse serum (PAA)), cells were incubated for 1h at room temperature, followed by three times washing with $PBS^{Mg+/Ca+}$ (Gibco), 0.05% Tween-80 (Sigma-Aldrich). After addition of the peroxidase substrate (True Blue, KPL) and incubation for 15-30 min, plaques were detected. The reaction was stopped by washing with H_2O (B. Braun) and plates were dried and stored at room temperature. The quantification of virus stocks or BALF was always performed in duplicates.

2.8 Quantitative real-time PCR

FACS sorted or cultured cells were washed once with $PBS^{Mg+/Ca+}$ followed by lysis with RLT buffer (Qiagen). RNA isolation was performed using RNeasy Kit (Qiagen) according to manufacturer's manual. After extraction, RNA concentration and quality were measured by Nanovue Plus (GE Healthcare). cDNA synthesis was prepared with a total volume of 13.5 µl containing 250 ng RNA in dH_2O (5 prime GmbH) which was denatured at 70°C for 5 min, followed by addition of 11.5 µl PCR mixture to the samples.

PCR mixture:

5x First stand buffer (Invitrogen)	5 µl
0.1 M Dithiothreitol (DTT) (Invitrogen)	2.5 µl
Random primer (Boehringer)	1.5 µl
Recombinant ribonuclease inhibitor 40 U/µl (Invitrogen)	0.5 µl
PCR Nucleotide Mix (Roche)	1 µl
M-MLV Reverse Transcriptase 200 U/µl (Invitrogen)	0.75 µl
dH_20 (5 Prime GmbH)	0.25 µl

Samples were incubated in a thermocycler machine (Peqlab) for 1h at 37°C until reaction was stopped by heating up the samples for 5 min at 95°C. cDNA was diluted in a 1:3 ratio with dH_2O (5 Prime GmbH) for qRT-PCR reaction. β-actin or ribosomal protein subunit S-18 (RSP18) expression served as normalization control. The reactions were performed with SYBR green I (Invitrogen) in the AB Step one plus Detection System (Applied Bioscience) with intron-spanning primers. The following qRT-PCR mixture was used for a reaction:

qRT-PCR mixture:

Sybr Green (Invitrogen)	13 µl
Forward primer [10 pmol/µl]	0.5 µl
Reverse primer [10 pmol/µl]	0.5 µl
50 mM $MgCl_2$ (Invitrogen)	1 µl
dH_2O (5 Prime GmbH)	5 µl

The following intron spanning primers were used for quantitative RT-PCR:

Gene	Primer sequence
murine Actin forward	5′-ACCCTAAGGCCAACCGTGA-3′
murine Actin reverse	5′-CAGAGGCATACAGGGACAGCA-3′
murine Aquaporine 5 forward	5’-TGGGGATCTACTTCACCGGC-3′
murine Aquaporine 5 reverse	5’-TACCCAGAAGACCCAGTGAGAGG-3′
murine β-tubulin forward	5’-CCACCACCATGCGGGAAA-3′
murine β-tubulin reverse	5’-CTGATGACCTCCCAGAACTTG-3′
murine Ccnd1 forward	5’- GCGTACCCTGACACCAAT-3′
murine Ccnd1 reverse	5’- GGTCTCCTCCGTCTTGAG-3′
murine CC10 forward	5’-CAGACACCAAAGCCTCCAACC-3′
murine CC10 reverse	5’-GGGCAGATGTCCGAAGAAGC-3′
murine Fgf7 forward	5’- TCGCACCCAGTGGTACCTG-3′;
murine Fgf7 reverse	5’- ACTGCCACGGTCCTGATTTC- 3’
murine Fgf10 forward	5’-CCATGAACAAGAAGGGGAAA-3′
murine Fgf10 reverse	5’-CCATTGTGCTGCCAGTTAAA-3′
murine Krt5 forward	5’-CCTTCGAAACACCAAGCACG-3′
murine Krt5 reverse	5’-AGGTTGGCACACTGCTTCTT-3′

Gene	Primer sequence
murine Podoplanin forward	5'-CCCCAATAGAGATAATGCAGGGG-3′
murine Podoplanin reverse	5'-GCCAATGGCTAACAAGACGC-3′
murine proSP-C forward	5'-TCCTGATGGAGAGTCCACCG-3′
murine proSP-C reverse	5'-CAGAGCCCCTACAATCACCAC-3′
murine p63 forward	5'-CAAAGAACGGCGATGGTACG-3′
murine p63 reverse	5'-CCTCTCACTGGTAGGTACAGC-3′
murine RPS-18 forward	5'- CCGCCATGTCTCTAGTGATCC-3′
murine RPS-18 reverse	5'- TTGGTGAGGTCGATGTCTGC-3′

The relative gene abundance compared to the housekeeping gene was calculated as ΔCt value ($Ct_{reference}$ – Ct_{target}). Comparison with control cells are presented as ΔΔCt ($\Delta Ct_{reference}$ - ΔCt_{target}). Data are presented as ΔCT or ΔΔCt.

2.9 Immunohistochemistry and immunofluorescence

For the preparation of cryosections, lungs were perfused with HBSS (Gibco) and filled with 1.5 ml Tissue Tek (O.C.T. Compounds, Sakura) mixed with $PBS^{-/-}$ (Gibco) in a 1:1 ratio. The lungs were embedded in Tissue Tek (Sakura) and snap-frozen in liquid nitrogen. 3-4 µm slices were cut with a Leica CM 1850 UV Cryotome and the slides were stored at -20°C. Lung sections or cytospins of FACS sorted cells were Hematoxylin-Eosin (H&E) or Pappenheim stained according to the following protocols.

For the H&E staining the cryosections were put in Hematoxylin solution (modified according to Gill III, Merck) for 10 to 20 sec. Slides were washed with tap water until staining solution was removed, followed by differentiation in 1% actetic acid for 10 sec and washing with tap water. After that, the slides were dipped in dH_2O (B. Braun) and stained with Eosin G-solution (0.5% aqueous, Merck) for 10-15 sec, followed by a stepwise dehydration with 70%, 96% and 100% ethanol (J.T. Baker).

For the Pappenheim staining, cytospins were stained with May Grünwald (Merck) for 5 min, followed by short washing with dH_2O (B. Braun). After that, the slides were stained for 10 min in Giemsa's azur eosin methylene blue solution (Merck) and finally washed with dH_2O (B. Braun) and subsequently dried and mounted (Neo-mount, Merck).

For immunofluorescence stainings, lung sections were fixed with 4% PFA (Sigma-Aldrich) for 20 min and subsequently incubated with 0.05% Tween-20 (Sigma-Aldrich), 5% BSA (Sigma-Aldrich), 5% horse serum (PAA) in $PBS^{-/-}$ for 30 min. Fluorochrome-labeled antibodies or corresponding isotype control antibodies were diluted in $PBS^{-/-}$, 0.1% BSA, 0.02% Triton X-100 (Roth) and incubated for 2h. For non-labeled antibodies the slides were washed with $PBS^{-/-}$, 0.1% BSA, 0.02% Triton X-100 (Roth) and incubated with corresponding fluorochrome-labeled secondary antibodies for 2h, followed by mounting with dapi-containing mounting medium (Vectashield, Vector Labs). Cultured cells were fixed in a 1:1 ratio of ice-cold acetone/methanol for 5 min and subsequently incubated with 3% BSA in $PBS^{-/-}$ for 30 min. Cells were stained with primary or isotype control antibodies, respectively, followed by addition of corresponding secondary antibodies for 2h and mounting with dapi-containing mounting medium. Images were taken with a Leica DM 2000 microscope using the Leica digital imaging software LAS. The following antibody dilutions were applied:

Immunofluorescence stainings:

Primary Antibodies	Dilution
α-SMA FITC (clone: 1A4, Sigma-Aldrich)	1:100
β-IV-tubulin (clone: ONS.1, Abcam) or isotype control IgG1 (clone: CT6, Abcam)	1:50
CC10 (clone: T-18, Santa Cruz) and isotype control normal goat IgG (Santa Cruz)	1:100
CD49f PE (clone: GoH3, Biolegend)	1:50
E-cadherin (clone: DECMA-1, Abcam)	1:200
EpCam FITC (clone: G8.8, Biolegend)	1:20
Keratin 5 FITC (Bioss)	1:100
Ki67 (Thermo Scientific)	1:100
Mucin5ac biotin (clone: 45M1, Abcam)	1:50
p63 protein A-555 (clone: P51A, Bioss)	1:100
pro-surfactant protein C (Millipore) or rabbit serum (Sigma-Aldrich)	1:500

Secondary Antibodies	Dilution
anti-streptavidin-APC (BD Pharmingen)	1:50
chicken anti-goat IgG Alexa Fluor 488 (Invitrogen)	1:800 to 1:1000
chicken anti-goat IgG Alexa Fluor 647 (Invitrogen)	1:800 to 1:1000
donkey anti-mouse IgG Alexa Fluor 555 (Invitrogen)	1:500
donkey anti-rabbit IgG Alexa Fluor 555 (Invitrogen)	1:800
donkey anti-rabbit IgG Alexa Fluor 488 (Invitrogen)	1:800 to 1:1000
donkey anti-rabbit IgG Alexa Fluor 647 (Invitrogen)	1:800 to 1:1000
donkey anti-rat IgG Alexa Fluor 555 (Abcam)	1:800 to 1:1000
donkey anti-rat IgG Alexa Fluor 488 (Invitrogen)	1:1000

2.10 Quantitative flow cytometry and FACS sorting

Multicolor flow cytometry or fluorescence activated cell sorting was performed with the LSR Fortessa (BD Bioscience) and the Aria III (BD Bioscience) using DIVA software (BD Bioscience) or Flowing Software. For analytical measurements 1-5 x 10^5 cells were freshly stained with fluorochrome-labeled antibodies for 20 min at 4°C. For intracellular stainings, permeabilization of cells was achieved by previous incubation with 0.2% saponin (Calbiochem) diluted in FACS buffer for 20 min at 4°C, followed by incubation with respective antibodies or isotype controls for 20 min at 4°C. For stainings with non-labeled primary antibodies, a fluorochrome-labeled secondary antibody was added and incubated for 20 min at 4°C. Finally, the cells were resuspended in the corresponding buffer. Annexin V staining for apoptosis measurements was performed on unfixed, non-permeabilized cells. Prior to antibody incubation, cells were washed and resuspended in Annexin V buffer (BD Bioscience) and incubated with Annexin V Alexa Fluor 647 and respective antibodies for 20 min at 4°C, followed by resuspension in Annexin V buffer. For the LipidTox staining (Invitrogen), cells were first stained with antibodies, followed by fixation in 4% PFA and incubation with diluted LipidTox for 30 min at 4°C. Immediately after staining, flow cytometric measurements or FACS sorting were performed. For dead cell exclusion 7-AAD (7-amino-actinomycin D; Biolegend) was added to the stained cell suspensions, or cells were treated with a fixable live/dead cell reagent (Life Technologies) according to the manual. FACS

sorting was performed with 85 or 100 µm nozzles. The sorted cells were counted and processed for RNA isolation, cell culture or cytospin stainings. Single cell sorting was performed with the automated cell deposition unit (ACDU) directly in a 24-well plate with 12 mm cell culture inserts (Millipore, 0.4 µm pore size). The following antibody mixtures were used for the different analysis:

- Fgrf2b detection:

Antibody	Dilution
CD24 PE-Cy7 (clone: M1/69, Biolegend)	1:200
CD49f PE (clone: GoH3, Biolegend)	1:50
EpCam APC-Cy7 (clone: G8.8, Biolgend)	1:50
Fgfr2b (clone: 133730, R&D Systems) or corresponding isotype control IgG2A (clone: 54447, R&D Systems)	150 µg/ml
goat anti-rat IgG Alexa Fluor 647 (Invitrogen)	1:1000
Influenza A virus nucleoprotein FITC (clone: 431, Abcam)	1:20
Sca-1 PerCP/Cy5.5 (clone: D7, Biolegend)	1:50

- Proliferation measurements:

Antibody	Dilution
CD24 PE-Cy7 (clone: M1/69, Biolegend)	1:200
CD49f PE or Pacific Blue (clone: GoH3, Biolegend)	1:50
EpCam APC-Cy7 (clone: G8.8, Biolgend)	1:50
Ki67 FITC or PE (clone: B56, BD Bioscience) and corresponding isotype control IgG1 κ FITC, PE (clone: MOPC-21, BD Bioscience)	undiluted

- Apoptosis measurements:

Antibody	Dilution
Annexin V Alexa Fluor 647 (Invitrogen)	1:100
CD24 PE-Cy7 (clone: M1/69, Biolegend)	1:200
CD31 Alexa Fluor 488 (clone: MEC13.3, Biolgend)	1:50
CD45 FITC (clone: 30-F11, Biolegend)	1:50
CD49f PE (clone: GoH3, Biolegend)	1:50
EpCam APC-Cy7 (clone: G8.8, Biolgend)	1:50

- Measurement of mesenchymal cells:

Antibody	Dilution
α-SMA FITC (clone: 1A4, Sigma-Aldrich)	1:100
CD31 PE (clone: MEC13.3, Biolgend)	1:50
CD45 APC-Cy7 (clone: 30-F11, Biolegend)	1:50
CD90.2 APC (clone: 53-2.1, Biolegend)	1:100
CD140a APC (clone: APA5, Biolegend)	1:100
EpCam APC-Cy7 (clone: G8.8, Biolgend)	1:50
Sca-1 Pacific Blue (clone: D7, Biolegend)	1:50

- Sorting of type I and type II pneumocytes:

Antibody	Dilution
CD24 PE-Cy7 (clone: M1/69, Biolegend)	1:200
CD31 Alexa Fluor 488 (clone: MEC13.3, Biolegend)	1:50
CD45 FITC (clone: 30-F11, Biolegend)	1:50
CD49f PE (clone: GoH3, Biolegend)	1:50
EpCam APC-Cy7 (clone: G8.8, Biolgend)	1:50
Podoplanin APC (clone: 8.1.1, Biolegend)	1:20
Sca-1 Pacific Blue (clone: D7, Biolegend)	1:50

- Sorting of leukocytes, mesenchymal cells, endothelial cells, epithelial cells

Antibody	Dilution
CD31 PE (clone: MEC13.3, Biolegend)	1:100
CD45 FITC (clone: 30-F11, Biolegend)	1:50
EpCam APC-Cy7 (clone: G8.8, Biolgend)	1:50
Sca-1 Pacific Blue (clone: D7, Biolegend)	1:50

- Sorting of human epithelial cells:

Antibody	Dilution
CD24 PE-Cy7 (clone: ML5, Biolegend)	1.50
CD49f PE (clone: GoH3, Biolegend)	1:50
EpCam FITC (clone: HEA-125, Miltenyi Biotec)	1.50
lgr6 Alexa Fluor 647 (Bioss), lgr6 (clone: EPR6874, LifeSpan Bioscience)	1:20

- Sorting of epithelial stem/progenitor cells, small airway epithelial cells and mesenchymal cells

Antibody	Dilution
CD24 PE-Cy7 (clone: M1/69, Biolegend)	1:200
CD31 Alexa Fluor 488 (clone: MEC13.3, Biolegend)	1:50
CD45 FITC (clone: 30-F11, Biolegend)	1:50
CD49f PE (clone: GoH3, Biolegend)	1:50
CD104 Alexa Fluor 647 (clone: 346-11A, AbD SeroTec)	1:20
EpCam APC-Cy7 (clone: G8.8, Biolgend)	1:50
Sca-1 Pacific Blue (clone: D7, Biolegend)	1:50

2.11 Murine lung epithelial cell isolation

Mice were scarified by cervical dislocation, thorax was opened and the *vena cava* was disconnected. A small incision was made in the left ventricle, and a 21-gauge butterfly cannula (Ecoflo) was installed in the right heart chamber to perfuse the lung with 20 ml HBSS (Gibco) until the lung was free of blood. A small incision was made in the dissected trachea and a blunt end 21-gauge cannula (B. Braun) was

fixed with a 4-0 surgical thread (Ethicon). The lung was filled with 1.5 ml dispase (5,000 caseinolytic units/100 ml, BD Bioscience), removed, washed in HBSS (Gibco) and incubated in dispase (BD Bioscience) for 40 min at room temperature. The lung was transferred into a petridish (Corning) with DMEM/HEPES 0.01% DNase I (Serva) and the bronchial tree, heart and trachea were removed. Lungs were homogenized (gentleMACS, MACS Miltenyi Biotech) in 7 ml DMEM/HEPES 0.01% DNase I (Serva) and afterwards incubated for 5-10 min while rotating (Heidolph). The cell suspension was filtered through 100 µm and 40 µm (both BD Bioscience) filters, followed by centrifugation (800 rpm, 8 min, 4°C). The pellet was recovered in 5 ml mAEC medium and the cell number was determined with a Neubauer chamber and trypan blue staining (0.4%, Gibco). By addition of mAEC medium, the cell suspension was set to 10 million cells/ml. According to the cell number the following calculations were performed for magnetic negative selection:

Calculation of biotinylated antibody volumes:

biotinylated anti-CD45 antibody (BD Pharmingen):

number of million cells x 0.45 x 2

biotinylated anti-CD16/32 antibody (BD Pharmingen):

number of million cells x 0.45 x 1.5

biotinylated anti-CD31 antibody (BD Pharmingen):

number of million cells x 0.2 x 2

Calculation of magnetic bead volumes:

A: Number of million cells x 0.65

B: A/3 ml

C: B x 50 µl

The calculated antibody volumes were added to the cell suspension to bind to leukocytes (anti-CD45, anti-CD16/32) and endothelial cells (anti-CD31), followed by incubation for 30 min at 37°C. The cell suspension was washed twice with DMEM/HEPES. The cell pellet was resuspended in a determined volume (calculated in B) of DMEM/HEPES and added to the biotin-binding magnetic beads (Dynabeads, Invitrogen), calculated in C. Prior to cell depletion, magnetic beads were washed three times and resuspended in $PBS^{-/-}$. The cell suspension

containing the magnetic beads (Dynabeads, Invitrogen) was incubated for 30 min at room temperature until the tube was placed in the magnetic separator (Invitrogen) for 15 min. After separation the suspension was removed and centrifuged for 8 min, 800 rpm at 4°C. The pellet was recovered and purity was determined by flow cytometry. Cells were either cultured in mAEC medium or further processed for flow cytometric analysis or cell sorting.

2.12 Isolation of primary human epithelial cells and fibroblasts

Lung tissue was minced and extensively washed with hAEC medium, followed by dispase II digestion (2.5 mg/ml, Roche) in PII-solution for 180 min at 37°C. The cell suspension was filtered through 100 µm, 40 µm (BD Bioscience) and 20 µm (Millipore) pore size filters. Cells were centrifuged at 1,500 rpm for 20 min at room temperature and the pellet was resuspended in PII-solution with 0.25% DNase (Serva). Separation of erythrocytes and lung cells was achieved by ficoll density centrifugation (Ficoll Paque; Amersham Pharmacia Biotech). Therefore, 20 ml Ficoll was overlayed with 15 ml cell suspension and centrifuged at 2,500 rpm for 15 min at room temperature. The interphase was collected and centrifuged at 1,500 rpm for 15 min at room temperature. The pellet was resuspended in hAEC medium and cells were counted in a Neubauer chamber with trypan blue to exclude dead cells. Cells were centrifuged at 1,500 rpm for 10 min at room temperature and resuspended in MACS buffer (10 million cells/ 80 µl MACS buffer), followed by subsequent depletion of leukocytes by anti-CD45 magnetic beads (Miltenyi Biotech). 20 µl anti-CD45 beads were added to 10 million cells, respectively, and incubated for 15 min at 4°C until cells were washed with MACS buffer and added to a washed MACS column (Miltenyi Biotec) for magnetic separation. The flow through was collected, centrifuged at 1,500 rpm for 20 min and the pellet was recovered with hAEC medium. Cells were counted and purity was determined by flow cytometry. Viability was analyzed by trypan blue exclusion and was always >95%.

For the isolation of primary human lung fibroblasts, cells were collected after ficoll density centrifugation, counted and seeded in well plates with Basal medium 2 to promote fibroblasts growth. Cells were passaged at a confluency of ~ 80% up to 4-5 times until they were directly used for co-cultures or frozen in liquid nitrogen.

Therefore, the cells were treated with trypsin EDTA (Biochrom), washed with Basal medium 2 and transferred to cryotubes (Thermo Scientific) with Basal medium 2 and DMSO (Sigma-Aldrich) in a 1:1 ratio. Cells were frozen overnight at -80°C and stored in liquid nitrogen until they were thawn at 37°C and cultured in Basal medium 2.

2.13 Culture of murine or human epithelial cells in 3D matrix

FACS sorted cells were centrifuged at 1,200 rpm for 10 min. After pellet recovery, cells were counted with trypan blue to exclude dead cells. The respective cell number was resuspended in 50 µl EpiSPC basic or expansion medium and mixed with growth factor reduced matrix (BD Biosciences) in a 1:1 ratio. After the cell suspension was shortly mixed with a vortex, 90 µl of the cell/ matrix suspension were seeded in 12 mm cell culture inserts, with a pore size of 0.4 µm (Millipore), and placed in a 24-well plate (Greiner bio-one). The plate was incubated for 5 min at 37°C, 5% CO_2 to solidify the matrix, followed by addition of 350 µl EpiSPC basic or expansion medium into the lower well chamber. The medium was changed every second day. For mono-cultures 1000 epithelial cells (murine or human), were seeded into the matrix. For co-cultures of epithelial stem cells with mesenchymal cells, endothelial cells or leukocytes, the cells were seeded in a 1:100 ratio into the matrix. For cell reseeding (clonality assay) or RNA isolation, the inserts were washed two times with $PBS^{Mg+/Ca+}$ and a prewarmed enzyme mix composed of 3 mg/ml collagenase I and dispase (Boehringer, Gibco) in $PBS^{Mg+/Ca+}$ (Gibco) was added to the wells and inserts. After 15-20 min of incubation, the enzyme mix containing lung organoids was pipetted in a reaction mix tube and incubated at 37°C for 30 min, followed by extensive mixing with a 1 ml syringe. Cells were washed two times with respective medium, counted and reseeded as described above (93), or processed for RNA isolation. For *ex vivo* Fgf10 blockade, 5 µg/ml of Fgf10 neutralizing antibody (clone: C17, Santa Cruz) or corresponding isotype control (normal goat IgG, Santa Cruz) were added to the medium, after 2d of culture. Images were taken with a Leica DM IL LED microscope and corresponding camera MC170 HD.

2.14 Influenza virus infection of murine and human epithelial cells *in vitro*

FACS sorted human or murine epithelial cells were infected with A/PR8 (murine cells) or A/Hamburg/04/09 (human cells) with the indicated MOIs. Cells were washed, counted and inoculum was added and incubated for 1h at room temperature. Inoculum was removed and 10,000 cells were seeded in matrix with corresponding medium and were further incubated, as already described. In selected experiments, FACS sorted murine or human epithelial cells were infected in liquid culture. The cells were incubated in a 1.5 ml tube while rotating for 8h at 37°C, 5% CO_2 until they were processed for flow cytometry.

2.15 *In vivo* treatment protocols

2.15.1 Orotracheal or intraperitoneal applications

Mice were pretreated with a subcutaneous injection of 0.05 mg/kg Atropinsulphate (0.5 mg/ml, B. Braun), 1:10 diluted in sterile 0.9% NaCl (Delta Select GmbH) with a 27-gauge cannula. Mice were anesthetized by intraperitoneal injection of ketamin/rompun (ketaminhydrochloride 100 mg/kg, Pfizer; xylazinhydrochloride 16mg/kg, Bayer). Mice were transferred to a heating plate (37 °C) and their eyes were covered with salve (Bepanthene, Bayer). When mice showed no reflexes to pain, an injection port of a safety intravenous catheter (B. Braun) was orotracheally applied and mice were inoculated with 500 PFU (except where otherwise indicated) A/PR8 (H1N1), A/X-31 (H3N2), A/Hamburg/04/09 (pandemic H1N1) diluted in 70 µl sterile $PBS^{-/-}$ or $PBS^{-/-}$ alone as mock control. In selected experiments, 5 µg of recombinant murine Fgf10 (R&D Systems) dissolved in sterile $PBS^{-/-}$ or $PBS^{-/-}$ alone was orotracheally applied after influenza virus infection. Intraperitoneal injections (i.p.) of 100 µl naphthalene diluted in corn oil (both Sigma-Aldrich) or corn oil alone was administered. For organ isolation of non-treated animals, mice were sacrified by cervical dislocation, after a short anesthesia with 4% isoflurane (Baxter). Mice were visited daily and scored for morbidity according to the approved protocol. A morbidity score of more than 20 or additional criteria, like cyanosis of the mucosa, gasping, apathy, low body temperature and loss of more than 25% body weight within two days leaded to the termination of an experiment.

2.15.2 Sample collection

After the given time points mice were exsanguinated in anesthesia. In selected experiments, lung permeability was determined by intravenous (i.v.) injection of 1 mg FITC-labeled albumin (Sigma-Aldrich) diluted in sterile 0.9% NaCl (B. Braun). After the incubation time, mice were anesthetized as previously described. The blood was collected from the *vena cava* with a 1 ml syringe (Dispomed). The trachea was dissected and a blunt 21-gauge cannula was fixed with a 4-0 surgical thread (Ethicon) and BALF was collected by intratracheal addition and retraction of PBS/EDTA. The BALF was centrifuged at 1,200 rpm for 10 min at 4°C and the supernatant was aliquoted. After the blood had clotted completely, it was centrifuged at 3,500 rpm for 15 min. The serum was collected, followed by 8 min of centrifugation until erythrocyte-free serum was left. The serum and BALF were aliquoted in 0.5 ml tubes and stored at -80°C. Lung permeability was determined by quantification of FITC fluorescence in BALF and serum with a fluorescence reader (FLX800, Bio-Tek instruments). A standard curve of FITC albumin was prepared by serial dilution of 1 µg to 0.1 pg.

Lung homogenates were obtained by instillation of 1.5 ml dispase (5,000 caseinolytic U/100 ml, BD Biosciences) through the trachea into the HBSS (Gibco) perfused lung, followed by incubation in dispase for 40 min. After removal of the heart, trachea and bronchial tree, the lung was homogenized (gentleMACS, MACS Miltenyi Biotech) in DMEM and 2.5% HEPES with 0.01% DNase (Serva) and filtered through 100 µm and 40 µm nylon filters. The single cell suspension was further processed for flow cytometric analysis and cell sorting or magnetic-assisted epithelial cell isolation.

2.16 Statistics

All data are given as mean ± SD. Statistical significance between 2 groups was estimated using the unpaired Student's *t* test or ANOVA and post-hoc Tukey for comparison of 3 groups calculated with GraphPad Prism. A *p* value less than 0.05 was considered significant.

3. Results

3.1 Characterization of distal airway epithelial stem/progenitor cells in the adult murine lung

3.1.1 Gating strategy of adult murine epithelial cell populations

For the enrichment of distal airway epithelial stem/progenitor cells (EpiSPC) in lung epithelial cell populations, flow cytometric analysis was performed with established surface markers (92). In a first enrichment step, biotin-labeled endothelial cells and leukocytes were depleted by biotin-binding magnetic beads. The majority of the remaining lung cells expressed the cell surface marker epithelial cell adhesion molecule (EpCam; CD326) and integrin α6 (CD49f). According to the expression levels of these two surface markers, the epithelial cell population was fractionated in $EpCam^{low}α6^{low}$ and $EpCam^{high}α6^{high}$ (Figure 3). In combination with the surface marker CD24, further division of the $EpCam^{high}α6^{high}$ cell population was achieved in CD24 low and high expressing cells. Therefore, the murine epithelial cells were fractionated into three major subpopulations. The high frequent $EpCam^{low}α6^{low}$ population included 91.3 ± 1.8% of the $EpCam^{+}$ population, whereas the $EpCam^{high}α6^{high}CD24^{low}$ made up 1.7 ± 0.3% and the $EpCam^{high}α6^{high}CD24^{high}$ comprised 6.3 ± 1.8 % of the $EpCam^{+}$ population.

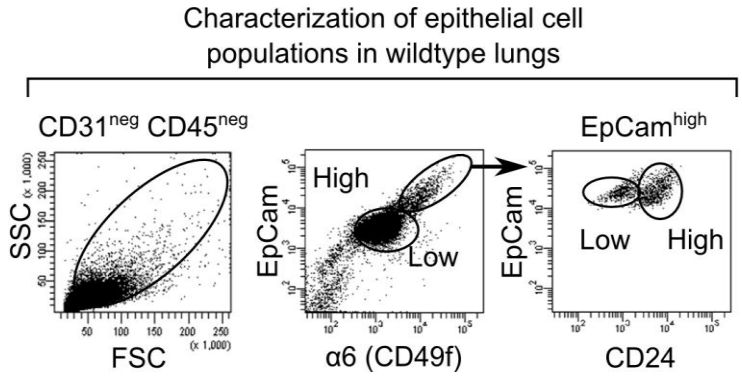

Figure 3: Flow cytometric characterization and gating strategy of primary murine distal airway epithelial cells.
CD45 and CD31 depleted lung homogenate of WT mice was analyzed with flow cytometry according to surface marker expression of EpCam, integrin α6 (CD49f) and CD24. Adult murine epithelial cells were fractionated into $EpCam^{low}α6^{low}$, $EpCam^{high}α6^{high}CD24^{low}$ and $EpCam^{high}α6^{high}CD24^{low}$ subpopulations. FSC; forward scatter; SSC, side scatter.

3.1.2 Characterization of epithelial stem/progenitor cells according to their proliferative response in vivo

Progenitor cells are characterized by their ablity to self-renew after injury and thereby contribute to repair processes (62, 144). Therefore, the proliferative response was analyzed in different injury models *in vivo* by quantitative flow cytometry. In addition to the gating strategy to differentiate lung epithelial cells (Figure 3), a nuclear marker for proliferation (Ki67) was included (145). Measurement of the proliferative response after bronchiolar injury induced by naphthalene revealed high renewal capacity in the EpCam^{high}α6^{high}CD24^{low} population, as compared to EpCam^{low}α6^{low} or EpCam^{high}α6^{high}CD24^{high} populations at d3 after treatment. At d10 after i.p. treatment, the proliferative response returned to baseline levels (Figure 4).

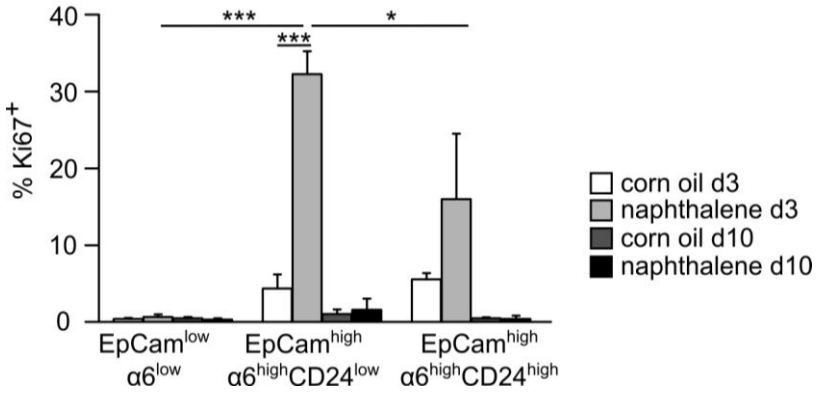

Figure 4: Proliferative response of epithelial cell subsets after naphthalene injury.
WT mice were treated with naphthalene or corn oil as a control. CD31$^+$ and CD45$^+$ cell subsets were depleted and the proliferative response of the different epithelial cell subsets was measured by quantitative flow cytometry and staining for Ki67 at d3 and d10 after i.p. treatment. Bar graphs represent mean ± SD of n=4 independent experiments; *p<0.05; **p<0.01; ***p<0.001; d, day.

Further investigation of the proliferative response after severe influenza virus-induced bronchoalveolar injury was performed (146). As shown in figure 5A, the highest proliferative response was observed in the EpCam^{high}α6^{high}CD24^{low} fraction. Analysis of different time points after infection revealed strong proliferation at d7 and d14 post infection, whereat baseline levels were reached at d21 post infection. A representative FACS plot of Ki67$^+$ EpCam^{high}α6^{high}CD24^{low} cell subset after influenza virus infection is shown in figure 5B. Analysis of apoptosis rates by Annexin V staining of EpCam$^+$ cells revealed injury resistance of the EpCam^{high}α6^{high}CD24^{low} population in A/PR8 infected WT mice at d7 post

infection (Figure 5C) which is a characteristic feature of lung progenitor/stem cells (144). Due to the ability of the EpCam^{high}α6^{high}CD24^{low} cell fraction to strongly proliferate after injury, the epithelial cell subset is defined as epithelial stem/progenitor cell (EpiSPC), as previously suggested (92, 93).

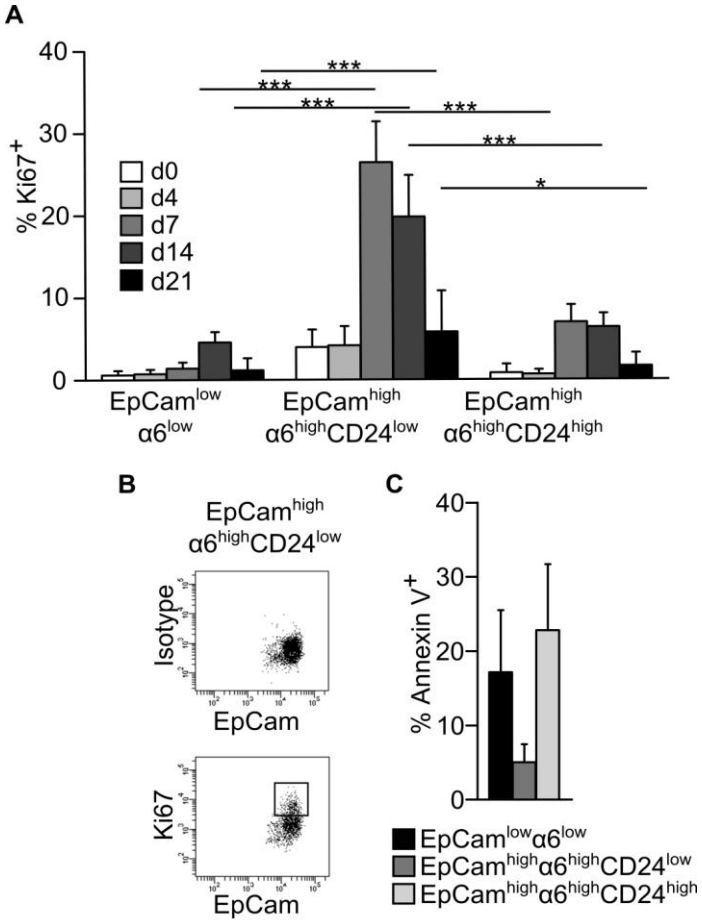

Figure 5: Proliferative response and apoptosis rates of epithelial cell subsets after influenza virus infection.
(A) WT mice were infected with 500 PFU A/PR8 and the proliferative response of epithelial cell fractions was measured at day 0, 4, 7, 14 and 21 post infection. CD31 and CD45 positive cells were depleted and Ki67 positive cells were analyzed by flow cytometry. (B) Representative FASC plots of Ki67 and isotype stained EpCam^{high}α6^{high}CD24^{low} at d7 post infection. (C) Apoptosis rates were measured by flow cytometric analysis of Annexin V^{+} cells in *in vivo* infected WT mice at d7. At least three animals/group were analyzed. EpCam^{low}α6^{low} and EpCam^{high}α6^{high}CD24^{high} were compared to EpCam^{high}α6^{high}CD24^{low} (EpiSPC); *p<0.05; **p<0.01; ***p<0.001; d, day.

3.1.3 Characterization of epithelial stem/progenitor cells according to endogenous marker expression

Further characterization of the EpiSPC population was performed by flow cytometry and immunofluorescence stainings according to markers which are associated with known epithelial stem/progenitor cells (80, 85, 90, 92, 95, 102).

Flow cytometric analysis of CD104 (integrin β4) and Sca-1 (stem cell antigen-1) revealed an ubiquitous expression in the EpiSPC population (Figure 6A). Cytospins of FACS sorted EpiSPC showed a morphologically homogenous population with a relatively large nucleus and a dense cytoplasm after Pappenheim staining. Immunofluoresence staining of FACS sorted EpiSPC revealed co-expression of proSP-C and CC10 in an EpiSPC subpopulation (Figure 6B) as described for the BASC stem cell phenotype (90).

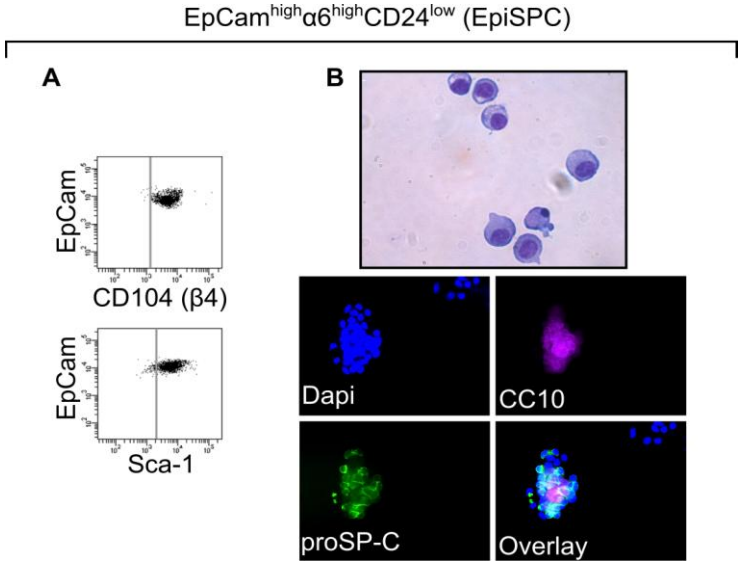

Figure 6: Characterization of EpiSPC according to endogenous marker expression.
(A) EpCam^{high}α6^{high}CD24^{low} cells were analyzed for expression of CD104 (integrin β4) and Sca-1 by flow cytometry. (B) Either Pappenheim or immunofluorescence stainings were performed with FACS sorted EpCam^{high}α6^{high}CD24^{low} cells with the indicated antibodies; EpiSPC, epithelial stem/progenitor cells.

Further investigation of Krt5 and p63 expression in WT non-infected and influenza virus infected mice was performed by immunofluorescence stainings and qRT-PCR. These markers were shown to be expressed by a so-called DASC (distal airway stem cell) population, which strongly contribute to repair processes and give rise to alveolar and bronchiolar lung tissue (98, 99). Another report described the contribution of lineage-negative epithelial progenitor cells (LNEP) to the p63/Krt5 repair program (99). Additionally, these markers are present in basal cells in the tracheal tissue (71). To investigate the Krt5 and p63 expression in EpiSPC of non-infected WT mice, lung and trachea digestions were prepared, followed by the preparation of cytospins of FACS sorted EpiSPC and tracheal cells, which served as a positive control. Immunofluorescence stainings showed high

expression of Krt5 and p63 in the tracheal cell compartment as compared to stained FACS sorted EpiSPC of non-infected WT animals (Figure 7A). To investigate the Krt5 and p63 expression after influenza virus infection, WT mice were infected with A/PR8 and EpiSPC were FACS sorted at d14 post infection. mRNA expression levels of Krt5 and p63 were compared to sorted EpiSPC of non-infected WT mice. Krt5 and p63 were highly upregulated in EpiSPC after influenza virus-induced injury, indicating a strong endogenous regenerative capacity and contribution to the Krt5 repair program.

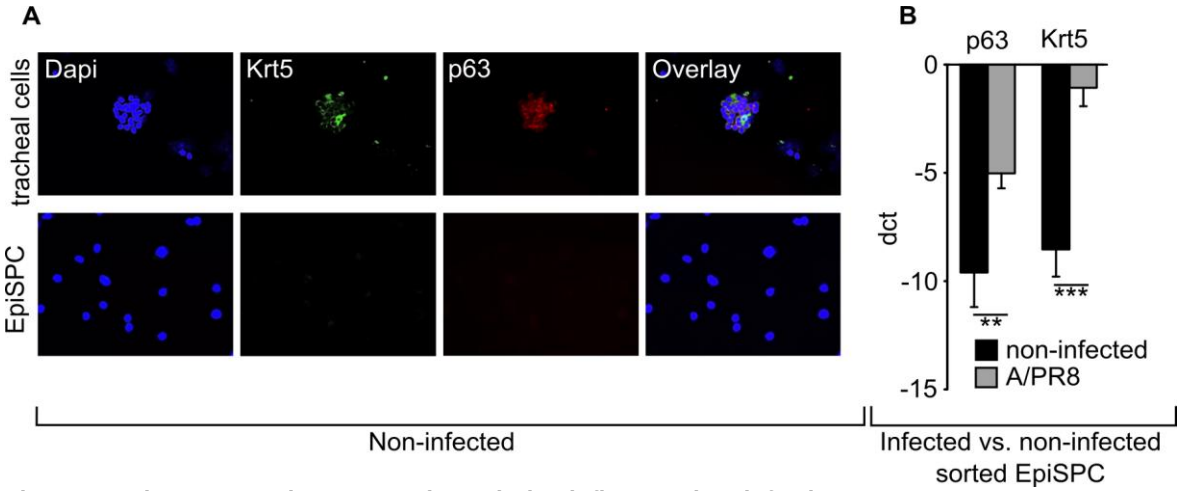

Figure 7: EpiSPC upregulate Krt5 and p63 during influenza virus infection.
(A) Cytospins of tracheal digests and FACS sorted EpiSPC of non-infected WT mice were stained with p63 and Krt5. (B) EpiSPC of A/PR8 infected WT mice were sorted at d14 post infection and compared to non-infected sorted EpiSPC of WT animals. Krt5 and p63 expression levels were analyzed by qRT-PCR. Bar graphs show mean ± SD of n=4 independent experiments; **p<0.01; ***p<0.001.

3.1.4 Characterization of the EpCam^{low}α6^{low} and EpCam^{high}α6^{high}CD24^{high} populations

Further characterization of the two remaining epithelial cell subsets was performed by cytospins of FACS sorted EpCam^{low}α6^{low} and EpCam^{high}α6^{high}CD24^{high} cell subsets and Pappenheim stainings. A characteristic feature of the EpCam^{low}α6^{low} population were large granular inclusions in the cytoplasm, which was likely to be surfactant protein stored in lamellar bodies (147, 148). Flow cytometric analysis of the EpCam^{low}α6^{low} subset identified that the majority of these cells expressed proSP-C, a marker for type II pneumocytes (58). A minor fraction of EpCam^{low}α6^{low} population expressed podoplanin (Figure 8A), indicating the presence of type I pneumocytes (149).

To characterize the EpCam^{high}α6^{high}CD24^{high} population, cells were FACS sorted and cytospins were made, followed by Pappenheim staining, which revealed

ciliated and non-ciliated cells (Figure 8B). Additionally, cells were cultured for 4d and stained for mucin5ac and β-tubulin, which revealed the presence of ciliated (β-tubulin^{+}) and goblet cells (mucin5ac^{+}) (54, 150). Flow cytometric analysis showed that there is also a minor population of CC10^{+} cells, but no proSP-C^{+} cells. Together, these data revealed that EpCam^{low}α6^{low} cells represented mainly alveolar epithelial cells (AEC) (type II and type I pneumocytes), whereas EpCam^{high}α6^{high}CD24^{high} cells were mainly composed of ciliated, goblet and club cells and were therefore termed small airway epithelial cells (SAEC).

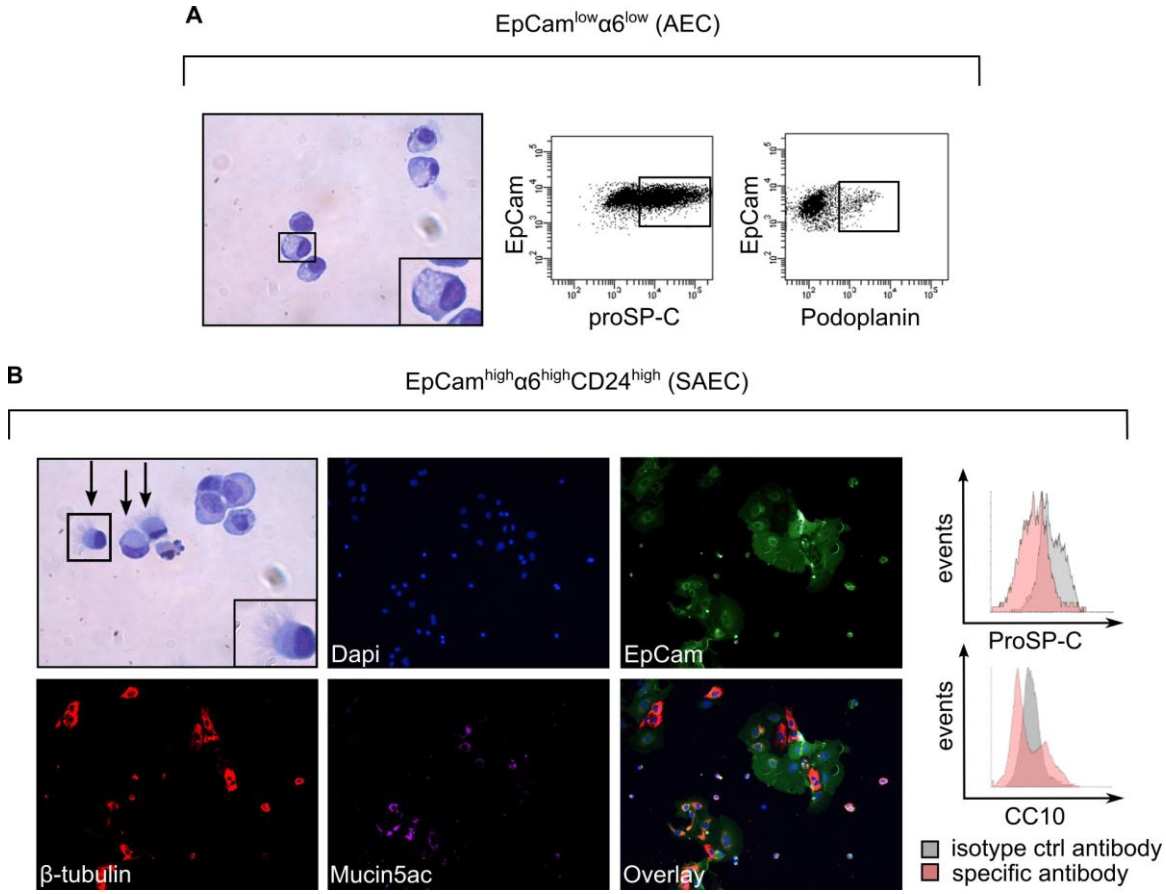

Figure 8: The EpCam^{low}α6^{low} and EpCam^{high}α6^{high}CD24^{high} cell fractions included terminally differentiated lung epithelial cells.
(A) Characterization of the EpCam^{low}α6^{low} (AEC) cell subset with FACS sorted and Pappenheim stained cytospins or by flow cytometry with the indicated antibodies. (B) FACS sorted and Pappenheim stained cytospins of the EpCam^{high}α6^{high}CD24^{high} cells subset revealed cilliated (arrow) and non-ciliated cell fractions. Immunofluorescence stainings of FACS sorted EpCam^{high}α6^{high}CD24^{high} epithelial cells cultured for 4d and stained with mucin5ac and β-tubulin. Flow cytometric analysis of EpCam^{high}α6^{high}CD24^{high} epithelial cells with CC10 and proSP-C was performed.

3.2 EpiSPC show organoid outgrowth, clonal expansion and terminal differentiation in 3D cultures

To identify the proliferative capacity and clonality of EpiSPC *in vitro*, the different

epithelial cell fractions were FACS sorted according to the gating strategy in figure 3, seeded in matrix and stimulated with hepatocyte growth factor (HGF) and fibroblast growth factor 10 (Fgf10) (Figure 9A). After 5, 8 and 14 days in culture, images were taken. EpiSPC responded to growth factors (GF) by proliferation and expansion which resulted in organoid outgrowth, as compared to AEC and SAEC. The clonality of EpiSPC was tested by serial passaging, therefore the matrix was digested and a single cell suspension of EpiSPC were reseeded with very low cell densities (~ 1000 cells/well), which again resulted in growth of organoids. The culture was repeatedly passaged for up to six times (Figure 9B). To further confirm the clonality of EpiSPC, a single cell sort was performed, which similarly resulted in organoid outgrowth (Figure 9C) and confirmed the robust clonogenic potential of EpiSPC.

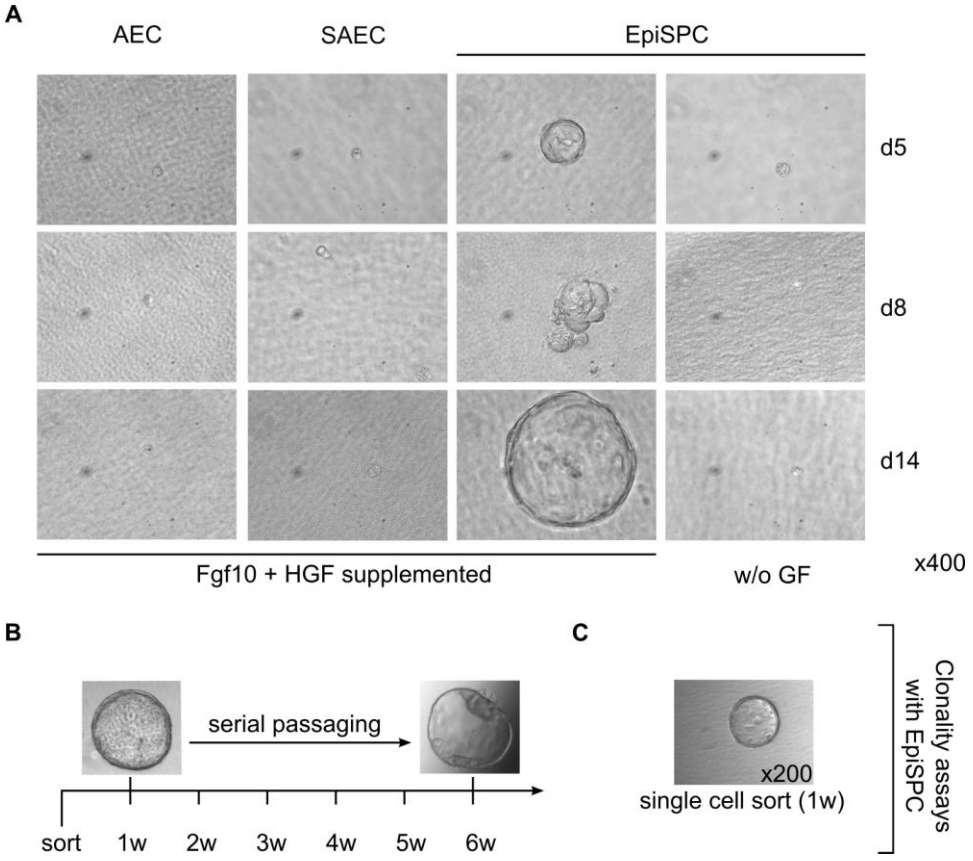

Figure 9: EpiSPC show high proliferative capacity and clonal expansion in the presence of growth factors.
(A) AEC, SAEC and EpiSPC were FACS sorted and seeded in matrix. Medium was either supplemented with 30 ng/ml hepatocyte growth factor (HGF) and 50 ng/ml fibroblast growth factor 10 (Fgf10) or left unsupplemented (w/o GF). Images were taken at d5, d8 and d14 after seeding. (B) Schematic illustration of serial passaging of the EpiSPC population in 3D culture. FACS sorted EpiSPC were seeded in matrix and supplemeted with HGF and Fgf10. After one week of culture, the matrix was digested and 1,000 cells were reseeded, which was performed for up to 6 weeks. (C) Single cell sort of EpiSPC was performed in matrix with supplemented medium. d, days; Fgf10, fibroblast growth factor 10; HGF, hepatocyte growth factor; w, weeks; w/o GF, without growth factors.

To determine the differentiation status of the EpiSPC *in vitro*, the matrix was digested after 10d of culture. RNA was extracted of cultured (d10) as well as freshly FACS sorted EpiSPC (d0), and analyzed for markers of differentiated cell types. Aquaporin 5 was significantly upregulated after 10d in culture, as compared to freshly sorted EpiSPC and in relation to flow sorted type I pneumocytes, defined by $CD31^{neg}CD45^{neg}EpCam^{low}\alpha6^{low}podoplanin^{+}$. Moreover, also β-tubulin was upregulated after EpiSPC culture in relation to expression in SAEC indicating upregulation of bronchiolar, as well as alveolar markers and the multilineage potential of EpiSPC (Figure 10A, B).

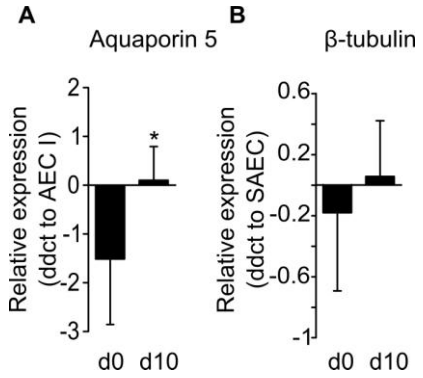

Figure 10: EpiSPC upregulate markers of terminal differentiated airway and alveolar epithelial cells in 3D culture.
RNA was extracted of FACS sorted EpiSPC (d0) and EpiSPC which were cultured in matrix for 10 days (d10) with growth factors. (A) Aquaporin 5 expression of EpiSPC was compared to freshly sorted type I pneumocytes. (B) β-tubulin expression of FACS sorted (d0) or cultured EpiSPC (d10) was compared to SAEC. Bar graphs represent mean ± SD of n=3 independent experiments; *p<0.05; ***p<0.001; d, days; ddCt, delta delta Ct; AEC I , Type I pneumocyte; SAEC, small airway epithelial cell.

3.3 Gating strategy and 3D culture of putative human lung epithelial progenitor cells

To identify a population of human lung epithelial progenitor cells (huEpiSPC) in distal airway tissue, healthy lung tissue was collected from lobectomy material. $CD45^{+}$ cells of human lung digests were depleted and remaining cells were FACS sorted according to the surface marker expression, which was already established for the murine system (Figure 11). The $EpCam^{+}$ epithelial cells were distinguished into $EpCam^{low}\alpha6^{low}$ and $EpCam^{high}\alpha6^{high}$ expressing cells, whereas the $EpCam^{high}\alpha6^{high}$ population was further divided into a $CD24^{low\text{-}neg}$ and $CD24^{+}$ fraction. Additionally, 95% of the $EpCam^{high}\alpha6^{high}CD24^{low\text{-}neg}$ fraction expressed lgr6 (leucine rich G protein coupled receptor), which is known to be expressed by epithelial progenitor cells in human lungs (66). FACS sorted

EpCam^{high}α6^{high}CD24$^{low-neg}$ (huEpiSPC) showed organoid outgrowth in 3D cultures and were dependent on the growth factors HGF and Fgf10 (Figure 11C).

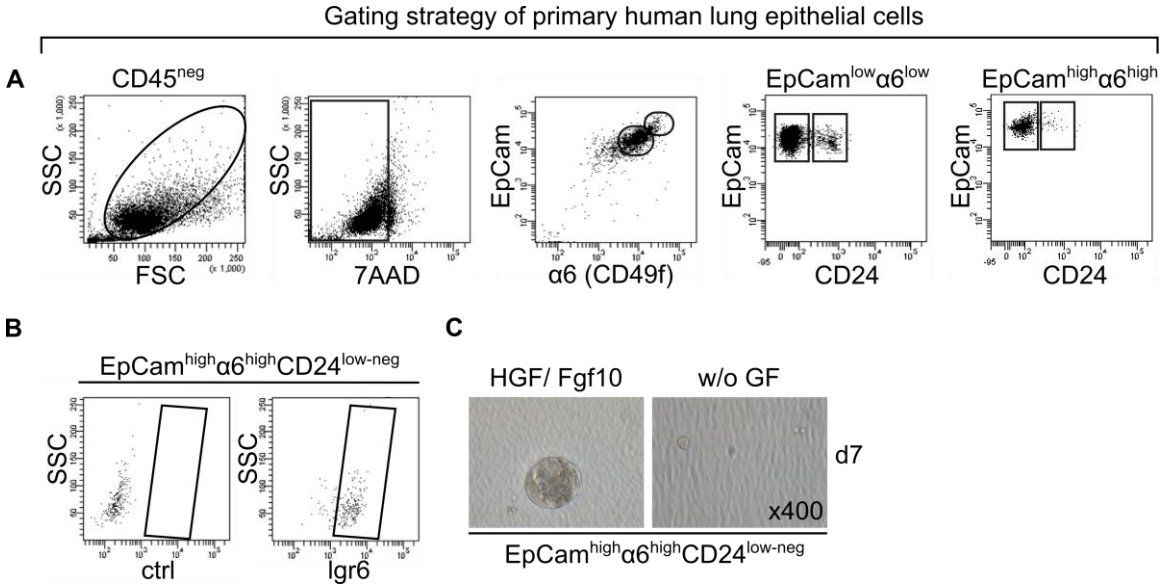

Figure 11: Gating strategy of putative primary human epithelial progenitor cells and 3D culture.
(A) Gating strategy of primary human epithelial progenitor cells, according to surface marker expression of EpCam, integrin α6 and CD24. (B) Flow cytometric analysis of the EpCam^{high}α6^{high}CD24$^{low-neg}$ cells with lgr6. (C) 3D culture of FACS sorted EpCam^{high}α6^{high}CD24$^{low-neg}$ primary human epithelial progenitor cells with and without addition of the growth factors HGF and Fgf10; ctrl, control; Fgf10, Fibroblast growth factor 10; HGF, Hepatocyte growth factor; w/o GF, without growth factors; FSC, forward scatter; SSC, side scatter.

3.4 EpiSPC renewal capacity is dependent on the Fgf10/Fgfr2b axis after influenza virus infection

To investigate the role of the Fgf10/Fgfr2b signaling pathway in the EpiSPC-mediated proliferative response, different inducible transgenic or gene-deficient mice were infected with A/PR8 and the renewal capacity was measured by flow cytometry and Ki67 expression. *Rosa26$^{rtTA/+}$;tet(O)sFgfr2b/+* mice overexpressed a dominant negative, soluble receptor (sFgfr2b) after treatment with doxycyline-containing food, which resulted in blockade of the Fgfr2b axis and decreased proliferative response of EpiSPC at d7 post infection (Figure 12A). Concomitantly, treatment of *Rosa26$^{rtTA/+}$;tet(O)Fgf10/+* animals with doxycycline-containing food, resulted in Fgf10 overexpression and led to an increased proliferative capacity of EpiSPC compared to mice which were fed with normal food (Figure 12B). Of note, Fgfr2b is able to bind Fgf10 as well as Fgf7 (112), therefore analysis of the proliferative response was performed using *Fgf7* knockout mice compared to WT littermates. However, *Fgf7* knockout mice showed only a slight, non-significant

decrease in EpiSPC proliferation (Figure 12C) which indicated that EpiSPC proliferation and renewal capacity was dependent on Fgf10 but not on Fgf7 *in vivo*.

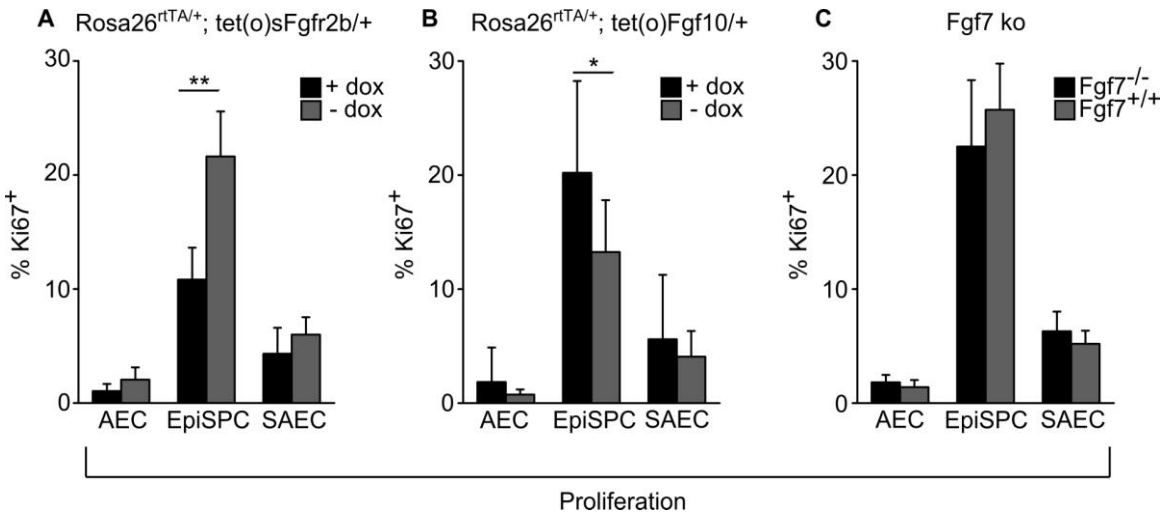

Figure 12: The proliferative capacity of EpiSPC is dependent on Fgf10 and the receptor Fgfr2b but not on Fgf7.
(A) *Rosa26$^{rtTA/+}$;tet(O)sFgfr2b/+* (induction of soluble, dominant negative Fgfr2b) or (B) *Rosa26$^{rtTA/+}$;tet(O)Fgf10/+* mice (induction of Fgf10) were infected with 500 PFU A/PR8 and the proliferative response of EpiSPC, AEC and SAEC was measured with flow cytometry and Ki67 staining at d7 post infection in doxycycline treated mice (+dox) and in non-induced (-dox) animals. (C) The proliferative capacity of A/PR8 infected *Fgf7* knockout animals or WT littermates was measured with flow cytometry at d7 post infection. Bar graphs represent mean ± SD of at least n=4 animals/group; *p<0.05; **p<0.01; dox, doxycycline.

3.5 Fgfr2b is upregulated on EpiSPC during influenza virus infection

To address whether lung injury resulted in regulation of the Fgf10/Fgfr2b axis on receptor level, WT mice were infected with 500 PFU A/PR8 and Fgfr2b expression was analyzed on the EpiSPC population by flow cytometry at different time points post infection. The Fgfr2b surface expression was highly upregulated on EpiSPC at d5 and d7 post infection and reached baseline levels at d14 post infection (Figure13A). To evaluate if this effect was influenza virus-specific, quantification of Fgfr2b surface expression on EpiSPC after naphthalene treatment was performed (Figure 13B). At d3 after treatment a robust proliferative response was observed in the EpiSPC subset (Figure 4) and additionally, Fgfr2b expression was upregulated as compared to the control. However, the Fgfr2b upregulation was most prominent after influenza virus-induced injury, suggesting a particular involvement of Fgfr2b in repair after influenza-induced injury.

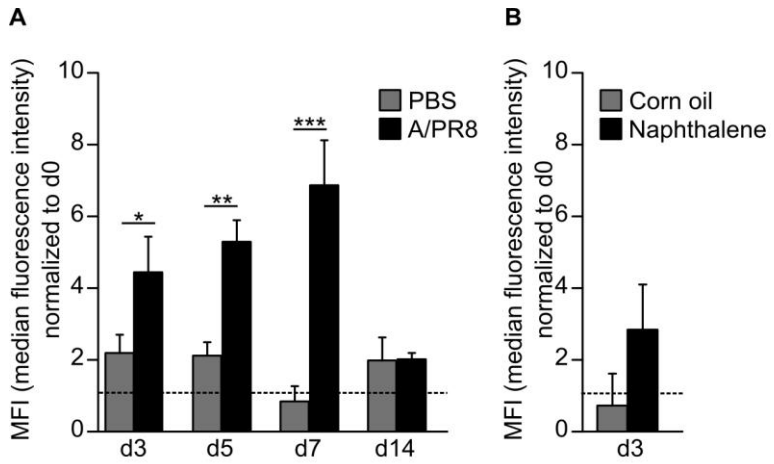

Figure 13: Fgfr2b is highly upregulated during influenza virus-induced injury.
(A) WT mice were infected with 500 PFU A/PR8 or treated with sterile PBS as a control and Fgfr2b expression was analyzed by flow cytometry at d3, d5, d7 and d14 post infection on the EpiSPC subset. (B) WT mice were treated with either naphthalene or corn oil as a control. Fgfr2b expression was measured by flow cytometry at d3 after treatment. Values are given in MFI (median fluorescence intensity) normalized to non-treated WT mice indicated as dotted lines. Bar graphs represent mean ± SD of at least n=3 independent experiments. *p<0.05; **p<0.01; ***p<0.001.

3.6 EpiSPC outgrowth and differentiation is mediated by cross-talk with lung resident mesenchymal cells

3.6.1 Characterization of lung resident mesenchymal cells

To further elucidate the Fgf10/Fgfr2b cross-talk mechanisms, the predominant source of the Fgfr2b ligands in adult murine lungs was determined. To achieve this, fractionation of whole lung homogenate into the four main cell subsets was performed by sorting of epithelial cells ($CD31^{neg}CD45^{neg}EpCam^{+}$), endothelial cells ($CD31^{+}CD45^{neg}EpCam^{neg}$), leukocytes ($CD31^{neg}CD45^{+}EpCam^{neg}$) and $CD31^{neg}CD45^{neg}EpCam^{neg}Sca\text{-}1^{+}$ cells (151) (Figure 14A). mRNA expression analysis revealed that the Fgfr2b ligands Fgf7 and Fgf10 were predominantely expressed by cells gated in R4 of non-infected and A/PR8 infected WT mice (Figure 14B and C). Of note, neither Fgf7, nor Fgf10 mRNA were significantly increased after influenza virus infection. Previous data suggested that the $CD31^{neg}CD45^{neg}EpCam^{neg}Sca\text{-}1^{+}$ population was associated with the fibroblast lineage (151). Further characterization of the R4 population revealed that ~ 5% expressed α-SMA representing myofibroblasts/smooth muscle cells, ~ 20% expressed CD90, a marker which indicate progenitor cells of the mesenchymal lineage, and ~ 12% were $LipidTox^{+}$ $PDGFR\alpha^{+}$ indicative of a lipofibroblast phenotype (102, 129, 152, 153). Pappenheim stained cytospins of the flow sorted R4 population showed a morphologically homogenous population with large

cytoplasm. Cultured cells revealed an upregulation of α-SMA (smooth muscle actin) expression after 6d, suggesting that the $CD31^{neg}CD45^{neg}EpCam^{neg}Sca\text{-}1^{+}$ population was composed of lung resident mesenchymal cells (rMC) with a fibroblast phenotype (Figure 14A).

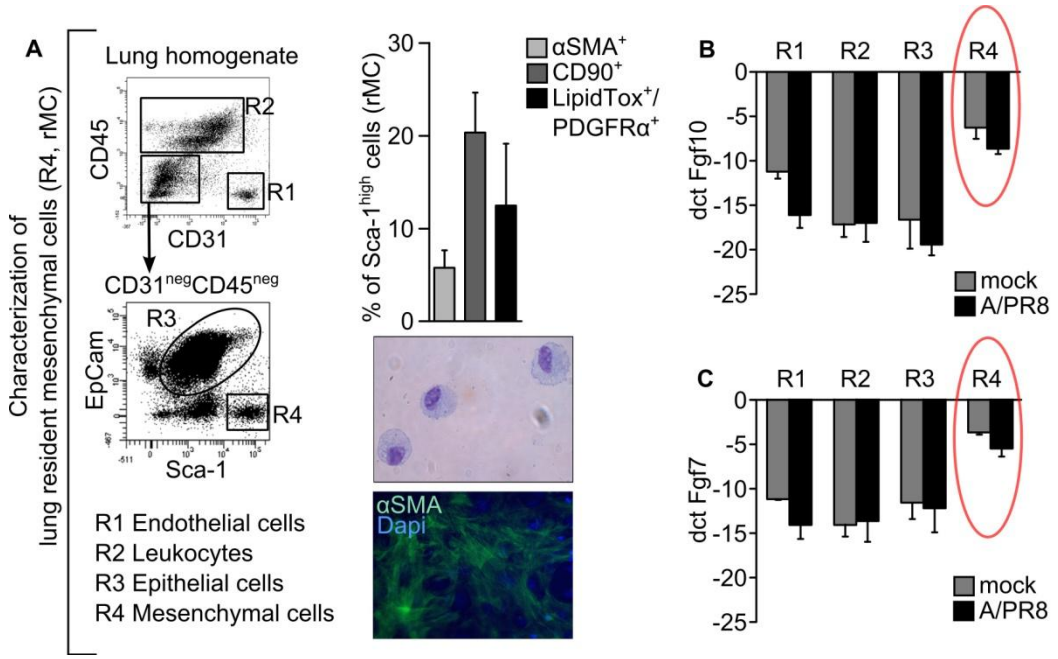

Figure 14: Characterization of lung resident mesenchymal cells and analysis of Fgfr2b ligand expression.
(A) Representative flow cytometry plots (left) of the gating strategy to fractionate total lung homogenate of WT mice into endothelium (R1), leukocytes (R2), epithelium (R3) and $Sca\text{-}1^{high}$ lung rMC (R4). Characterization of the $Sca\text{-}1^{high}$ population according to mesenchymal cell markers was performed by flow cytometry (right panel). The FACS sorted $Sca\text{-}1^{high}$ population was either Pappenheim stained or α-SMA expression was analysed after 6d of culture. (B) mRNA expression of Fgf10 (C) or Fgf7 in FACS sorted lung cell populations was determined by qRT-PCR analysis. Bar graphs represent mean ± SD of at least n=3 independent experiments.

3.6.2 Lung resident mesenchymal cells mediate EpiSPC expansion

To investigate if Fgfr2b ligand-expressing rMC support organoid growth and/or differentiation of EpiSPC, FACS sorted rMC and EpiSPC were co-cultured in 3D matrix without growth factor supplementation (93). The presence of Fgf10-expressing rMC was sufficient to promote the proliferative response of EpiSPC and the formation of organoids at d5 (Figure 15). Additionally, rMC supported saccular outgrowth of EpiSPC at d10 and the formation of lung-like structures at d16, as compared to growth factor supplemented EpiSPC mono-cultures (Figure 9), or co-cultures with $CD31^{+}$ or $CD45^{+}$ cells (R1 and R2, figure 14), respectively. The role of the Fgf10-mediated cross-talk between EpiSPC and rMC was

addressed by the addition of an Fgf10 blocking antibody in the co-culture system. Treatment with the blocking antibody resulted in decreased proliferative response, at an early stage, which was indicated by reduced organoid outgrowth and showed the important role of Fgf10 in EpiSPC proliferation and outgrowth in the cross-talk with rMC.

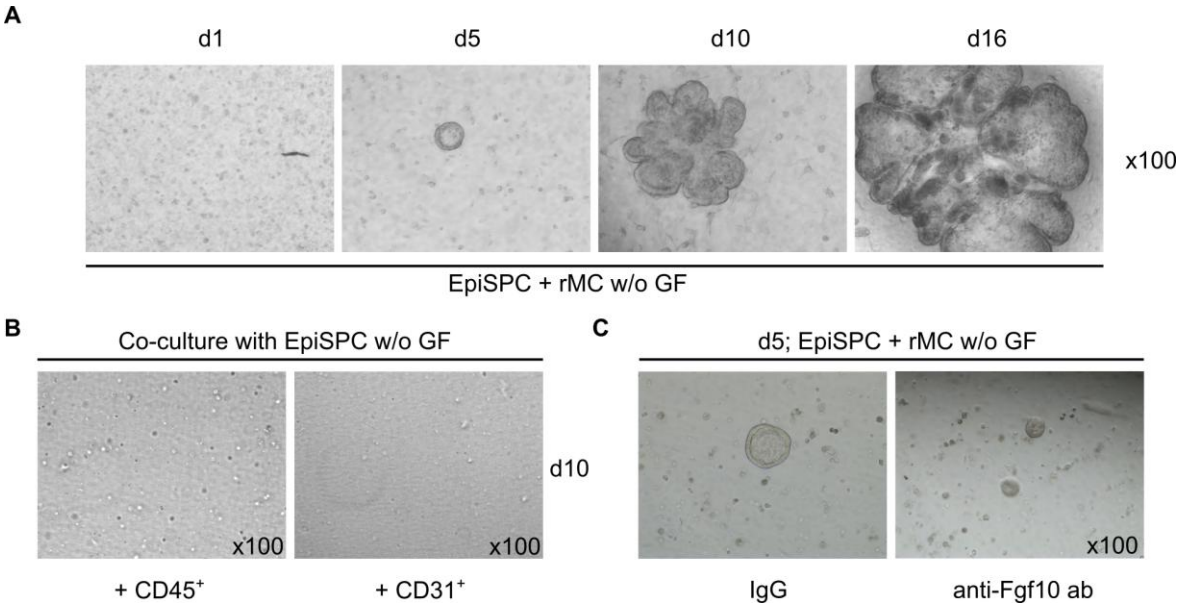

Figure 15: Lung resident mesenchymal cells promote EpiSPC organoid outgrowth which is mediated by Fgf10.
(A) FACS sorted EpiSPC and rMC were co-cultured in 3D matrix without addition of growth factors. (B) $CD45^+$ leukocytes and $CD31^+$ endothelial cells were co-cultured with EpiSPC without growth factor supplementation. (C) Co-culture of EpiSPC and rMC with a Fgf10 neutralizing antibody, compared to IgG control of n=3 independent experiments. ab, antibody; GF, growth factors; IgG, Immunoglobulin; rMC, resident mesenchymal cells; w/o, without.

To evaluate whether Fgf10-expressing rMC have an influence on the EpiSPC differentation capacity, RNA was extracted after 10d and 28d of EpiSPC mono-cultures or EpiSPC-rMC co-cultures and expression levels of markers for differentiated airway and alveolar epithelium were analyzed and compared to freshly FACS sorted EpiSPC (Figure 16). Podoplanin, a marker for type I pneumocytes (149) was highly upregulated in the co-culture model as compared to EpiSPC mono-cultures after 10d of culture, suggesting that the rMC promoted differentiation into alveolar epithelium. After 28d of EpiSPC mono-culture, podoplanin was also highly upregulated, which suggested, that EpiSPC in mono-culture differentiated much slower, than in the co-culture system. Similar to

podoplanin, β-tubulin was highly upregulated in the co-culture, as compared to mono-cultures, indicating that rMC may promote the differentiation of EpiSPC into ciliated airway epithelium (154). In contrast, cyclin D1, a marker for proliferation (155) showed less expression in co-cultures, which suggested that rMC rather promote differentiation compared to proliferation of EpiSPC at later stages of culture.

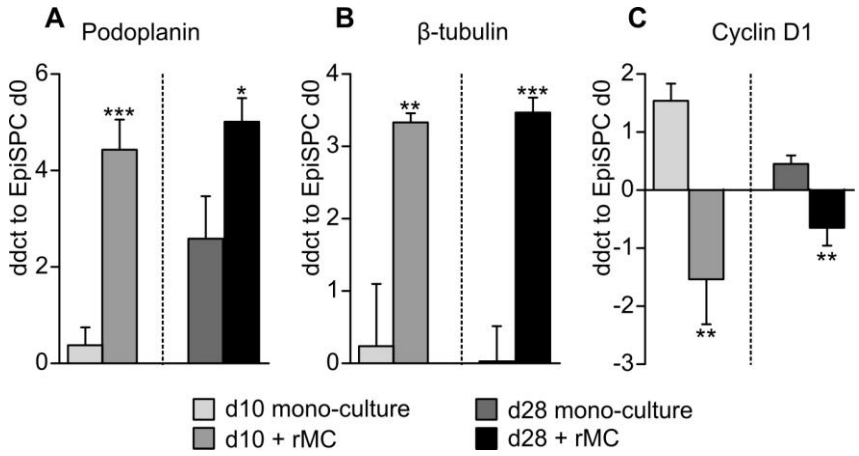

Figure 16: EpiSPC differentiation is accelerated in co-cultures with rMC.
FACS sorted EpiSPC were either mono- or co-cultured with rMC. Mono-cultured EpiSPC were supplied with HGF and Fgf10, whereas co-cultured EpiSPC were left unsupplemented. After 10d and 28d of culture, RNA was isolated and expression of (A) podoplanin, (B) β-tubulin and (C) cyclin D1 was analysed by qRT-PCR. Bar graphs show ddct values compared to freshly FACS sorted EpiSPC. Bar graphs represent mean ± SD of n=3 independent experiments; *p<0.05; **p<0.01; ***p<0.001; rMC, lung resident mesenchymal cells.

3.6.3 Human lung fibroblast cross-talk with huEpiSPC to promote organoid formation

To investigate if primary human fibroblasts similary cross-talk with huEpiSPC, FACS sorted huEpiSPC ($EpCam^{high}\alpha6^{high}CD24^{low\text{-}neg}$) were co-cultured with primary human lung fibroblasts, without addition of growth factors. Figure 17 shows that lung resident human fibroblasts supported organoid outgrowth of huEpiSPC, as observed by co-cultures of murine EpiSPC and rMC, suggesting a similar supportive phenotype of primary lung fibroblasts in the human lung.

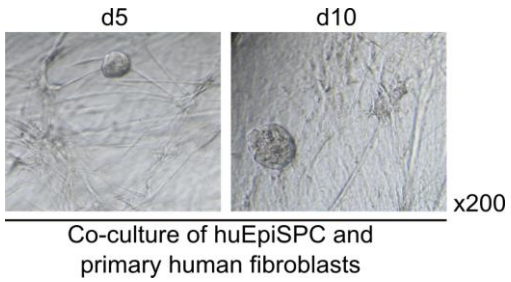

Figure 17: huEpiSPC show organoid outgrowth in co-culture with primary human fibroblasts.
Isolated primary human fibroblasts were co-cultured with FACS sorted huEpiSPC without addition of growth factors in matrix. Images were taken at day 5 and 10 after seeding. Representative images of n=3 independent experiments.

3.7 Influenza virus targets EpiSPC resulting in reduced proliferative capacity

3.7.1 Ex vivo infection of EpiSPC results in reduced organoid formation

To analyze the proliferative response and the ability to form organoids in 3D culture after influenza virus infection, FACS sorted EpiSPC were *ex vivo* infected with MOIs of 0.1 up to 5 and seeded in matrix. After 6d of culture, organoids were counted and revealed that higher MOIs of A/PR8 resulted in less organoid formation and decreased proliferative capacity (Figure 18A). Control staining with influenza virus NP after 8h of *ex vivo* infected EpiSPC revealed a robust infection rate of ~ 44% (Figure 18B).

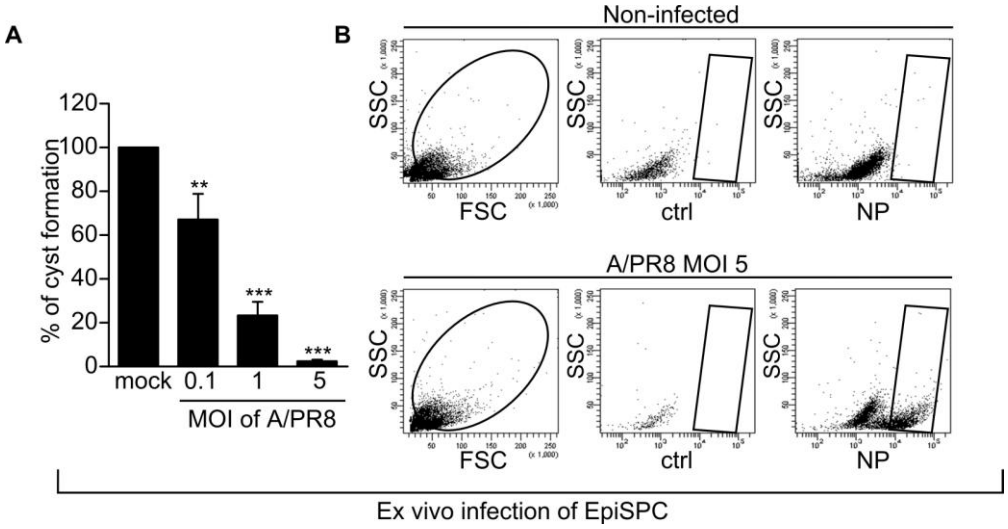

Figure 18: EpiSPC show impaired organoid formation after influenza virus infection.
(A) Organoid formation in 3D culture was evaluated of FACS sorted and *ex vivo* A/PR8 infected EpiSPC with different MOIs at d6 post infection. (B) Representative FACS plots of *ex vivo* A/PR8 infected and NP stained EpiSPC after 8h showed an infection rate of ~ 44%. Bar graphs represent mean ± SD of n=3 independent experiments; *p<0.05; **p<0.01; ***p<0.001; MOI, multiplicity of infection; ctrl, control; NP, nucleoprotein.

3.7.2 Influenza virus infected EpiSPC show reduced proliferative capacity and impaired Fgfr2b upregulation

To investigate if an impaired reparative response after influenza virus infection is caused by the extent of EpiSPC infection, different influenza virus strains varying in their pathogenicity were analyzed. WT mice were infected with 500 PFU of low pathogenic H3N2 (x-31), pandemic H1N1 (A/Hamburg/04/09; pH1N1) causing mild to moderate injury and high pathogenic, mouse adapted A/PR8 (20, 156). After 21d post infection H&E stained lung sections of A/PR8 infected mice still showed alveolar wall thickening and impaired re-epithelialization (arrows), in contrast to x-31 or pH1N1 infected mice which represented an almost intact lung structure (Figure 19A). Interestingly, the pathogenicity of the different influenza virus strains correlated with EpiSPC infection rates, measured by influenza virus nucleoprotein (NP) staining in infected WT mice at d4 post infection (Figure 19B). Additionally, A/PR8 infected EpiSPC were limited in their proliferative response, indicated by reduced proliferation rates, measured by $Ki67^+$ cell fractions of the corresponding epithelial cell subsets. Most importantly, the infected (NP^+) EpiSPC cell fraction showed impaired Fgfr2b upregulation after influenza virus infection, as compared to the non-infected (NP^-) EpiSPC cell fraction (Figure 19C, D), which indicated that the influenza virus-infected EpiSPC fraction were limited in their proliferative response due to impaired Fgfr2b upregulation.

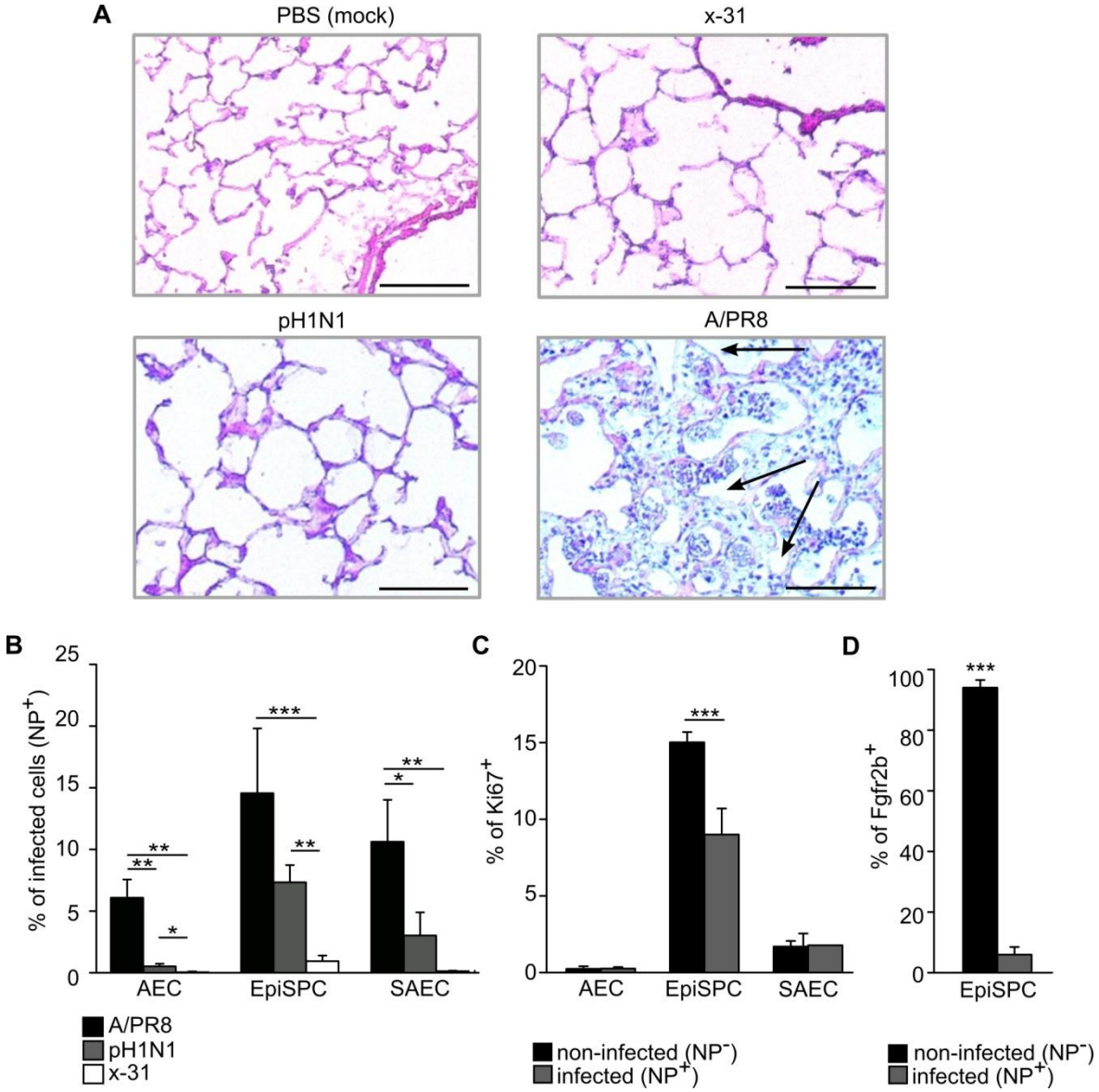

Figure 19: The extent of EpiSPC infection correlates with the pathogenicity of different virus strains and the regenerative response is impaired by reduced Fgfr2b upregulation.
(A) Lung sections were stained with H&E of mock-infected ($PBS^{-/-}$) or influenza virus infected WT mice at d21 post influenza virus infection. The different influenza virus strains varied in their pathogenicity from low (x-31), intermediate (pandemic H1N1) to high (A/PR8). Arrows indicate non-epithelialized areas. (B) WT mice were infected with 500 PFU A/PR8, pandemic H1N1 or x-31, respectively. Infection rates were determined with NP staining by flow cytometry. (C) WT mice were infected with 500 PFU A/PR8 and the proliferative response was measured by Ki67 staining of infected and non-infected epithelial subpopulations. (D) $Fgfr2b^{+}$ EpiSPC were subdivided in infected (NP^{+}) and non-infected (NP^{-}) by flow cytometry at d7 post A/PR8 infection of WT mice. Bar graphs show mean ± SD of at least n=3 independent experiments; *p<0.05; **p<0.01; ***p<0.001; NP, nucleoprotein.

3.7.3 Ex vivo infection of primary human epithelial cells results in reduced cyst formation

To investigate if primary huEpiSPC were targeted by influenza virus, FACS sorted huEpiSPC were infected with different MOIs of the pandemic H1N1 influenza virus strain A/Hamburg/04/09. Infection of huEpiSPC resulted in reduced proliferative

response, indicated by reduced organoid formation with increasing MOI in 3D cultures. The infection rate of *ex vivo* infected huEpiSPC was measured with influenza virus NP staining by flow cytometry and revealed to be ~ 20% (Figure 20A, B).

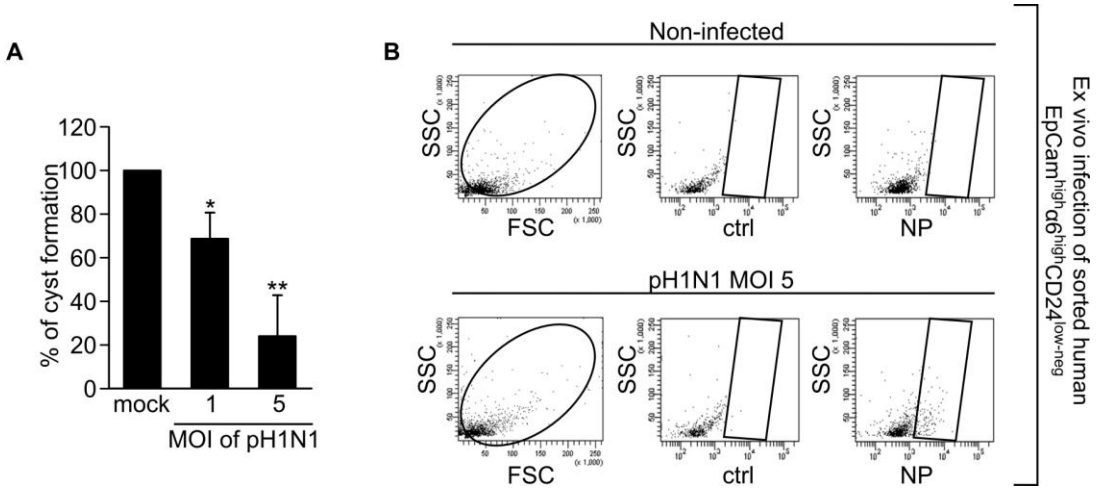

Figure 20: HuEpiSPC show reduced organoid formation after *ex vivo* infection with influenza virus. (A) Organoid formation in 3D culture was evaluated of FACS sorted and *ex vivo* infected huEpiSPC with different MOIs at d6 post infection. (C) Representative FACS plots of *ex vivo* infected and NP stained huEpiSPC after 8h of infection showed an infection rate of ~ 20%. Bar graphs represent mean ± SD of n=3 independent experiments; *p<0.05;**p<0.01; MOI, multiplicity of infection; ctrl, control; NP, nucleoprotein; pH1N1, pandemic H1N1.

3.8 Targeting the Fgf10/Fgfr2b axis during influenza virus infection *in vivo*

3.8.1 Fgf10/Fgfr2b blockade impairs lung regeneration and restoration of barrier function

To evaluate the role of the Fgf10/Fgfr2b axis in lung regeneration and outcome *in vivo*, inducible, transgenic *Rosa26$^{rtTA/+}$;tet(O)sFgfr2b/+* mice were treated with doxycycline food to inhibit Fgfr2b signaling. After influenza virus infection, lung permeability of induced and non-induced mice was measured by i.v. administration of FITC-albumin and determination of the FITC fluorescence in BALF and serum. At d14 post influenza virus infection, the alveolar leakeage was increased in doxycycline-induced mice (Figure 21A). Additionally, induced mice showed an increased mortality rate compared to non-induced mice. Moreover, the weight curve revealed that induced animals did not fully recover after influenza virus infection (Figure 21B and C). However, analysis of virus titers in BALF at d7 post infection revealed no significant difference between induced and non-induced mice, indicating that morbidity and mortality differences were not associated to altered host defense (Figure 21D).

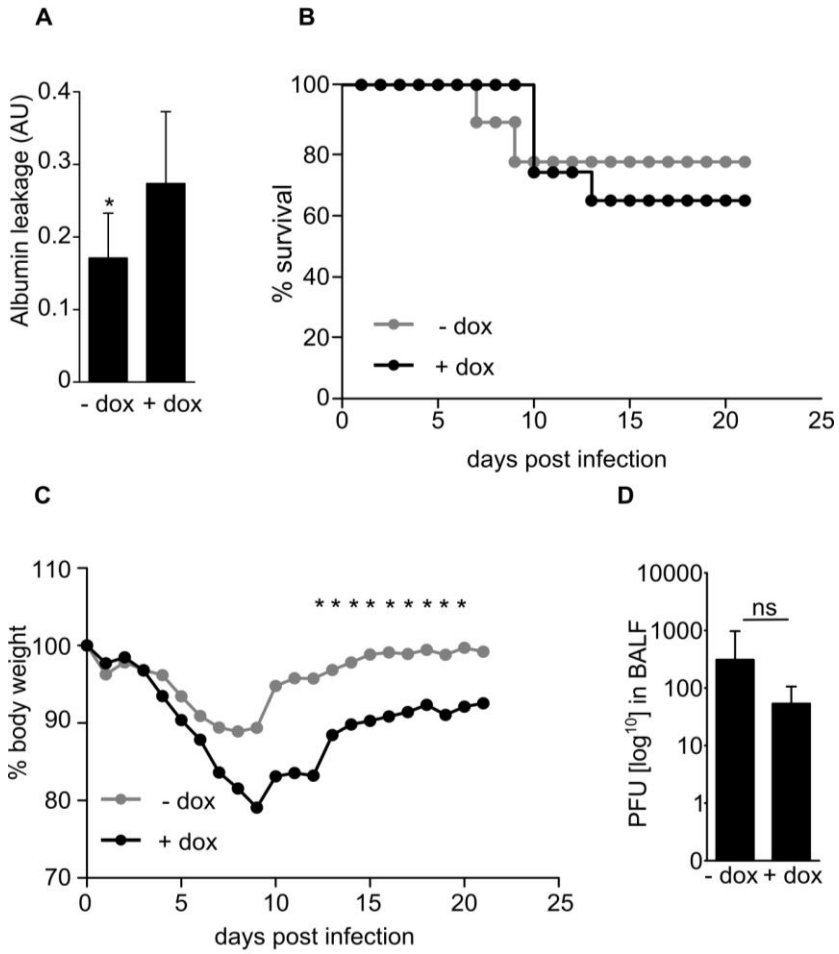

Figure 21: Blockade of Fgf10/Fgfr2b signaling results in increased lung permeability, morbidity and mortality.
Rosa26$^{rtTA/+}$*;tet(O)sFgfr2b/+* animals were infected with A/PR8. Doxycycline induced animals (+ dox) overexpressed soluble, dominant negative Fgfr2b and were compared with mice with normal food (- dox). Alveolar leakage was measured (A) by i.v. injection of FITC-albumin and quantification of FITC fluorescence in serum and BALF. (B) Induced and non-induced mice were analysed for their survival rates in % (Kaplan-Maier curve; n=8 respectively) and their corresponding body weight loss in % (C). (D) Virus titers were determined in BALF of induced and non-induced mice at d7 post infection of n=5 independent experiments. Bar graphs represent mean ± SD; *p<0.05; AU, Arbitrary units; BALF, bronchoalveolar lavage fluid; dox, doxycyline; PFU, plaque forming units.

3.8.2 Therapeutic Fgf10 application restores lung barrier function and improves outcome after influenza virus infection

To evaluate whether recombinant Fgf10 (rFgf10) treatment would improve outcome after influenza virus infection, orotracheal application of 5 µg rFgf10, diluted in PBS$^{-/-}$, or sterile PBS$^{-/-}$ alone as control was applied in WT animals at d6 after influenza virus infection. Measurement of the proliferative response by Ki67 staining at d7 post infection revealed an enhanced proliferative response in the EpiSPC fraction of rFgf10 treated mice as compared to PBS$^{-/-}$ treatment (Figure 22A). Additionally, the percentage of EpCam^{+} epithelial cells in lung homogenates

was increased after rFgf10 treatment at d14 post infection (Figure 22B). To evaluate if the enhanced proliferative response of EpiSPC was accompanied by decreased alveolar permeability, measurement of alveolar leakage by i.v. FITC albumin injection and determination of FITC fluorescence in BALF and serum at d14 post infection was performed, which revealed a significant decrease of alveolar permeability by a single dose of rFgf10. Moreover, the mortality rate of rFgf10 treated WT mice was decreased as compared to $PBS^{-/-}$ treated WT mice after influenza virus infection (Figure 22C and D).

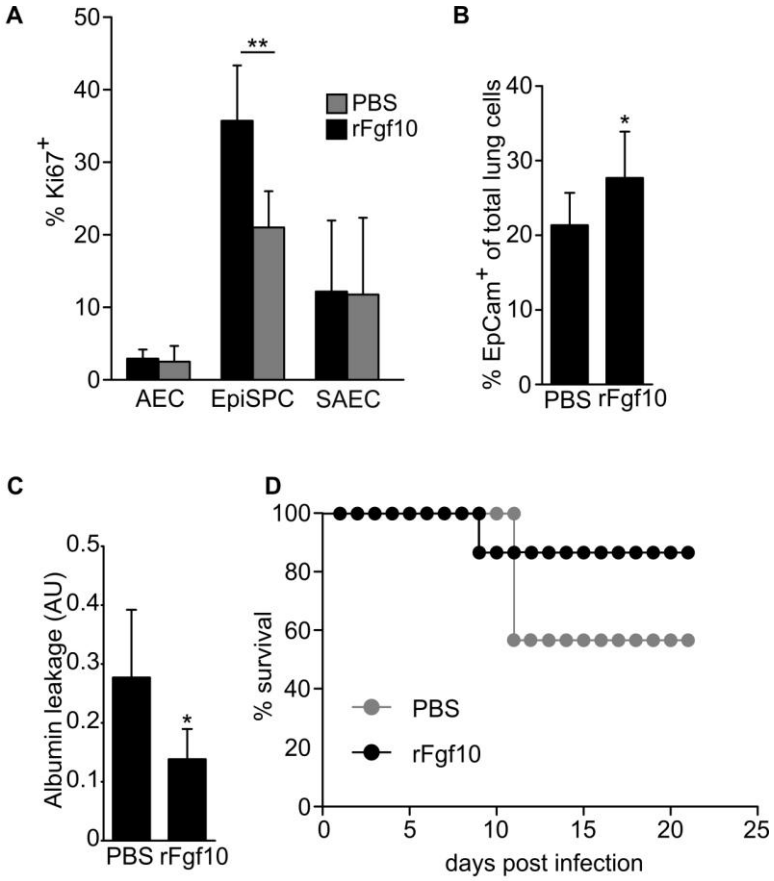

Figure 22: Therapeutic application of recombinant Fgf10 improves alveolar barrier function and survival.
WT mice were infected with A/PR8 and treated with either 5 µg recombinant Fgf10 or sterile $PBS^{-/-}$ at d6 post infection. (A) Flow cytometric measurements of $Ki67^+$ cells in the different epithelial cell subsets at d7 post infection was analyzed. (B) $EpCam^+$ epithelial cells were analyzed in total lung homogenates at d14 post infection. Alveolar permeability (C) was measured by quantification of i.v. injected FITC-albumin in serum and BALF. The mortality rate (D) of rFgf10 and $PBS^{-/-}$ treated WT mice was analyzed of n=8 mice/group after influenza virus infection. Bar graphs represent mean ± SD of at least n=5 independent experiments; *p<0.05; **p<0.01; AU, Arbitrary units; rFgf10, recombinant fibroblast growth factor 10.

Additionally, analysis of the lung structure in rFgf10 or $PBS^{-/-}$ treated WT mice after influenza virus infection revealed a reduced number of alveolar septa in $PBS^{-/-}$ treated mice (see lower magnification). At d21 post infection, the rFgf10 treated

mice showed re-epithelialization and restoration of the lung structure (arrowheads), in contrast to PBS$^{-/-}$ treated mice which still showed an increased area of non-epithelialized lung tissue (arrows) (Figure 23). To evaluate the lung structure in terms of proliferation and cell to cell contact re-establisment, lung sections were stained for the adherence junction protein E-cadherin and the proliferation marker Ki67 (Figure 24). rFgf10 treated mice showed robust E-cadherin expression, as compared to infected and PBS$^{-/-}$ treated or mock-infected mice. Furthermore, increased Ki67 expression of rFgf10 treated mice revealed a prolonged effect of the rFgf10 treatment until d21.

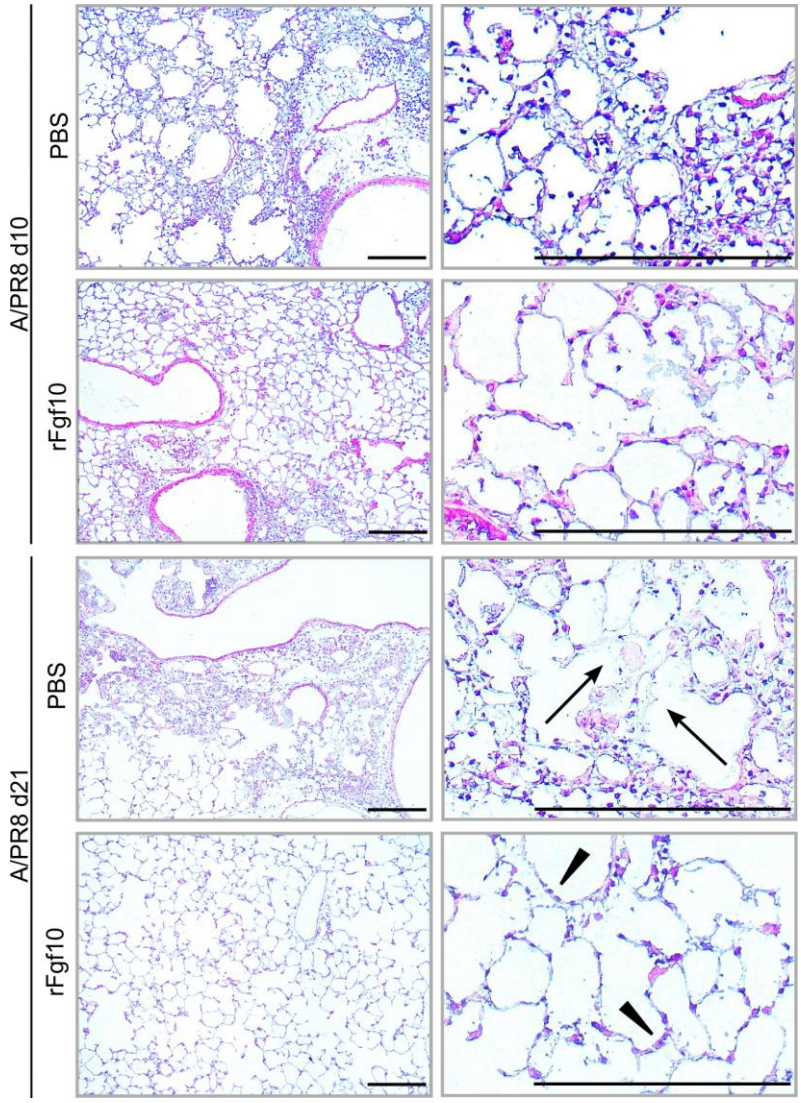

Figure 23: Influenza virus infected and recombinant Fgf10 treated WT mice show re-epithelialization in hematoxylin/eosin stained lung sections.
WT mice were infected with A/PR8 and treated with either 5 µg recombinant Fgf10 or PBS$^{-/-}$ at d6 post infection. Lung sections were obtained at d10 and d21 post infection and stained with Hematoxylin-Eosin. Arrows indicate areas of unrepaired non-epithelialized alveolar tissue. Arrow heads represent areas of re-epithelialization; bars= 200 µm; rFgf10, recombinant fibroblast growth factor 10.

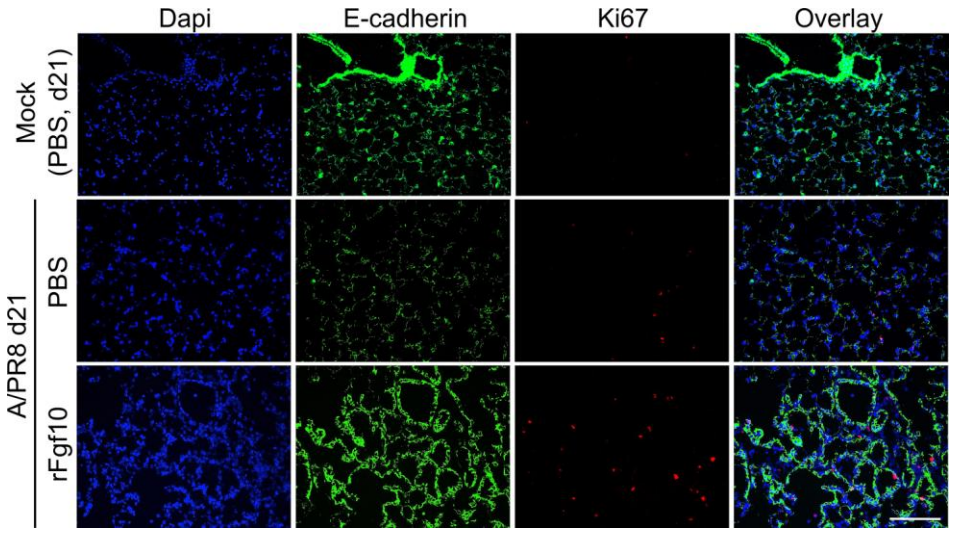

Figure 24: Influenza virus infected and recombinant Fgf10 treated WT mice show re-establishment of cell to cell contacts and prolonged proliferation.
WT mice were infected with A/PR8 or mock infected with $PBS^{-/-}$ (mock). Orotracheal instillation of infected mice was performed using either recombinant Fgf10 or $PBS^{-/-}$ at d6 post infection. Lung sections were obtained at d21 post infection and immunofluorescence stainings for E-cadherin and Ki67 were performed and compared to mock infected WT animals; bars= 200 µm; rFgf10, recombinant fibroblast growth factor 10.

To investigate the contribution of rFgf10 treatment on the Krt5 repair program, lung sections of $PBS^{-/-}$ or rFgf10 treated mice were stained for Krt5 after influenza virus infection. The Krt5 repair program was initiated in both treatment groups (Figure 25), but enhanced Krt5 expression was observed in the mice which were treated with rFgf10, suggesting that Fgf10 enhances the Krt5-dependent repair program after influenza virus-induced injury, which was shown to be cruical for the regeneration of lung tissue (98, 99).

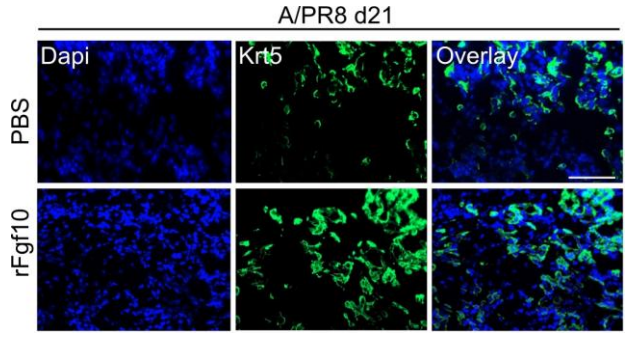

Figure 25: Recombinant Fgf10 treatment increases the Krt5 expression after influenza virus-induced injury.
WT mice were infected with A/PR8 and treated with $PBS^{-/-}$ or recombinant Fgf10 at d6 post infection. At d21 lung sections were stained for Krt5 and dapi; bars= 100 µm; rFgf10, recombinant fibroblast growth factor 10; Krt5, Keratin 5.

4. Discussion

Influenza virus pneumonia is characterized by epithelial cell apoptosis resulting in increased alveolar permeability and infiltration of protein-rich fluid into the air filled alveoli impairing gas exchange. Structural and functional re-establishment of the distal alveolar epithelial barrier after severe influenza virus pneumonia is crucial for survival and recovery.

This project demonstrates that distal epithelial stem/progenitor cells (EpiSPC) drive renewal processes after severe influenza virus pneumonia, which involves cross-talk with lung resident mesenchymal cells and Fgf10/Fgfr2b-mediated repair. Additionally, EpiSPC show high infection rates, correlating with the pathogenicity of different virus strains. Importantly, infected EpiSPC show reduced renewal capacity and impaired upregulation of the Fgf10 receptor Fgfr2b. Therapeutic application of recombinant Fgf10 after influenza virus infection enhances the proliferative response which leads to increased survival rates and improved lung function and structure. These data show that Fgf10 plays a cruical role in promoting the regenerative phenotype of EpiSPC which provides a new therapeutic approach after severe influenza virus infection.

4.1 EpiSPC characterization and proliferative response

It has been shown that the lung comprises different region-specific epithelial stem/progenitor cells in the tracheobronchial as well as in the distal compartment, which contribute to lung restoration after injury (63). Regeneration of the distal epithelial compartment was shown to involve different epithelial stem/progenitor cell populations, including $p63^{+}Krt5^{+}$ lineage-negative epithelial progenitors (LNEP), distal airway stem cells (DASC) (98, 99), an $\alpha6\beta4^{+}$ alveolar epithelial cell population or more lineage committed $CC10^{+}$ and/or $proSP\text{-}C^{+}$ epithelial cells (55, 90, 92, 95, 97, 102).

The analysis of a popuation with the signature $EpCam^{high}\alpha6^{high}CD24^{low}\beta4^{+}Sca\text{-}1^{+}$ (EpiSPC) (92, 93) showed stem cell characteristics as identified by clonogenic potential, injury resistance and organoid outgrowth in the presence of growth factors including Fgf10. Of note, organoid outgrowth could only be observed in the EpiSPC population and was not observed for terminally differentiated AEC

(EpCam^{low}α6^{low}) or SAEC (EpCam^{high}α6^{high}CD24^{high}) populations. The clonality was demonstrated by single cell sorting and clonal passaging which included digestion of organoids and reseeding of single cell suspensions with a low cell density (92). This could be performed for up to 6 passages until cystic outgrowth was dramatically decreased, possibly due to terminal differentiation of EpiSPC in culture. To test the differentiation potential of EpiSPC *in vitro*, cysts were digested after ten days in culture, RNA was extracted and qRT-PCR analysis of β-tubulin and aquaporin 5 revealed expression of terminally differentiated airway and alveolar markers, suggesting the potential of EpiSPC to contribute to bronchial as well as alveolar lineages (54, 56, 154). EpiSPC showed a high proliferative response after bronchiolar injury induced by naphthalene (84) and bronchoalveolar injury caused by influenza virus infection (19), in contrast to other distal lung epithelial cell populations. This suggests, that EpiSPC contributed to alveolar and bronchiolar repair processes, indicated by their proliferative capacity after naphthalene treatment and influenza virus-induced injury. In the influenza virus model, the proliferative response of EpiSPC was especially observed at d7 post infection, continued until d14 and reached baseline levels at d21 post infection. This renewal response was associated to a strong induction of the p63/Krt5 regeneration program, which was highly upregulated after influenza virus infection and absent in FACS sorted EpiSPC of non-infected mice. Of note, the p63/Krt5 repair program was found to be crucial for distal lung repair (95, 98, 99).

Analysis of the EpiSPC profile revealed that a fraction of these cells co-expressed low levels of CC10 and proSP-C, suggesting that a part of these proliferating EpiSPC differentiated into more lineage committed cells of the alveolar or bronchiolar tissue. Conflicting data exsist on the contribution of lineage committed cells to repair programs after injury (97-99, 157). It was previously suggested that most of the p63^{+} cells which were found during repair processes derived from the CC10^{+} pool, whereas a recent report suggested that the p63/Krt5 repair program is initiated by lineage-negative cells (97-99). Another report highlighted the type II pneumoncytes as a progenitor for alveolar tissue after bleomycin injury (102). However, the proliferative response of type II pneumocytes in the EpCam^{low}α6^{low} AEC subset was limited after influenza virus infection *in vivo*. This suggests that the contribution of different progenitor cell polulations which are involved in

alveolar repair processes is injury-specific, and dependent on the injury severity as well as microenvironmental factors.

4.2 Characterization of human epithelial stem/progenitor cells

In order to identify epithelial stem/progenitor cells (huEpiSPC) in primary distal human lung tissue, the same gating strategy which identified EpiSPC in the murine model was applied. Interestingly, analogies between human and murine epithelial cells were found. The human $EpCam^{high}\alpha6^{high}CD24^{low\text{-}neg}$ fraction was strictly dependend on growth factors, including Fgf10 and showed organoid outgrowth in 3D cultures. Additionally, the majority of these cells were $lgr6^{+}$, which was previously found to be expressed by an E-$cadherin^{+}$ population in the adult human lung that was able to form bronchoalveolar tissue in kidney capsules. Of note, the E-$cadherin^{+}lgr6^{+}$ cells were a subpopulation of $\alpha6^{+}$ cells (103). Therefore, the E-$cadherin^{+}lgr6^{+}\alpha6^{+}$ population may be included in the $EpCam^{high}\alpha6^{high}CD24^{low\text{-}neg}$ subpopulation. Nevertheless, it is necessary to define specific markers for huEpiSPC characterization to determine their differentiation potential to alveolar or bronchiolar tissue after injury.

Ex vivo co-culture of primary human lung fibroblasts and huEpiSPC revealed a supportive phenotype of fibroblasts in the human system, although huEpiSPC co-culture did not result in the formation of lung-like structures. This could be explained by the variability of patient samples, concerning both epithelial cells and fibroblasts or due to reduced differentiation capacity of the cells *ex vivo*. Nevertheless, these data clearly show that fibroblasts composed a miroenvironment required for huEpiSPC outgrowth.

Furthermore, huEpiSPC were effectively infected by a pandemic influenza virus strain, and whether pathogenicity of different virus strains also affects the infection rates of huEpiSPC needs to be addressed in future studies.

4.3 The Fgf10/Fgfr2b axis during influenza virus infection

It has been described that the Fgf10/Fgfr2b pathway plays a crucial role during lung development. Fgf10 and Fgfr2b knockout mice are not viable due to failure of organ formation which includes the absence of distal lung tissue (120-122). The

Fgf10/Fgfr2b pathway is usually inactive in adults but it has been shown that this pathway can be reactivated after naphthalene injury (134). To evaluate the impact of Fgf10 during influenza virus infection, the proliferative response was analyzed in different inducible transgenic animals. *Rosa26$^{rtTA/+}$; tet(o)sFgfr2b/+* or *Rosa26$^{rtTA/+}$; tet(o)Fgf10/+* mice either express a dominant negative, soluble Fgfr2b (sFgfr2b) which block the ligands before binding to cell-adherent Fgfr2b and therefore prevent Fgfr2b signaling, or overexpress the ligand Fgf10. Moreover, the proliferative response in *Fgf7* knockout animals was investigated, since Fgf10 and Fgf7 share the same receptor (123, 124).

Evaluation of Ki67^{+} cells showed that Fgf10 had a crucial role in the proliferative phenotype of the EpiSPC. Fgfr2b blockade resulted in reduced EpiSPC proliferation. Additionally, Fgf10 overexpression displayed an increased EpiSPC renewal capacity. The *Fgf7* knockout animals only showed a slight, non-significant decrease in the EpiSPC proliferation, which lead to the conclusion that EpiSPC proliferation clearly depends on Fgf10 after influenza virus infection. Although Fgf7 also acts as a ligand for Fgfr2b (124, 128), Fgf7 deficiency has not such a fatal effect during lung development (120, 125). Another report highlighted the different function of the two ligands with respect to Fgfr2b signaling and recycling. Fgf7 stimulation leads to rapid receptor degradation, whereas Fgf10 receptor binding leads to recycling and prolonged signaling (128), suggesting ligand-specific effects on the EpiSPC renewal capacity and importance of the Fgf10 induced receptor maintainance on the cell surface. Evaluation of Fgfr2b surface expression on EpiSPC during influenza virus infection revealed an upregulation of the receptor especially during the acute phase of the infection. In naphthalene treated mice, the effect of Fgfr2b upregulation was moderate, indicating an injury-specific response with particular engagement of the Fgf10/Fgfr2b axis after influenza virus-induced injury.

4.4 Lung resident mesenchymal cells mediate EpiSPC expansion

During lung development, the Fgfr2b ligands Fgf7/10 are expressed by mesenchymal cells (158). With respect to the cellular source of the Fgfr2b ligands, the EpCam^{neg}CD31^{neg}CD45^{neg}Sca-1^{high} popluation was found to primarily express Fgf7/10. Further characterization of the EpCam^{neg}CD31^{neg}CD45^{neg}Sca-1^{high}

popluation revealed a mixture of α-SMA$^+$ cells, a marker for myofibroblasts/smooth muscle cells, resident mesenchymal cells which may have stem cell potential characterized by CD90, and LipidTox$^+$ PDGFRα$^+$ indicating lipofibroblasts (102, 129, 152, 153). Of note, Fgfr2b ligand expression did not remarkably change in non-treated and influenza virus infected mice suggesting that previously described Fgf10 upregulation in bleomycin and naphthalene treated mice (134) is an injury-specific observation. Moreover, it indicates that the Fgf10/Fgfr2b axis is mainly regulated by receptor, and not by ligand expression, during influenza infection.

Given that Fgf10 plays a role in stem cell maintenance by preventing differentiation during development (130), and that Fgfr2b ligands are expressed by the mesenchymal lineage, co-culture of lung resident mesenchymal cells (rMC) and EpiSPC was sufficient to support organoid outgrowth and formation of lung-like structures without growth factor supplementation. Of note, CD45$^+$ leukocytes or CD31$^+$ endothelial cells did not have any supportive effect on EpiSPC outgrowth. In accordance to the *in vivo* data, blockade of the Fgf10 signaling by a neutralizing antibody *ex vivo* resulted in reduced proliferative responses of EpiSPC at an early stage of cystic outgrowth. At later stages, EpiSPC formed organoid, lung-like stuctures and increased the expression of terminal differentiation markers. These data confirm that EpiSPC are able to contribute to the restoration of lung organoids by proliferation *in vivo* and differentiation *ex vivo*. Whether EpiSPC expansion and differentiation requires additional factors induced by Fgf10 itself or other microenvironmental factors which are released during injury has to be elucidated.

4.5 Influenza virus targets EpiSPC thereby limiting EpiSPC mediated regeneration by restriction of Fgfr2b upregulation

To evaluate the impact of influenza virus infection on the proliferative capacity, EpiSPC were FACS sorted and *ex vivo* infected. EpiSPC showed high infection rates after 8h post infection. Increasing virus dose of A/PR8 (MOI 0-5) resulted in reduced organoid outgrowth and size after *ex vivo* infection demonstrating a reduced proliferative response. Of note, EpiSPC showed reduced apoptosis indicating resistance to injury and resulting in survival of previously infected

EpiSPC. Whether surviving EpiSPC reveal disturbed regeneration programs in forms of induction of aberrant repair responses later on, such as promotion of tissue fibrosis, needs to be addressed.

Importantly, infection of EpiSPC prevented EpiSPC-mediated repair processes by impaired Fgfr2b upregulation, resulting in limited proliferative capacity of infected EpiSPC compared to the non-infected EpiSPC subset of the same lung. In addition to that, the pathogenicity of different virus strains correlated to the infection rates of EpiSPC, indicating a previously undefined factor for the pathogenicity of influenza virus strains. Whether a specific tropism to EpiSPC determines pathogenicity of different influenza virus stains is currently investigated.

Recent data, obtained in this research group showed that influenza virus interferes with the β-catenin-dependent gene transcription by inhibition of Fgfr2b expression in the infected EpiSPC fraction and thereby limits the proliferative response. Additionally, culture of distal lung epithelial cells with a β-catenin activator resulted in reduced viral replication, whereas an inhibitor showed increased viral load. The activation of Wnt signaling pathways can result in activation of various cell signaling cascades which may be cross-connected and regulate differentiation, proliferation, polarity and migration (159). During lung development it has been demonstrated that Wnt/β-catenin signaling is upstream of the Fgf signaling cascade (160). Additionally, it has been demonstrated that β-catenin expression is inhibited during influenza virus infection, and active β-catenin is an important regulator of the antiviral immune response (161). In accordance to that, recent unpublished data support the observation that canonical Wnt/β-catenin has an anti-viral effect and inhibition of the Wnt/β-catenin represents an immune evasion strategy of the virus, which additionally impairs the EpiSPC regeneration program.

4.6 Targeting the Fgf10/Fgfr2b axis during influenza virus infection

To elucidate the role of the Fgf10/Fgfr2b axis during influenza virus infection *in vivo*, induced and non-induced *Rosa26*$^{rtTA/+}$*; tet(o)sFgfr2b/+* were infected and analyzed for weight loss, survival and alveolar permeability. The data demonstrate that inhibition of the Fgf10/Fgfr2b axis resulted in increased alveolar leakage, higher mortality rates and increased weight loss after influenza virus infection.

Additionally, the induced mice showed incomplete recovery, indicated by reduced weight gain. Due to the fact that the Fgf10/Fgfr2b signaling pathway was mainly regulated by receptor expression and not by altered ligand secretion, the effects observed in the *Rosa26*$^{rtTA/+}$*; tet(o)sFgfr2b/+* mice seemed to be moderate in comparison with recombinant Fgf10 (rFgf10) treatment after influenza virus infection, demonstrating a strong benefit in outcome. WT mice which were treated with either rFgf10 or sterile PBS$^{-/-}$ after influenza virus infection showed enhanced proliferative response, likely by targeting the Fgfr2b^{high}, non-infected EpiSPC subset. Additionally, the alveolar permeability was reduced, and the survival rate increased. H&E stained lung sections confirmed re-epithelialization and restoration of distal lung tissue in rFgf10 treated mice. The establishment of cell to cell contacts was demonstrated by E-cadherin stained lung sections. These findings indicate that, even after severe influenza virus-induced injury, excess Fgf10 can promote alveolar and airway repair processes by enganging the non-infected EpiSPC pool. Moreover, the prolonged proliferative effect of rFgf10 treatment is shown by Ki67 stained lung sections, which may be due to Fgfr2b recycling and prolonged singnaling (128). Furthermore, rFgf10 treated mice showed increased Krt5 expression in the distal lung tissue, indicating that the p63/Krt5 expressing EpiSPC subset contribute to the expansion of Krt5^{+} cells during repair processes which are fostered by rFgf10 application.

Altogether, these data demonstrate that influenza virus infection of epithelial stem/progenitor cells severely impairs their Fgfr2b-mediated regenerative response, and that therapeutic treatment of influenza virus pneumonia with rFgf10 promotes epithelial renewal capacity. Fgf10 therefore represents a putative treatment to drive epithelial repair to re-establish lung structure and improve gas exchange after a severe influenza virus pneumonia (Figure 26).

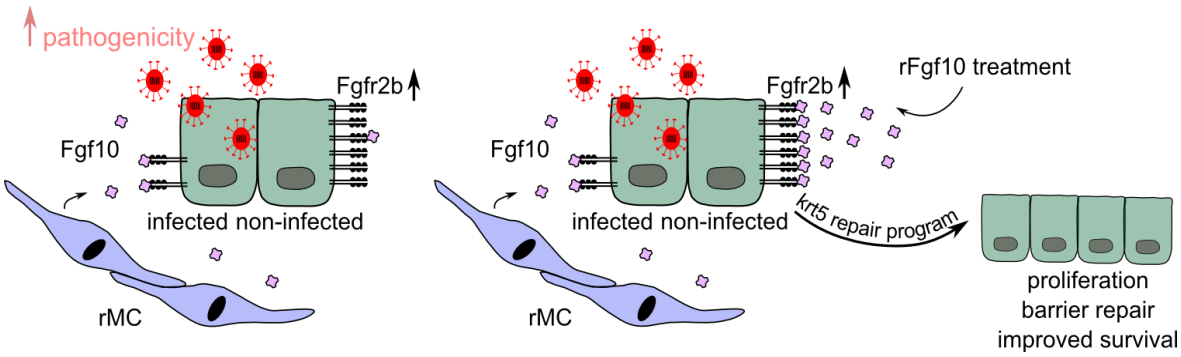

Figure 26: Proposed model of the EpiSPC repair program after influenza virus infection.
Highly pathogenic influenza virus infect a substantial fraction of EpiSPC, which results in reduced Fgfr2b upregulation and impaired epithelial repair, partially mediated by Fgf10-expressing resident mesenchymal cells. Therapeutic application of recombinant Fgf10 overcomes influenza virus-induced regeneration failure by engagement of Fgfr2b-expressing EpiSPC which increases proliferation and leads to barrier repair and improved survival with the involvement of the Krt5 repair program.

5. Summary

Influenza virus pneumonia causes apoptosis of alveolar epithelial cells, disruption of the epithelial barrier and edema formation that affects gas exchange dramatically, resulting in the acute respiratory distress syndrome with poor outcome. The pathology of influenza virus-induced injury is well studied, but repair mechanisms of the distal lung epithelium, which may influence the outcome are not well understood. It has been demonstrated that epithelial progenitor cells in the adult murine lung can repopulate injured tracheobronchial or alveolar regions. Therefore, this project investigated repair mechanisms of distal epithelial stem/progenitor cell (EpiSPC) after severe influenza virus pneumonia. The EpiSPC express the surface markers $EpCam^{high}\alpha6^{high}CD24^{low}\beta4^{+}Sca\text{-}1^{+}$. They highly proliferate after influenza virus injury, but show low apoptosis rates after infection as compared to other epithelial subsets. Characterization of their phenotype in *ex vivo* 3D cultures revealed that flow sorted EpiSPC clonally expand in presence of growth factors, including Fgf10, and upregulate markers associated with terminally differentiated bronchiolar and alveolar cells. Lung resident mesenchymal cells defined as $CD45^{neg}CD31^{neg}EpCam^{neg}Sca\text{-}1^{high}$ revealed to be the primary source of Fgf10, and supported lung-like outgrowth in the absence of further growth factors. During influenza virus infection, the Fgf10 receptor Fgfr2b was highly upregulated on non-infected EpiSPC, whereas the infected population poorly upregulated the Fgfr2b, resulting in severe limitation of their proliferative response. Interestingly, the pathogenicity of different influenza virus strains correlated with infection rates of EpiSPC *in vivo*, suggesting a causal relation between the extent of EpiSPC infection and their capacity to restore lung function. Targeting the Fgf10/Fgfr2b axis by induction of dominant negative soluble Fgfr2b in transgenic mice resulted in increased alveolar permeability, weight loss, and decreased proliferative capacity of EpiSPC. Application of recombinant Fgf10 (rFgf10) as a therapeutic approach in the acute phase of influenza virus infection enhanced the proliferative response of EpiSPC, decreased alveolar leakage and improved survival rates. Additionally, lung sections revealed better resolution of inflammation and restoration of lung structure after rFgf10 application. In accordance with decreased alveolar leakage, staining of lung sections revealed improved cell to cell connections in the alveolar compartment. With respect to the

human lung, a population similar to EpiSPC, expressing EpCam^{high}α6^{high}CD24$^{low-neg}$Igr6^{+} was identified, which similarly depended on growth factors, including Fgf10 and formed cystic spheres in 3D culture. As demonstrated in murine organoid cultures, co-cultures of human EpiSPC with primary human lung fibroblasts promoted outgrowth without addition of growth factors, whereas infection with pandemic influenza virus resulted in a reduced proliferative response.

In conclusion, this work identifies Fgf10/Fgfr2b-dependent EpiSPC as primary drivers of lung regeneration after influenza virus-induced lung injury. Influenza virus-induced inhibition of Fgf10-mediated repair caused by influenza virus infection could be overcome by therapeutic application of Fgf10, highlighting this approach as putative therapy for patients with influenza virus-induced ARDS.

6. Zusammenfassung

Influenzaviren infizieren vorwiegend die Epithelzellen der oberen Atemwege. Dennoch kann das Virus in den distalen Bereich der Lunge vordringen und Pneumonien verursachen, die schließlich zum akuten Lungenversagen führen. Die Reparatur und Wiederherstellung eines funktionstüchtigen Epithels ist deshalb für die Genesung des Patienten von besonderer Bedeutung. Dabei spielen epitheliale Progenitorzellen eine zentrale Rolle. Diese können nach einer Schädigung des Epithels proliferieren und zu alveolärem und/oder bronchialem Epithel differenzieren und somit die alveoläre Schrankenfunktion wieder herstellen und die Sauerstoffversorgung gewährleisten.

In dieser Arbeit wurde eine Progenitorzellpopulation mit der Oberflächensignatur $EpCam^{high}\alpha6^{high}CD24^{low}\beta4^{+}Sca\text{-}1^{+}$ untersucht, die maßgeblich an der Regeneration des Lungenepithels nach einer Influenzavirus-induzierten Pneumonie beteiligt ist. Diese epithelialen Stamm/Progenitorzellen (EpiSPC) sind im Gegensatz zu terminal ausdifferenzierten Epithelzellen Apoptose-resistent. Durchflusszytometrisch separierte und in Matrix kultivierte EpiSPC bilden organoide Strukturen in Abhängigkeit von der Verfügbarkeit des Wachstumsfaktors Fgf10. Die Fgf10-abhängige Proliferation der EpiSPC konnte auch *in vivo* in verschiedenen transgenen murinen Infektionsmodellen gezeigt werden. Eine gezielte Inhibierung des Fgf10/Fgfr2b Signalweges führte in diesen Tieren zu verringerten EpiSPC-Proliferationsraten, wohingegen eine Aktivierung des Signalweges die Proliferationsraten erhöhte. Dabei stellte sich heraus, dass der Ligand Fgf7, der wie Fgf10 den Rezeptor Fgfr2b aktivieren kann, keinen Einfluss auf die Proliferationsraten der EpiSPC ausübt. Desweiteren wurde der Rezeptor Fgfr2b durch eine Influenzavirusinfektion verstärkt auf den EpiSPC exprimiert, wohingegen die Expression seines Liganden Fgf10 nicht massgeblich beeinflusst wurde. Die erhöhte Expression des Rezeptors wurde insbesondere auf nicht infizierten EpiSPC nachgewiesen, deren Proliferationsrate, im Gegensatz zu infizierten EpiSPC, erheblich verstärkt ist. Desweiteren weisen die EpiSPC *in vivo* eine hohe Infektionsrate auf, wobei diese mit der Pathogenität verschiedener Influenzavirus Stämme korreliert. In *in vitro* Ko-Kulturen mit primären, Fgf10-exprimierenden mesenchymalen Zellen der Lunge konnte ein verstärktes Wachstum der EpiSPC beobachtet werden, das in Abhängigkeit von Fgf10 zur

Ausbildung von Lungenorganoiden führte. Eine gezielte Inhibierung des Fgf10/Fgfr2b Signalweges *in vivo* führte zu einer höheren alveolären Permeabilität sowie Mortalität. Behandlung mit intratracheal appliziertem rekombinantem Fgf10 resultierte in erhöhten EpiSPC Proliferationsraten, sowie geringerer Mortalität. Desweiteren konnte die alveoläre Schrankenstörung verringert, und die Regeneration des distalen Lungengewebes verbessert werden. Im distalen humanen Lungengewebe konnte eine, den murinen EpiSPC entsprechende Progenitorzellpopulation mit der Oberflächensignatur $EpCam^{high}\alpha6^{high}CD24^{low\text{-}neg}$ nachgewiesen werden, deren Wachstum ebenfalls Fgf10-abhängig war.

Zusammenfassend wurde gezeigt, dass der Fgf10/Fgfr2b Signalweg nach einer Influenzavirusinfektion eine wesentliche Rolle in der EpiSPC abhängigen Regeneration des distalen Lungengewebes spielt. Eine durch Influenzaviren hervorgerufene Inhibierung der Regeneration konnte durch eine gezielte Behandlung mit rekombinantem Fgf10 kompensiert werden. Diese Ergebnisse weisen darauf hin, dass eine Behandlung mit rekombinantem Fgf10 zu einem Therapieerfolg bei Influenzavirus-induziertem ARDS-Patienten führen könnte.

7. References

1. Medina, R.A., and García-Sastre, A. 2011. Influenza A viruses: new research developments. *Nat Rev Micro* 9:590-603.

2. Taubenberger, J.K., and Kash, J.C. 2010. Influenza virus evolution, host adaptation, and pandemic formation. *Cell Host Microbe* 7:440-451.

3. Samji, T. 2009. Influenza A: understanding the viral life cycle. *Yale J Biol Med* 82:153-159.

4. Szewczyk, B., Bienkowska-Szewczyk, K., and Krol, E. 2014. Introduction to molecular biology of influenza a viruses. *Acta Biochim Pol* 61:397-401.

5. Fukuyama, S., and Kawaoka, Y. 2011. The pathogenesis of influenza virus infections: the contributions of virus and host factors. *Curr Opin Immunol* 23:481-486.

6. Couch, R.B. 1996. Orthomyxoviruses. *Medical Microbiology* 4th edition:Chapter 58.

7. Taubenberger, J.K., and Morens, D.M. 2013. Influenza viruses: breaking all the rules. *MBio* 4:00365-00313.

8. Karlsson Hedestam, G.B., Fouchier, R.A., Phogat, S., Burton, D.R., Sodroski, J., and Wyatt, R.T. 2008. The challenges of eliciting neutralizing antibodies to HIV-1 and to influenza virus. *Nat Rev Microbiol* 6:143-155.

9. Hutchinson, E.C., and Fodor, E. 2013. Transport of the influenza virus genome from nucleus to nucleus. *Viruses* 5:2424-2446.

10. Rossman, J.S., and Lamb, R.A. 2011. Influenza virus assembly and budding. *Virology* 411:229-236.

11. Herold, S., Becker, C., Ridge, K.M., and Budinger, G.R. 2015. Influenza virus-induced lung injury: pathogenesis and implications for treatment. *Eur Respir J* 45:1463-1478.

12. Hale, B.G., Albrecht, R.A., and Garcia-Sastre, A. 2010. Innate immune evasion strategies of influenza viruses. *Future Microbiol* 5:23-41.

13. Osterlund, P., Strengell, M., Sarin, L.P., Poranen, M.M., Fagerlund, R., Melen, K., and Julkunen, I. 2012. Incoming influenza A virus evades early host recognition, while influenza B virus induces interferon expression directly upon entry. *J Virol* 86:11183-11193.

14. Pulendran, B., and Maddur, M.S. 2015. Innate immune sensing and response to influenza. *Curr Top Microbiol Immunol* 386:23-71.

15. Bergmann, M., Garcia-Sastre, A., Carnero, E., Pehamberger, H., Wolff, K., Palese, P., and Muster, T. 2000. Influenza virus NS1 protein counteracts PKR-mediated inhibition of replication. *J Virol* 74:6203-6206.

16. Krug, R.M. 2015. Functions of the influenza A virus NS1 protein in antiviral defense. *Curr Opin Virol* 12:1-6.

17. Kochs, G., Garcia-Sastre, A., and Martinez-Sobrido, L. 2007. Multiple anti-interferon actions of the influenza A virus NS1 protein. *J Virol* 81:7011-7021.

18. Hale, B.G., Randall, R.E., Ortin, J., and Jackson, D. 2008. The multifunctional NS1 protein of influenza A viruses. *J Gen Virol* 89:2359-2376.

19. Taubenberger, J.K., and Morens, D.M. 2008. The pathology of influenza virus infections. *Annu Rev Pathol* 3:499-522.

20. Bouvier, N.M., and Lowen, A.C. 2010. Animal Models for Influenza Virus Pathogenesis and Transmission. *Viruses* 2:1530-1563.

21. Lyles, D.S. 2000. Cytopathogenesis and inhibition of host gene expression by RNA viruses. *Microbiol Mol Biol Rev* 64:709-724.

22. Bouvier, N.M., and Palese, P. 2008. The biology of influenza viruses. *Vaccine* 26 Suppl 4:D49-53.

23. Kuiken, T., and Taubenberger, J.K. 2008. Pathology of human influenza revisited. *Vaccine* 26 Suppl 4:D59-66.

24. Yin, L., Zheng, D., Limmon, G.V., Leung, N.H., Xu, S., Rajapakse, J.C., Yu, H., Chow, V.T., and Chen, J. 2014. Aging exacerbates damage and delays repair of alveolar epithelia following influenza viral pneumonia. *Respir Res* 15:116.

25. Belshe, R.B. 2005. The origins of pandemic influenza--lessons from the 1918 virus. *N Engl J Med* 353:2209-2211.

26. Short, K.R., Kroeze, E.J., Fouchier, R.A., and Kuiken, T. 2014. Pathogenesis of influenza-induced acute respiratory distress syndrome. *Lancet Infect Dis* 14:57-69.

27. Ashbaugh, D.G., Bigelow, D.B., Petty, T.L., and Levine, B.E. 1967. Acute respiratory distress in adults. *Lancet* 2:319-323.

28. Phua, J., Badia, J.R., Adhikari, N.K., Friedrich, J.O., Fowler, R.A., Singh, J.M., Scales, D.C., Stather, D.R., Li, A., Jones, A., et al. 2009. Has mortality from acute respiratory distress syndrome decreased over time?: A systematic review. *Am J Respir Crit Care Med* 179:220-227.

29. Matthay, M.A., and Zemans, R.L. 2011. The acute respiratory distress syndrome: pathogenesis and treatment. *Annu Rev Pathol* 6:147-163.

30. Ochiai, R. 2015. Mechanical ventilation of acute respiratory distress syndrome. *J Intensive Care* 3:25.

31. Fanelli, V., Vlachou, A., Ghannadian, S., Simonetti, U., Slutsky, A.S., and Zhang, H. 2013. Acute respiratory distress syndrome: new definition, current and future therapeutic options. *J Thorac Dis* 5:326-334.

32. Matthay, M.A., Ware, L.B., and Zimmerman, G.A. 2012. The acute respiratory distress syndrome. *J Clin Invest* 122:2731-2740.

33. El-Khatib, M.F., and Jamaleddine, G.W. 2008. Clinical relevance of the PaO2/FiO2 ratio. *Crit Care* 12:407.

34. Beiderlinden, M. 2011. Akutes Lungenversagen. In *Praxis der Intensivmedizin*. Wilhelm, W., editor. Heidelberg: Springer-Verlag.

35. Ranieri, V.M., Rubenfeld, G.D., Thompson, B.T., Ferguson, N.D., Caldwell, E., Fan, E., Camporota, L., and Slutsky, A.S. 2012. Acute respiratory distress syndrome: the Berlin Definition. *JAMA* 307:2526-2533.

36. Ferguson, N.D., Fan, E., Camporota, L., Antonelli, M., Anzueto, A., Beale, R., Brochard, L., Brower, R., Esteban, A., Gattinoni, L., et al. 2012. The Berlin definition of ARDS: an expanded rationale, justification, and supplementary material. *Intensive Care Med* 38:1573-1582.

37. Howell, D.C.J., Bellingan, G.J. 2009. Acute lung injury and acute respiratory distress syndrome (ALI/ARDS). In *Respiratory disease and its management*. McLuckie, A., editor. London: Springer.

38. Bellingan, G.J. 2002. The pulmonary physician in critical care * 6: The pathogenesis of ALI/ARDS. *Thorax* 57:540-546.

39. Wynn, T.A. 2011. Integrating mechanisms of pulmonary fibrosis. *J Exp Med* 208:1339-1350.

40. Burnham, E.L., Janssen, W.J., Riches, D.W., Moss, M., and Downey, G.P. 2014. The fibroproliferative response in acute respiratory distress syndrome: mechanisms and clinical significance. *Eur Respir J* 43:276-285.

41. Ricard, J.D., Dreyfuss, D., and Saumon, G. 2002. Ventilator-induced lung injury. *Curr Opin Crit Care* 8:12-20.

42. Ranieri, V.M., Suter, P.M., Tortorella, C., De Tullio, R., Dayer, J.M., Brienza, A., Bruno, F., and Slutsky, A.S. 1999. Effect of mechanical ventilation on inflammatory mediators in patients with acute respiratory distress syndrome: a randomized controlled trial. *JAMA* 282:54-61.

43. Roze, H., Repusseau, B., and Ouattara, A. 2014. Extracorporeal membrane oxygenation in adults for severe acute respiratory failure. *Ann Fr Anesth Reanim* 33:492-494.

44. Marasco, S.F., Lukas, G., McDonald, M., McMillan, J., and Ihle, B. 2008. Review of ECMO (extra corporeal membrane oxygenation) support in critically ill adult patients. *Heart Lung Circ* 17 Suppl 4:S41-47.

45. Raghavendran, K., Pryhuber, G.S., Chess, P.R., Davidson, B.A., Knight, P.R., and Notter, R.H. 2008. Pharmacotherapy of acute lung injury and acute respiratory distress syndrome. *Curr Med Chem* 15:1911-1924.

46. Han, S., and Mallampalli, R.K. 2015. The acute respiratory distress syndrome: from mechanism to translation. *J Immunol* 194:855-860.

47. Standiford, T.J., and Ward, P.A. 2015. Therapeutic targeting of acute lung injury and acute respiratory distress syndrome. *Transl Res*.

48. Beitler, J.R., Schoenfeld, D.A., and Thompson, B.T. 2014. Preventing ARDS: progress, promise, and pitfalls. *Chest* 146:1102-1113.

49. Herold, S., Hoegner, K., Vadasz, I., Gessler, T., Wilhelm, J., Mayer, K., Morty, R.E., Walmrath, H.D., Seeger, W., and Lohmeyer, J. 2014. Inhaled granulocyte/macrophage colony-stimulating factor as treatment of pneumonia-associated acute respiratory distress syndrome. *Am J Respir Crit Care Med* 189:609-611.

50. Curley, G.F., and Laffey, J.G. 2015. Future therapies for ARDS. *Intensive Care Med* 41:322-326.

51. Weibel, E.R. 2009. What makes a good lung? *Swiss Med Wkly* 139:375-386.

52. Weibel, E.R. 2012. It takes more than cells to make a good lung. *Am J Respir Crit Care Med* 187:342-346.

53. Jeffery, P.K., Gaillard, D., and Moret, S. 1992. Human airway secretory cells during development and in mature airway epithelium. *Eur Respir J* 5:93-104.

54. Tam, A., Wadsworth, S., Dorscheid, D., Man, S.F., and Sin, D.D. 2011. The airway epithelium: more than just a structural barrier. *Ther Adv Respir Dis* 5:255-273.

55. Reynolds, S.D., and Malkinson, A.M. 2010. Clara cell: progenitor for the bronchiolar epithelium. *Int J Biochem Cell Biol* 42:1-4.

56. Dobbs, L.G., Johnson, M.D., Vanderbilt, J., Allen, L., and Gonzalez, R. 2010. The great big alveolar TI cell: evolving concepts and paradigms. *Cell Physiol Biochem* 25:55-62.

57. Herzog, E.L., Brody, A.R., Colby, T.V., Mason, R., and Williams, M.C. 2008. Knowns and unknowns of the alveolus. *Proc Am Thorac Soc* 5:778-782.

58. Fehrenbach, H. 2001. Alveolar epithelial type II cell: defender of the alveolus revisited. *Respir Res* 2:33-46.

59. Bonner, J.C. 2010. Mesenchymal cell survival in airway and interstitial pulmonary fibrosis. *Fibrogenesis Tissue Repair* 3:15.

60. Vaccaro, C., and Brody, J.S. 1978. Ultrastructure of developing alveoli. I. The role of the interstitial fibroblast. *Anat Rec* 192:467-479.

61. El Agha, E., and Bellusci, S. 2014. Walking along the Fibroblast Growth Factor 10 Route: A Key Pathway to Understand the Control and Regulation of Epithelial and Mesenchymal Cell-Lineage Formation during Lung Development and Repair after Injury. *Scientifica (Cairo)* 2014:538379.

62. Leeman, K.T., Fillmore, C.M., and Kim, C.F. 2014. Lung stem and progenitor cells in tissue homeostasis and disease. *Curr Top Dev Biol* 107:207-233.

63. McQualter, J.L., and Bertoncello, I. 2012. Concise review: Deconstructing the lung to reveal its regenerative potential. *Stem Cells* 30:811-816.

64. Rawlins, E.L., and Hogan, B.L. 2006. Epithelial stem cells of the lung: privileged few or opportunities for many? *Development* 133:2455-2465.

65. Kajstura, J., Rota, M., Hall, S.R., Hosoda, T., D'Amario, D., Sanada, F., Zheng, H., Ogorek, B., Rondon-Clavo, C., Ferreira-Martins, J., et al. 2011. Evidence for human lung stem cells. *N Engl J Med* 364:1795-1806.

66. Ruiz, E.J., Oeztuerk-Winder, F., and Ventura, J.J. 2014. A paracrine network regulates the cross-talk between human lung stem cells and the stroma. *Nat Commun* 5:3175.

67. Urbanek, K., Cesselli, D., Rota, M., Nascimbene, A., De Angelis, A., Hosoda, T., Bearzi, C., Boni, A., Bolli, R., Kajstura, J., et al. 2006. Stem cell niches in the adult mouse heart. *Proc Natl Acad Sci U S A* 103:9226-9231.

68. Berika, M., Elgayyar, M.E., and El-Hashash, A.H. 2014. Asymmetric cell division of stem cells in the lung and other systems. *Front Cell Dev Biol* 2:33.

69. Hong, K.U., Reynolds, S.D., Giangreco, A., Hurley, C.M., and Stripp, B.R. 2001. Clara cell secretory protein-expressing cells of the airway neuroepithelial body microenvironment include a label-retaining subset and are critical for epithelial renewal after progenitor cell depletion. *Am J Respir Cell Mol Biol* 24:671-681.

70. Li, F., He, J., Wei, J., Cho, W.C., and Liu, X. 2015. Diversity of epithelial stem cell types in adult lung. *Stem Cells Int* 2015:728307.

71. Rock, J.R., Randell, S.H., and Hogan, B.L. 2010. Airway basal stem cells: a perspective on their roles in epithelial homeostasis and remodeling. *Dis Model Mech* 3:545-556.

72. Rock, J.R., Onaitis, M.W., Rawlins, E.L., Lu, Y., Clark, C.P., Xue, Y., Randell, S.H., and Hogan, B.L.M. 2009. Basal cells as stem cells of the mouse trachea and human airway epithelium. *Proc Natl Acad Sci U S A* 106:12771-12775.

73. Rock, J.R., Gao, X., Xue, Y., Randell, S.H., Kong, Y.Y., and Hogan, B.L. 2011. Notch-dependent differentiation of adult airway basal stem cells. *Cell Stem Cell* 8:639-648.

74. Rock, J.R., and Hogan, B.L. 2011. Epithelial progenitor cells in lung development, maintenance, repair, and disease. *Annu Rev Cell Dev Biol* 27:493-512.

75. Schoch, K.G., Lori, A., Burns, K.A., Eldred, T., Olsen, J.C., and Randell, S.H. 2004. A subset of mouse tracheal epithelial basal cells generates large colonies in vitro. *Am J Physiol Lung Cell Mol Physiol* 286:L631-642.

76. Ghosh, M., Helm, K.M., Smith, R.W., Giordanengo, M.S., Li, B., Shen, H., and Reynolds, S.D. 2011. A single cell functions as a tissue-specific stem cell and the in vitro niche-forming cell. *Am J Respir Cell Mol Biol* 45:459-469.

77. Borthwick, D.W., Shahbazian, M., Krantz, Q.T., Dorin, J.R., and Randell, S.H. 2001. Evidence for stem-cell niches in the tracheal epithelium. *Am J Respir Cell Mol Biol* 24:662-670.

78. Duan, D., Sehgal, A., Yao, J., and Engelhardt, J.F. 1998. Lef1 transcription factor expression defines airway progenitor cell targets for in utero gene therapy of submucosal gland in cystic fibrosis. *Am J Respir Cell Mol Biol* 18:750-758.

79. Hegab, A.E., Ha, V.L., Gilbert, J.L., Zhang, K.X., Malkoski, S.P., Chon, A.T., Darmawan, D.O., Bisht, B., Ooi, A.T., Pellegrini, M., et al. 2011. Novel stem/progenitor cell population from murine tracheal submucosal gland ducts with multipotent regenerative potential. *Stem Cells* 29:1283-1293.

80. Rawlins, E.L., Okubo, T., Xue, Y., Brass, D.M., Auten, R.L., Hasegawa, H., Wang, F., and Hogan, B.L. 2009. The role of Scgb1a1+ Clara cells in the long-term maintenance and repair of lung airway, but not alveolar, epithelium. *Cell Stem Cell* 4:525-534.

81. Fanucchi, M.V., Murphy, M.E., Buckpitt, A.R., Philpot, R.M., and Plopper, C.G. 1997. Pulmonary cytochrome P450 monooxygenase and Clara cell differentiation in mice. *Am J Respir Cell Mol Biol* 17:302-314.

82. Warren, D.L., Brown, D.L., Jr., and Buckpitt, A.R. 1982. Evidence for cytochrome P-450 mediated metabolism in the bronchiolar damage by naphthalene. *Chem Biol Interact* 40:287-303.

83. Mahvi, D., Bank, H., and Harley, R. 1977. Morphology of a naphthalene-induced bronchiolar lesion. *Am J Pathol* 86:558-572.

84. Van Winkle, L.S., Buckpitt, A.R., Nishio, S.J., Isaac, J.M., and Plopper, C.G. 1995. Cellular response in naphthalene-induced Clara cell injury and bronchiolar epithelial repair in mice. *Am J Physiol* 269:L800-818.

85. Giangreco, A., Reynolds, S.D., and Stripp, B.R. 2002. Terminal bronchioles harbor a unique airway stem cell population that localizes to the bronchoalveolar duct junction. *Am J Pathol* 161:173-182.

86. Zheng, D., Limmon, G.V., Yin, L., Leung, N.H., Yu, H., Chow, V.T., and Chen, J. 2013. A cellular pathway involved in Clara cell to alveolar type II cell differentiation after severe lung injury. *PLoS One* 8:e71028.

87. Song, H., Yao, E., Lin, C., Gacayan, R., Chen, M.H., and Chuang, P.T. 2012. Functional characterization of pulmonary neuroendocrine cells in lung development, injury, and tumorigenesis. *Proc Natl Acad Sci U S A* 109:17531-17536.

88. Linnoila, R.I. 2006. Functional facets of the pulmonary neuroendocrine system. *Lab Invest* 86:425-444.

89. Reynolds, S.D., Giangreco, A., Power, J.H., and Stripp, B.R. 2000. Neuroepithelial bodies of pulmonary airways serve as a reservoir of progenitor cells capable of epithelial regeneration. *Am J Pathol* 156:269-278.

90. Kim, C.F., Jackson, E.L., Woolfenden, A.E., Lawrence, S., Babar, I., Vogel, S., Crowley, D., Bronson, R.T., and Jacks, T. 2005. Identification of bronchioalveolar stem cells in normal lung and lung cancer. *Cell* 121:823-835.

91. Tropea, K.A., Leder, E., Aslam, M., Lau, A.N., Raiser, D.M., Lee, J.H., Balasubramaniam, V., Fredenburgh, L.E., Alex Mitsialis, S., Kourembanas, S., et al. 2012. Bronchioalveolar stem cells increase after mesenchymal stromal cell treatment in a mouse model of bronchopulmonary dysplasia. *Am J Physiol Lung Cell Mol Physiol* 302:L829-837.

92. McQualter, J.L., Yuen, K., Williams, B., and Bertoncello, I. 2010. Evidence of an epithelial stem/progenitor cell hierarchy in the adult mouse lung. *Proc Natl Acad Sci U S A* 107:1414-1419.

93. Bertoncello, I., and McQualter, J. 2011. Isolation and clonal assay of adult lung epithelial stem/progenitor cells. *Curr Protoc Stem Cell Biol* Chapter 2:Unit 2G 1.

94. McQualter, J.L., McCarty, R.C., Van der Velden, J., O'Donoghue, R.J., Asselin-Labat, M.L., Bozinovski, S., and Bertoncello, I. 2013. TGF-beta signaling in stromal cells acts upstream of FGF-10 to regulate epithelial stem cell growth in the adult lung. *Stem Cell Res* 11:1222-1233.

95. Chapman, H.A., Li, X., Alexander, J.P., Brumwell, A., Lorizio, W., Tan, K., Sonnenberg, A., Wei, Y., and Vu, T.H. 2011. Integrin alpha6beta4 identifies an adult distal lung epithelial population with regenerative potential in mice. *J Clin Invest* 121:2855-2862.

96. Kumar, P.A., Hu, Y., Yamamoto, Y., Hoe, N.B., Wei, T.S., Mu, D., Sun, Y., Joo, L.S., Dagher, R., Zielonka, E.M., et al. 2011. Distal airway stem cells yield alveoli in vitro and during lung regeneration following H1N1 influenza infection. *Cell* 147:525-538.

97. Zheng, D., Yin, L., and Chen, J. 2014. Evidence for Scgb1a1(+) cells in the generation of p63(+) cells in the damaged lung parenchyma. *Am J Respir Cell Mol Biol* 50:595-604.

98. Zuo, W., Zhang, T., Wu, D.Z., Guan, S.P., Liew, A.A., Yamamoto, Y., Wang, X., Lim, S.J., Vincent, M., Lessard, M., et al. 2014. p63+ Krt5+ distal airway stem cells are essential for lung regeneration. *Nature* 517:616-620.

99. Vaughan, A.E., Brumwell, A.N., Xi, Y., Gotts, J.E., Brownfield, D.G., Treutlein, B., Tan, K., Tan, V., Liu, F.C., Looney, M.R., et al. 2015. Lineage-negative progenitors mobilize to regenerate lung epithelium after major injury. *Nature* 517:621-625.

100. Desai, T.J., Brownfield, D.G., and Krasnow, M.A. 2014. Alveolar progenitor and stem cells in lung development, renewal and cancer. *Nature* 507:190-194.

101. Adamson, I.Y., and Bowden, D.H. 1975. Derivation of type 1 epithelium from type 2 cells in the developing rat lung. *Lab Invest* 32:736-745.

102. Barkauskas, C.E., Cronce, M.J., Rackley, C.R., Bowie, E.J., Keene, D.R., Stripp, B.R., Randell, S.H., Noble, P.W., and Hogan, B.L. 2013. Type 2 alveolar cells are stem cells in adult lung. *J Clin Invest* 123:3025-3036.

103. Oeztuerk-Winder, F., Guinot, A., Ochalek, A., and Ventura, J.-J. 2012. Regulation of human lung alveolar multipotent cells by a novel p38α MAPK/miR-17-92 axis. *The EMBO Journal* 31:3431-3441.

104. Engelhardt, J.F., Schlossberg, H., Yankaskas, J.R., and Dudus, L. 1995. Progenitor cells of the adult human airway involved in submucosal gland development. *Development* 121:2031-2046.

105. Hackett, T.L., Shaheen, F., Johnson, A., Wadsworth, S., Pechkovsky, D.V., Jacoby, D.B., Kicic, A., Stick, S.M., and Knight, D.A. 2008. Characterization of side population cells from human airway epithelium. *Stem Cells* 26:2576-2585.

106. Goodell, M.A., Brose, K., Paradis, G., Conner, A.S., and Mulligan, R.C. 1996. Isolation and functional properties of murine hematopoietic stem cells that are replicating in vivo. *J Exp Med* 183:1797-1806.

107. Gonzalez, R.F., Allen, L., Gonzales, L., Ballard, P.L., and Dobbs, L.G. 2010. HTII-280, a biomarker specific to the apical plasma membrane of human lung alveolar type II cells. *J Histochem Cytochem* 58:891-901.

108. Gospodarowicz, D., Bialecki, H., and Greenburg, G. 1978. Purification of the fibroblast growth factor activity from bovine brain. *J Biol Chem* 253:3736-3743.

109. Bohlen, P., Esch, F., Baird, A., and Gospodarowicz, D. 1985. Acidic fibroblast growth factor (FGF) from bovine brain: amino-terminal sequence and comparison with basic FGF. *EMBO J* 4:1951-1956.

110. Gospodarowicz, D. 1975. Purification of a fibroblast growth factor from bovine pituitary. *J Biol Chem* 250:2515-2520.

111. Nobuyuki Itoh, and Ornitz, D.M. 2011. Fibroblast growth factors: from molecular evolution to roles in development, metabolism and disease. *J Biochem* 149 121-130.

112. Eswarakumar, V.P., Lax, I., and Schlessinger, J. 2005. Cellular signaling by fibroblast growth factor receptors. *Cytokine Growth Factor Rev* 16:139-149.

113. Plotnikov, A.N., Hubbard, S.R., Schlessinger, J., and Mohammadi, M. 2000. Crystal structures of two FGF-FGFR complexes reveal the determinants of ligand-receptor specificity. *Cell* 101:413-424.

114. Wuechner, C., Nordqvist, A.C., Winterpacht, A., Zabel, B., and Schalling, M. 1996. Developmental expression of splicing variants of fibroblast growth factor receptor 3 (FGFR3) in mouse. *Int J Dev Biol* 40:1185-1188.

115. Gong, S.G. 2014. Isoforms of receptors of fibroblast growth factors. *J Cell Physiol* 229:1887-1895.

116. Carter, E.P., Fearon, A.E., and Grose, R.P. 2014. Careless talk costs lives: fibroblast growth factor receptor signalling and the consequences of pathway malfunction. *Trends Cell Biol* 4:221-233.

117. Jean, J.-C., Lü, J., Joyce-Brady, M., and Cardoso, W.V. 2008. Regulation of Fgf10 gene expression in murine mesenchymal cells. *Journal of Cellular Biochemistry* 103:1886-1894.

118. Ramasamy, S.K., Mailleux, A.A., Gupte, V.V., Mata, F., Sala, F.G., Veltmaat, J.M., Del Moral, P.M., De Langhe, S., Parsa, S., Kelly, L.K., et al. 2007. Fgf10 dosage is critical for the amplification of epithelial cell progenitors and for the formation of multiple mesenchymal lineages during lung development. *Dev Biol* 307:237-247.

119. Cardoso, W.V., and Lu, J. 2006. Regulation of early lung morphogenesis: questions, facts and controversies. *Development* 133:1611-1624.

120. Fairbanks, T.J., Kanard, R.C., De Langhe, S.P., Sala, F.G., Del Moral, P.M., Warburton, D., Anderson, K.D., Bellusci, S., and Burns, R.C. 2004. A

genetic mechanism for cecal atresia: the role of the Fgf10 signaling pathway. *J Surg Res* 120:201-209.

121. Sekine, K., Ohuchi, H., Fujiwara, M., Yamasaki, M., Yoshizawa, T., Sato, T., Yagishita, N., Matsui, D., Koga, Y., Itoh, N., et al. 1999. Fgf10 is essential for limb and lung formation. *Nat Genet* 21:138-141.

122. De Moerlooze, L., Spencer-Dene, B., Revest, J.M., Hajihosseini, M., Rosewell, I., and Dickson, C. 2000. An important role for the IIIb isoform of fibroblast growth factor receptor 2 (FGFR2) in mesenchymal-epithelial signalling during mouse organogenesis. *Development* 127:483-492.

123. Ohuchi, H., Hori, Y., Yamasaki, M., Harada, H., Sekine, K., Kato, S., and Itoh, N. 2000. FGF10 Acts as a Major Ligand for FGF Receptor 2 IIIb in Mouse Multi-Organ Development. *Biochem Biophys Res Commun* 277:643-649.

124. Ware, L.B., and Matthay, M.A. 2002. Keratinocyte and hepatocyte growth factors in the lung: roles in lung development, inflammation, and repair. *Am J Physiol Lung Cell Mol Physiol* 282:L924-940.

125. Guo, L., Degenstein, L., and Fuchs, E. 1996. Keratinocyte growth factor is required for hair development but not for wound healing. *Genes Dev* 10:165-175.

126. Shannon, J.M., and Hyatt, B.A. 2004. Epithelial-mesenchymal interactions in the developing lung. *Annu Rev Physiol* 66:625-645.

127. Partanen, J., Schwartz, L., and Rossant, J. 1998. Opposite phenotypes of hypomorphic and Y766 phosphorylation site mutations reveal a function for Fgfr1 in anteroposterior patterning of mouse embryos. *Genes Dev* 12:2332-2344.

128. Francavilla, C., Rigbolt, K.T., Emdal, K.B., Carraro, G., Vernet, E., Bekker-Jensen, D.B., Streicher, W., Wikstrom, M., Sundstrom, M., Bellusci, S., et al. 2013. Functional proteomics defines the molecular switch underlying FGF receptor trafficking and cellular outputs. *Mol Cell* 51:707-722.

129. El Agha, E., Herold, S., Al Alam, D., Quantius, J., MacKenzie, B., Carraro, G., Moiseenko, A., Chao, C.M., Minoo, P., Seeger, W., et al. 2014. Fgf10-positive cells represent a progenitor cell population during lung development and postnatally. *Development* 141:296-306.

130. Volckaert, T., Campbell, A., Dill, E., Li, C., Minoo, P., and De Langhe, S. 2013. Localized Fgf10 expression is not required for lung branching morphogenesis but prevents differentiation of epithelial progenitors. *Development* 140:3731-3742.

131. Bellusci, S., Grindley, J., Emoto, H., Itoh, N., and Hogan, B.L. 1997. Fibroblast growth factor 10 (FGF10) and branching morphogenesis in the embryonic mouse lung. *Development* 124:4867-4878.

132. Park, W.Y., Miranda, B., Lebeche, D., Hashimoto, G., and Cardoso, W.V. 1998. FGF-10 is a chemotactic factor for distal epithelial buds during lung development. *Dev Biol* 201:125-134.

133. Hokuto, I., Perl, A.K., and Whitsett, J.A. 2003. Prenatal, but not postnatal, inhibition of fibroblast growth factor receptor signaling causes emphysema. *J Biol Chem* 278:415-421.

134. Volckaert, T., Dill, E., Campbell, A., Tiozzo, C., Majka, S., Bellusci, S., and De Langhe, S.P. 2011. Parabronchial smooth muscle constitutes an airway epithelial stem cell niche in the mouse lung after injury. *J Clin Invest* 121:4409-4419.

135. Shu, W., Jiang, Y.Q., Lu, M.M., and Morrisey, E.E. 2002. Wnt7b regulates mesenchymal proliferation and vascular development in the lung. *Development* 129:4831-4842.

136. Weidenfeld, J., Shu, W., Zhang, L., Millar, S.E., and Morrisey, E.E. 2002. The WNT7b promoter is regulated by TTF-1, GATA6, and Foxa2 in lung epithelium. *J Biol Chem* 277:21061-21070.

137. Gupte, V.V., Ramasamy, S.K., Reddy, R., Lee, J., Weinreb, P.H., Violette, S.M., Guenther, A., Warburton, D., Driscoll, B., Minoo, P., et al. 2009. Overexpression of fibroblast growth factor-10 during both inflammatory and

fibrotic phases attenuates bleomycin-induced pulmonary fibrosis in mice. *Am J Respir Crit Care Med* 180:424-436.

138. Hokuto, I., Perl, A.K., and Whitsett, J.A. 2004. FGF signaling is required for pulmonary homeostasis following hyperoxia. *Am J Physiol Lung Cell Mol Physiol* 286:L580-587.

139. Gossen, M., and Bujard, H. 1992. Tight control of gene expression in mammalian cells by tetracycline-responsive promoters. *Proc Natl Acad Sci U S A* 89:5547-5551.

140. Belteki, G., Haigh, J., Kabacs, N., Haigh, K., Sison, K., Costantini, F., Whitsett, J., Quaggin, S.E., and Nagy, A. 2005. Conditional and inducible transgene expression in mice through the combinatorial use of Cre-mediated recombination and tetracycline induction. *Nucleic Acids Res* 33:e51.

141. Parsa, S., Kuremoto, K., Seidel, K., Tabatabai, R., Mackenzie, B., Yamaza, T., Akiyama, K., Branch, J., Koh, C.J., Al Alam, D., et al. 2010. Signaling by FGFR2b controls the regenerative capacity of adult mouse incisors. *Development* 137:3743-3752.

142. Clark, J.C., Tichelaar, J.W., Wert, S.E., Itoh, N., Perl, A.K., Stahlman, M.T., and Whitsett, J.A. 2001. FGF-10 disrupts lung morphogenesis and causes pulmonary adenomas in vivo. *Am J Physiol Lung Cell Mol Physiol* 280:L705-715.

143. Schwenk, F., Baron, U., and Rajewsky, K. 1995. A cre-transgenic mouse strain for the ubiquitous deletion of loxP-flanked gene segments including deletion in germ cells. *Nucleic Acids Res* 23:5080-5081.

144. Warburton, D., Perin, L., Defilippo, R., Bellusci, S., Shi, W., and Driscoll, B. 2008. Stem/progenitor cells in lung development, injury repair, and regeneration. *Proc Am Thorac Soc* 5:703-706.

145. Schluter, C., Duchrow, M., Wohlenberg, C., Becker, M.H., Key, G., Flad, H.D., and Gerdes, J. 1993. The cell proliferation-associated antigen of antibody Ki-67: a very large, ubiquitous nuclear protein with numerous

repeated elements, representing a new kind of cell cycle-maintaining proteins. *J Cell Biol* 123:513-522.

146. Thangavel, R.R., and Bouvier, N.M. 2014. Animal models for influenza virus pathogenesis, transmission, and immunology. *J Immunol Methods*.

147. Mason, R.J. 2006. Biology of alveolar type II cells. *Respirology* 11:S12-15.

148. Oosterlaken-Dijksterhuis, M.A., van Eijk, M., van Buel, B.L., van Golde, L.M., and Haagsman, H.P. 1991. Surfactant protein composition of lamellar bodies isolated from rat lung. *Biochem J* 274:115-119.

149. Ramirez, M.I., Millien, G., Hinds, A., Cao, Y., Seldin, D.C., and Williams, M.C. 2003. T1alpha, a lung type I cell differentiation gene, is required for normal lung cell proliferation and alveolus formation at birth. *Dev Biol* 256:61-72.

150. Rawlins, E.L., Ostrowski, L.E., Randell, S.H., and Hogan, B.L. 2007. Lung development and repair: contribution of the ciliated lineage. *Proc Natl Acad Sci U S A* 104:410-417.

151. McQualter, J.L., Brouard, N., Williams, B., Baird, B.N., Sims-Lucas, S., Yuen, K., Nilsson, S.K., Simmons, P.J., and Bertoncello, I. 2009. Endogenous fibroblastic progenitor cells in the adult mouse lung are highly enriched in the sca-1 positive cell fraction. *Stem Cells* 27:623-633.

152. Martin, J., Helm, K., Ruegg, P., Varella-Garcia, M., Burnham, E., and Majka, S. 2008. Adult lung side population cells have mesenchymal stem cell potential. *Cytotherapy* 10:140-151.

153. Kaplan, N.B., Grant, M.M., and Brody, J.S. 1985. The lipid interstitial cell of the pulmonary alveolus. Age and species differences. *Am Rev Respir Dis* 132:1307-1312.

154. Jensen-Smith, H.C., Luduena, R.F., and Hallworth, R. 2003. Requirement for the betaI and betaIV tubulin isotypes in mammalian cilia. *Cell Motil Cytoskeleton* 55:213-220.

155. Alao, J.P. 2007. The regulation of cyclin D1 degradation: roles in cancer development and the potential for therapeutic invention. *Mol Cancer* 6:24.

156. Otte, A., and Gabriel, G. 2011. 2009 pandemic H1N1 influenza A virus strains display differential pathogenicity in C57BL/6J but not BALB/c mice. *Virulence* 2:563-566.

157. Zheng, D., Limmon, G.V., Yin, L., Leung, N.H., Yu, H., Chow, V.T., and Chen, J. 2012. Regeneration of alveolar type I and II cells from Scgb1a1-expressing cells following severe pulmonary damage induced by bleomycin and influenza. *PLoS One* 7:e48451.

158. Lebeche, D., Malpel, S., and Cardoso, W.V. 1999. Fibroblast growth factor interactions in the developing lung. *Mech Dev* 86:125-136.

159. Lien, W.H., and Fuchs, E. 2014. Wnt some lose some: transcriptional governance of stem cells by Wnt/beta-catenin signaling. *Genes Dev* 28:1517-1532.

160. Shu, W., Guttentag, S., Wang, Z., Andl, T., Ballard, P., Lu, M.M., Piccolo, S., Birchmeier, W., Whitsett, J.A., Millar, S.E., et al. 2005. Wnt/beta-catenin signaling acts upstream of N-myc, BMP4, and FGF signaling to regulate proximal-distal patterning in the lung. *Dev Biol* 283:226-239.

161. Hillesheim, A., Nordhoff, C., Boergeling, Y., Ludwig, S., and Wixler, V. 2014. beta-catenin promotes the type I IFN synthesis and the IFN-dependent signaling response but is suppressed by influenza A virus-induced RIG-I/NF-kappaB signaling. *Cell Commun Signal* 12:29.

8. Declaration

I declare that I have completed this dissertation single-handedly without the unauthorized help of a second party and only with the assistance acknowledged therein. I have appropriately acknowledged and referenced all text passages that are derived literally from or are based on the content of published or unpublished work of others, and all information that relates to verbal communications. I have abided by the principles of good scientific conduct laid down in the charter of the Justus Liebig University of Giessen in carrying out the investigations described in the dissertation.

J. Quantius